

**UNIVERSITÄTSKLINIKUM HAMBURG-EPPENDORF**

Institut für Immunologie

Prof. Dr. med. Marcus Altfeld

**USE OF FLUORESCENT SENSORS TO VISUALIZE P2X7-MEDIATED  
CHANGES IN LOCAL ATP CONCENTRATIONS IN THE CYTOSOL  
AND AT THE CELL SURFACE**

**Dissertation**

zur Erlangung des Doktorgrades Dr. rer. biol. hum./ PhD  
an der Medizinischen Fakultät der Universität Hamburg

vorgelegt von:

Klaus Eric Kaschubowski  
aus Hamburg

Hamburg 2020

**Angenommen von der  
Medizinischen Fakultät der Universität Hamburg am: 16.12.2020**

**Veröffentlicht mit Genehmigung der  
Medizinischen Fakultät der Universität Hamburg.**

**Prüfungsausschuss, der/die Vorsitzende: Prof. Dr. Friedrich Haag**

**Prüfungsausschuss, 2. Gutachter/in: Prof. Dr. Viacheslav Nikolaev**

## PUBLICATIONS

Some ideas and figures have appeared previously in the following publications:

- Johnsen, B., K. E. Kaschubowski, S. Nader, E. Schneider, J.-A. Nicola, R. Fliegert, I. M. A. Wolf, A. H. Guse, V. O. Nikolaev, F. Koch-Nolte, and F. Haag (June 2019). “P2X7-mediated ATP secretion is accompanied by depletion of cytosolic ATP.” In: *Purinergic signalling* 15 (2), pp. 155–166. DOI: [10.1007/s11302-019-09654-5](https://doi.org/10.1007/s11302-019-09654-5).
- Kaschubowski, K. E., A. E. Kraft, V. O. Nikolaev, and F. Haag (2020). “Using FRET-Based Fluorescent Sensors to Monitor Cytosolic and Membrane-Proximal Extracellular ATP Levels.” In: *Methods in molecular biology (Clifton, N.J.)* 2041, pp. 223–231. DOI: [10.1007/978-1-4939-9717-6\\_16](https://doi.org/10.1007/978-1-4939-9717-6_16).

# CONTENTS

1	INTRODUCTION	1
1.1	An overview of the Immune System	1
1.1.1	Innate immune system	1
1.1.2	Adaptive immune system	2
1.2	Purinergic Signaling	3
1.2.1	P1/adenosine Receptors	3
1.2.2	P2 Receptors	4
1.2.3	The P2X7 Receptor	5
1.2.4	Inflammation and P2X7	8
1.2.5	ATP release and metabolism	9
1.3	ATP measurement and sensors	10
1.3.1	Genetically encoded ATP sensors	11
1.3.2	Small molecule ATP sensors	14
1.4	Aim of this work	15
2	MATERIAL AND METHODS	16
2.1	Materials	16
2.1.1	Antibodies/nanobodies	16
2.1.2	Bacterial strains	17
2.1.3	Buffers and solutions	17
2.1.4	Cell lines	19
2.1.5	Chemicals and reagents	20
2.1.6	Consumables	23
2.1.7	Enzymes	25
2.1.8	Kits	26
2.1.9	Laboratory equipment	26
2.1.10	Mouse lines	28
2.1.11	Plasmids	28
2.1.12	Primers	29
2.1.13	Software	29
2.2	Methods	31
2.2.1	Methods in cell biology	31
2.2.2	Immunological methods	35
2.2.3	Microscopy and image processing	37
2.2.4	Methods in molecular biology	39
2.2.5	Methods in protein chemistry	42
2.2.6	Labeling of proteins, beads and other surfaces using click chemistry	44
3	RESULTS	46
3.1	Hallmarks of P2X7 activity	46

3.1.1	Shedding of CD62L and PI uptake . . . . .	47
3.1.2	Calcium uptake after P2X7 activation . . . . .	48
3.1.3	ATP release after gating of P2X7 by NAD <sup>+</sup> -dependent ADP-ribosylation . . . . .	49
3.2	FRET-based ATP sensors for measurement of cytosolic and extracellular ATP . . . . .	51
3.2.1	Generation of cell lines expressing FRET-based ATP sensors . . . . .	51
3.2.2	Functional validation of the sensor and visualization of cytosolic ATP . . . . .	52
3.2.3	Use of FRET-based ATP sensors to monitor cytosolic depletion of ATP following complement-dependent cytotoxicity (CDC) . . . . .	56
3.2.4	Use of FRET-based ATP sensors to monitor cytosolic depletion of ATP following gating of P2X7 . . . . .	57
3.2.5	Use of FRET-based ATP sensors to visualize extracellular ATP . . . . .	59
3.2.6	Transgenic mice, AAV and lentiviral production of FRET-based ATP sensors . . . . .	61
3.3	Small-molecule sensors for detection of extracellular ATP . . . . .	62
3.3.1	Soluble Zn-DPA sensors . . . . .	62
3.3.2	Targeting of Zn-DPA-azide sensor variants to cell membranes . . . . .	63
3.3.3	Direct membrane anchors of Zn-DPA-C(n) variants . . . . .	67
3.4	Single wavelength sensors for measurement of cytosolic and extracellular ATP . . . . .	70
4	DISCUSSION . . . . .	74
4.1	Hallmarks of P2X7 activation . . . . .	74
4.1.1	P2X7 mediated ATP release . . . . .	75
4.2	ATP imaging using FRET based sensors . . . . .	75
4.2.1	Validating the function of FRET-based ATP sensors . . . . .	76
4.2.2	ATP depletion after gating of P2X7 . . . . .	76
4.3	Small-molecule ATP sensors . . . . .	78
4.4	Conclusion and outlook . . . . .	81
5	ABSTRACT . . . . .	84
6	ZUSAMMENFASSUNG . . . . .	85
7	ACRONYMS . . . . .	86
8	BIBLIOGRAPHY . . . . .	90
9	LIST OF FIGURES AND TABLES . . . . .	106
	Curriculum Vitae . . . . .	109
	Eidesstattliche Versicherung . . . . .	110

# 1 | INTRODUCTION

## 1.1 AN OVERVIEW OF THE IMMUNE SYSTEM

The immune system is a complex host defense system that protects against body invading pathogens like viruses, bacteria, parasites or fungi. In jawed vertebrates, this humoral and cellular immune system consists of an innate and adaptive system (Boehm and Swann, 2014), which are dependent on each other to guarantee an efficient response against said pathogens. All cells of the immune system derive from hematopoietic stem cells (HSC) of the bone marrow and can be divided in lymphoid and myeloid cells. One hallmark of the immune system is to discriminate between self and non-self (and therefore foreign antigens). Another crucial function of the immune system is the ability to sustain long-term protection (immunological memory) against pathogens (Farber et al., 2016).

### 1.1.1 *Innate immune system*

The innate immune system is the so-called “first line of defense”. It includes myeloid and innate lymphoid cells (e.g., antigen-presenting cells (APC)) like macrophages or dendritic cells (DC), the innate humoral system (complement, pentaxins and defensins), and epithelial cells of the intestine, skin and lungs. (Hazlett and M. Wu, 2011; Netea et al., 2019). The main functions of the innate immune system are:

- serving as a physical barrier to keep pathogens outside of the body (provided by epithelial cells of the intestine, skin and the lung).
- to give a fast initial response (within minutes) after coming in contact with a pathogen.

The innate immune system can fulfill these roles because of its ubiquitous distribution in the tissue, and this unspecific response will either lead to successful clearance of the pathogen or the recruitment of more innate cells. The whole process is often accompanied by inflammation leading to swelling, pain, redness and heat (see [Section 1.2.4 “Inflammation and P2X7”](#)). It also initiates tissue repair and presents antigens to cells of the adaptive immune system. APC such as DC and macrophages, present antigens to T cells through their major histocompatibility complex (MHC) II molecules (Haan, Arens, and Zelm, 2014).

### 1.1.2 *Adaptive immune system*

The adaptive immune system allows a specific response against unknown antigens (i.e., molecules like proteins or lipids that are recognized as foreign/pathogenic). It can develop an immunological memory, which allows a faster response after a second or multiple encounter with an already known foreign antigen. This memory can last over decades or life-long for some pathogens (Crotty et al., 2003; Stefanati et al., 2019). The main cell populations of the adaptive immune system are B and T cells. T cells can be roughly divided into helper ( $CD4^+$ ), cytotoxic ( $CD8^+$ ) T cells, with a special subset of  $CD4^+$  T cells being the T regulatory cells (Tregs). During their maturation process, T cells undergo positive and negative selection in the thymus to eliminate self-reacting cells that could cause autoimmunity. The V(D)J recombination is an important process during the maturation of the T cells that leads to a tremendous expansion of the T cell receptor (TCR) repertoire and allows the recognition of a variety of antigens.

After DCs take up antigens in the periphery, they digest them and load peptides onto the MHC class II molecules, which are then presented on the cell surface. They then migrate into the lymph nodes where they come into contact with specific T cells to activate them, acting as a link between innate and adaptive immunity (Neeffjes et al., 2011). Antigens presented on MHC class I molecules are recognized by  $CD8^+$  T cells, which induce apoptosis of the presenting cells. Activation of  $CD4^+$  T cells via the MHC class II molecule on DCs leads to cytokine release, T cell differentiation, and B cell activation.

In B cells, the B cell receptor (BCR) also undergoes V(D)J recombination during maturation in the bone marrow. Additionally, after their encounter with antigens, B cells experience somatic hyper-mutation and subsequently clonal expansion. The activation of B cells through  $CD4^+$  T cells ultimately leads to the differentiation of B cells into plasma cells (antibody-producing cells) (Nutt et al., 2015; Park, Yoon, and Jung, 2016).

Purinergic signaling plays an essential role in the interplay of innate and adaptive immunity. It is essential to regulate the inflammatory response, including cytokine release, chemotaxis, and T cell activation. This will be discussed further in the following chapters.

#### *Conventional and heavy chain antibodies*

Antibodies (Ab) belong to the immunoglobulin superfamily (IgSF) and consist of two heavy and two light chains. Upon digestion with proteases, light and heavy chains form two fragments: fragment antigen-binding (Fab) regions for antigen recognition, and the fragment crystallizable (Fc) region, formed by the constant regions of the two heavy chains. This fragment allows communication with the immune system e.g., the complement system resulting in the clearance of pathogens (Nutt et al., 2015; Park, Yoon, and Jung, 2016). In some mammals (camelids), heavy chain antibodies (hcAb) are expressed next to conventional Ab. These hcAb lack the light chains of a conventional Ab. They recognize antigens by one single variable domain that can be produced as a recombinant protein, which because of its small size, is called a nanobody (Wesolowski et al., 2009; Danquah et al., 2016).

## 1.2 PURINERGIC SIGNALING

Adenine nucleotides are small ubiquitous molecules, among them are adenosine triphosphate (ATP) and nicotinamide adenine dinucleotide (NAD<sup>+</sup>), mainly known for their roles in energy metabolism inside of cells. In ATP, the energy is stored in the phosphoanhydride bonds and released via hydrolyzation of said bonds (Knowles, 1980). NAD<sup>+</sup>, on the other hand, is a co-factor for oxidoreductase and acts as a substrate for the ATP production in mitochondria.

In 1972 Burnstock et al. first described that ATP and NAD<sup>+</sup>, besides their role in energy metabolism, also play important roles as second messengers for intra- and extracellular signal transduction (Burnstock 1972). In 1978 Burnstock et al. described receptors that are the targets of these purine nucleotides. He proposed the division into two families of receptors, respectively P1 and P2 receptors. In general P1 receptors are more sensitive to adenosine (Ado) and adenosine monophosphate (AMP), whereas P2 receptors are more sensitive to adenosine diphosphate (ADP) and ATP (Burnstock et al., 1978). Figure 1.1 shows an overview of the essential members involved in purinergic signaling. In the following, these members are discussed in more detail.

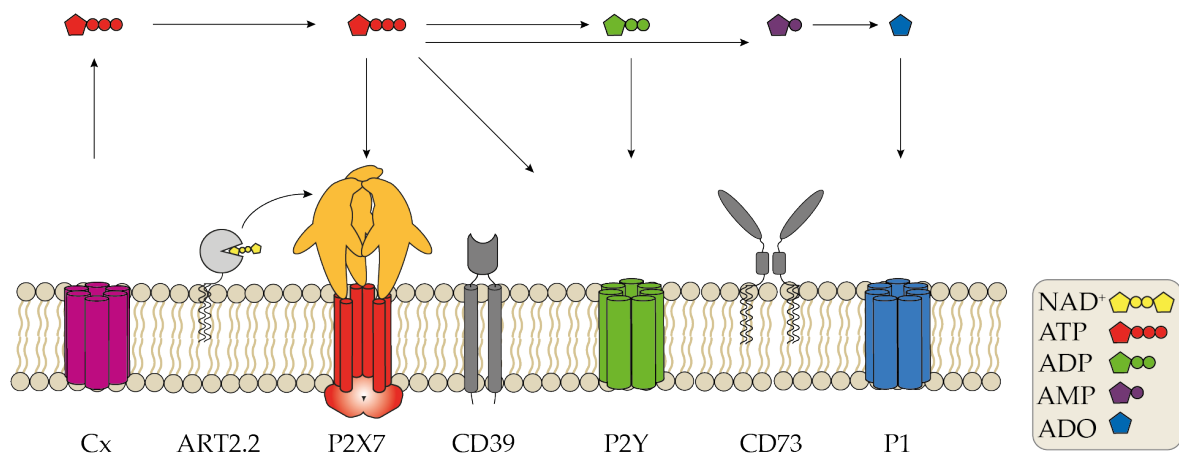


Figure 1.1: Schematic overview of receptors, channels and enzymes taking part in the purinergic signalling cascade

ATP is released from damaged cells, through various channels (connexins, hemichannels, P2X7) or exocytosis into the extracellular space, causing inflammation by activating P2X (e.g., P2X7) and P2Y receptors. ATP and ADP are hydrolyzed to AMP via NTP-Dase 1 (CD39). ADP can activate P2Y receptors, and AMP is further hydrolyzed by 5'-Nucleotidase (CD73) to adenosine, which in turn can activate P1 receptors and thus dampen the immune response.

### 1.2.1 P1/adenosine Receptors

P1 or adenosine receptors are G-protein-coupled receptors (GPCR) that are characterized by seven transmembrane domains. The binding of extracellular ligands leads to an activation of intracellular heterotrimeric bound G proteins. These consist of three subunits  $G\alpha$ ,  $G\beta$ , and  $G\gamma$ . After the ligand is bound to the GPCR, the induced conformational change allows the G protein complex to bind to the GPCR. Thereafter, the G protein dissociates into the  $\alpha$  and  $\beta\gamma$

subunits, which can activate other proteins. The  $G\alpha$  hydrolyzes the guanosine triphosphate (GTP) to guanosine diphosphate (GDP), which allows the  $\alpha$  and  $\beta\gamma$  to reassemble (Borea et al., 2017).

The adenosine receptor family has four members, the A1, A2A, A2B, and A3 receptors. They differ for example in the tissue expression, the associated G protein, and the adenosine affinity. These adenosine receptors are ubiquitously distributed in the body and have important roles in the central nervous and the cardiovascular systems. Furthermore, they are expressed on different cells of the immune system. The A2A receptor is the most common Ado receptor found on immune cells. A2B and A3 are lesser abundant in immune cells. The primary function of these receptors is limiting inflammation. After activation through Ado, cyclic adenosine monophosphate (cAMP) concentrations rise in cells, inducing activation of protein kinase A (PKA) and thus further downstream effects, including inhibition of the deletion of naive T cells and the proliferation of T helper cells, as well as reduced production of pro-inflammatory cytokines and proliferation of regulatory T cells (Cekic and Linden, 2016). In macrophages, the production of Tumor necrosis factor alpha (TNF- $\alpha$ ) is down- and the production of interleukin (IL)-10 and the expression of CD73 are upregulated (Borea et al., 2017).

### 1.2.2 P2 Receptors

Next to the anti-inflammatory P1 receptors, the P2 receptors play a fundamental role in the inflammatory process. There are 15 members of this family divided into P2X and P2Y receptors (Boeynaems et al., 2005; Kügelgen, 2006).

The P2Y receptors are similar to the P1 family, G protein-coupled receptors. Their main agonists are adenine nucleotides (ATP, ADP) for P2Y1, P2Y11-13, pyrimidine nucleotides (P2Y4, P2Y6), ATP/uridine triphosphate (UTP) (P2Y2), and uridine diphosphate (UDP)-glucose for P2Y14 (Le Duc et al., 2017; K. A. Jacobson et al., 2015). There are two subgroups which are associated either with the G protein  $G_q$  (P2Y1, P2Y2, P2Y4, P2Y6, and P2Y11) or  $G_i$  (P2Y12, P2Y13, and P2Y14). These receptors are also found in various tissues, such as the central nervous system (neurons and glial cells) (Weisman et al., 2012) and are expressed on most immune cells. They function through phospholipase C (PLC) and inositol phosphate (IP), which leads to chemotaxis of granulocytes, maturation of dendritic cells, platelets aggregation and increase of intracellular calcium in macrophages (Le Duc et al., 2017). Their function in B and T cells is predominantly unknown.

In comparison to P1 and P2Y, the P2X receptors are ionotropic. There are seven known members of this family (P2X1-7) and they are formed out of three subunits. P2X channels can form either homo- or heteromers. Except for P2X6, every other subunit can form homotrimers. Described heteromers are P2X1/2, P2X2/3, P2X2/6, and P2X4/6 (Dal Ben et al., 2015). Every unit consists of an intracellular carboxy and amino terminus, two  $\alpha$  helical transmembrane domains (TM1 and TM2), which are connected via an extracellular loop and they are highly conserved (Duckwitz et al., 2006; Kawate et al., 2009). The extracellular loop contains the binding site of the ligand, which is ATP for all P2X receptors. For the

activation of P2X receptors, all three ATP binding sites must be occupied. In turn, the P2X channels undergo a conformational change (“gating”), which leads to an opening of the channel, allowing the efflux or influx of positively charged ions (efflux of potassium ions (K<sup>+</sup>) and influx of calcium ions (Ca<sup>2+</sup>)/sodium ions (Na<sup>+</sup>)). This cation exchange leads to a desensitization of the cell membrane, and prolonged activation can lead to an increase in the opening of the channel, which in turn allows bigger molecules to pass through the channel. The sensitivity to ATP varies among the different channels. It ranges from higher nanomolar to higher micromolar/lower millimolar ATP concentrations, with P2X7 being the least sensitive (Xing et al., 2016). Similar to the other purine receptors, P2X channels are expressed in almost every tissue. In hemopoietic cells, these receptors are responsible for e.g., the activation of T cells (T<sub>Reg</sub>), microglia, and platelets.

### 1.2.3 The P2X7 Receptor

#### *Structure*

P2X7 is one of the most thoroughly investigated P2X channels in the context of immunology. It has a length of 595 amino acids and a molecular weight between 75 and 85 kDa. The structure of a single subunit of the P2X7 receptor is often described as dolphin-shaped (see [Figure 1.3](#)). The structures of other P2X receptors (P2X3 and P2X4) were solved (Kawate et al., 2009; Hattori and Gouaux, 2012; Mansoor et al., 2016) and used to make predictions for the P2X7 receptor (Schwarz, Drouot, et al., 2012; Hattori and Gouaux, 2012; Kasuya et al., 2017). Recently the complete structure of P2X7 was published. As expected, the structure of P2X7 is similar to other P2X receptors, with the difference of a longer carboxy-terminal tail (200 amino acids longer than the other P2X members) and a cysteine-rich region (“cytoplasmic ballast”) (Allsopp and Evans, 2015). The lack of a resolved crystal structure of P2X7 receptor tail domain led to the assumption of an unstructured/unfolded tail. Crystallizations of C- and N-terminal truncated versions were performed (Karasawa and Kawate, 2016). Recently, McCarthy et al. could provide a defined structure of the intracellular domains of the P2X7 receptor (rat), showing that it forms a dinuclear zinc ion complex and a guanosine nucleotide-binding site (McCarthy, Yoshioka, and Mansoor, 2019). There are palmitoylation sites predicted in the cysteine-rich region, which could also be shown to be associated with lipid rafts. This post-translational modification, in turn, seems to be important for the localization of P2X7 in the cell membrane, as it plays a role in trafficking the channel to the cell membrane (Gonnord et al., 2009).

#### *Splice variants and SNPs*

There are many known splice variants and single nucleotide polymorphisms (SNPs) of the P2X7 receptor. There are five known splice variants in mice, named P2X7a /b/c/d/k. P2X7a is the common variant with 13 exons. P2X7k is the only splice variant besides P2X7a without a truncated C-terminal. The b and c variants show a lower channel activity and the d variant is the shortest. With a truncation of the N-terminal tail, P2X7k has a higher sensitivity and a

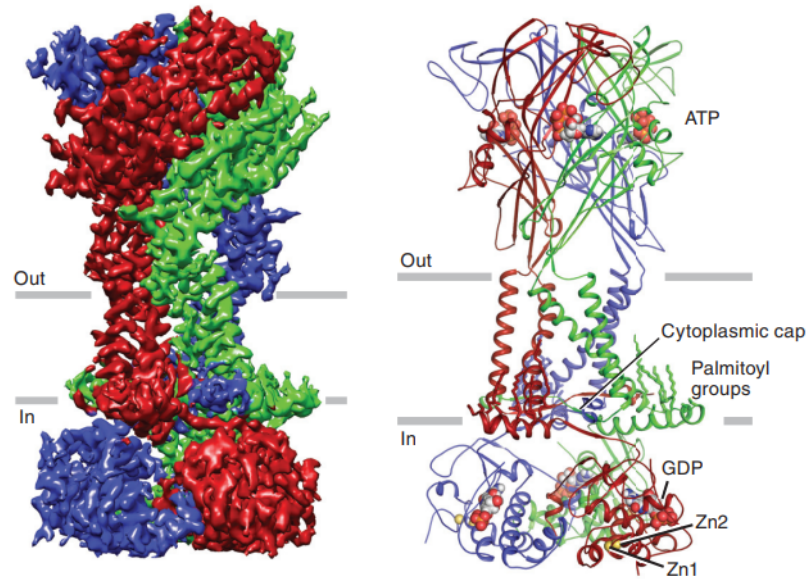


Figure 1.2: The Structure of the P2X7 Receptor

Shown is the P2X7 receptor, with extracellular and transmembrane domains, as well as the intracellular C- and N-termini for each subunit. The intracellular domains (cytoplasmic cap) contain a dinuclear zinc ion complex and a guanosine binding site, as well as a cysteine-rich region harboring palmitoylation sites (McCarthy, Yoshioka, and Mansoor, 2019).

faster kinetics in response to ATP compared to the other splice variants (Nicke et al., 2009). P2X7k is solely expressed in T cells, whereas P2X7a is mostly expressed in macrophages (Schwarz, Drouot, et al., 2012; X. J. Xu et al., 2012). The P2X7k splice variant has only been described for mouse P2X7.

Next to the splice variants, different SNPs are described in the literature. In humans, there are over 150 known SNPs (Di Virgilio, Dal Ben, et al., 2017), but only a few are characterized. Among them are loss and gain of function variants. However, the P2X7 receptor in mice is less polymorphic. One known SNP is the P451L. In C57BL/6 mice a point mutation in position 451, which is located in the domain of the C-terminal tail, results in an expression of leucine instead of proline. This mutation leads to a reduced sensitivity to ATP in C57BL/6 compared to BALB/c mice, which can, in part, be explained by a reduced expression level in T cells of C57BL/6 mice (Adriouch, Dox, et al., 2002; Schwarz, Fliegert, et al., 2009).

### Functions

The P2X7 receptor is the least sensitive receptor of the P2X family, requiring ATP concentrations within the high micromolar to low millimolar range for activation. Another possibility to activate P2X7 is by  $\text{NAD}^+$ -dependent ADP-ribosylation via the glycosylphosphatidylinositol (GPI) anchored ADP-ribosyltransferases (ARTs) (Adriouch, Haag, et al., 2012). ARTs can transfer the ADP-ribose moiety from  $\text{NAD}^+$  covalently to cell surface proteins. These enzymes are structurally similar to cholera toxin and are therefore classified as cholera toxin-like-ADP-ribosyltransferases (ARTCs) (Hottiger et al., 2010). In case of the P2X7 receptor,

ADP-ribose is transferred by two isoforms of ARTC2 to arginine at position 125, close to the ATP binding site, which leads to the permanent opening of the receptor. Isoform ARTC2.2 is commonly expressed on mouse T cells and activates P2X7 (Glowacki et al., 2002; Adriouch, Bannas, et al., 2008; Schwarz, Fliegert, et al., 2009), while ARTC2.1 is preferentially expressed in cells of the innate immune system such as macrophages (Hong et al., 2009). Humans do not express ARTC2 proteins, since in this species the single copy of the ancestral ARTC2 gene is disrupted by premature stop codons (Haag, Koch-Nolte, et al., 1994; B. Rissiek, Haag, et al., 2015a).

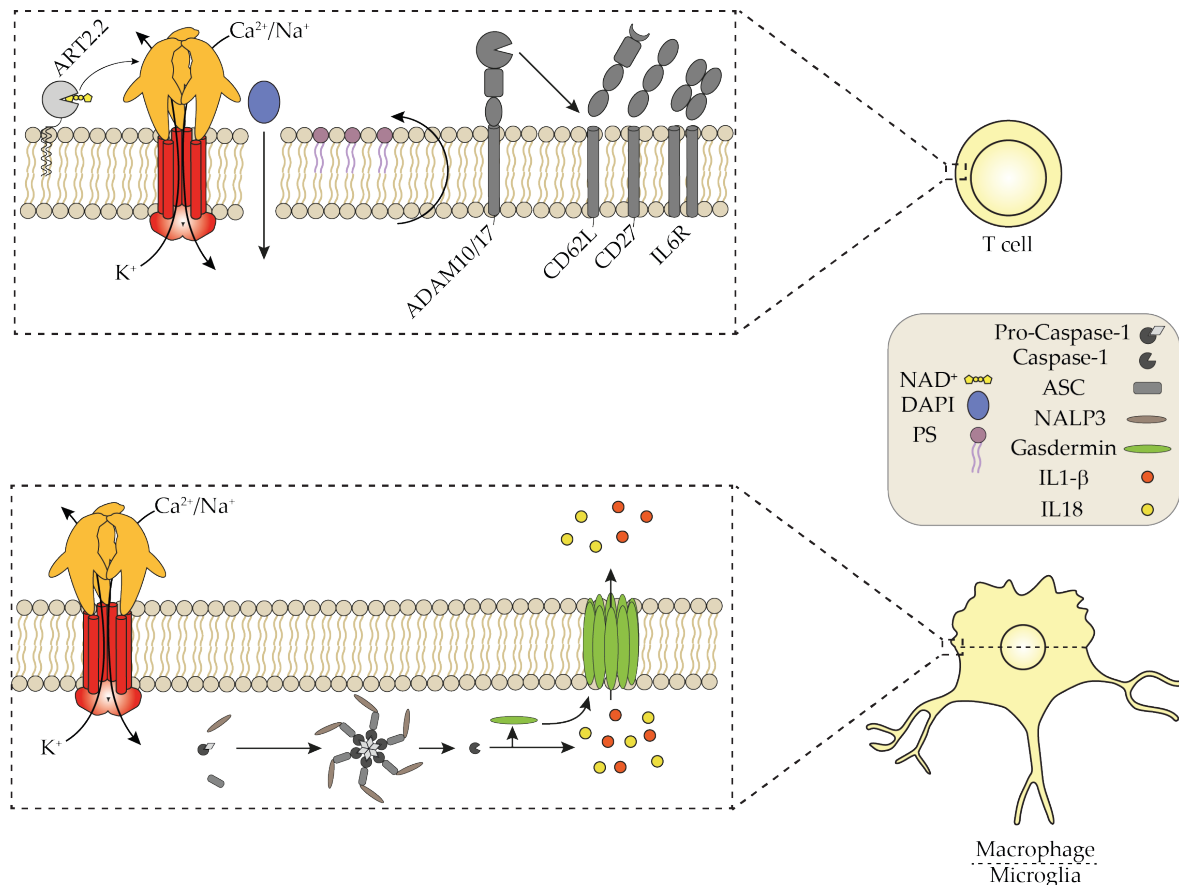


Figure 1.3: Functions of P2X7 in T cells, macrophages and microglia

On T cells, activation of P2X7 through extracellular ATP or via ADP-ribosylation leads to activation of the metalloproteases ADAM10 and 17, which in turn shed CD62L, CD27 and IL6R from the cell surface. Prolonged activation of P2X7 results in pore formation (passage of molecules up to 900 Da) in the cell membrane, phosphatidylserine (PS) exposure and ultimately cell death. In microglia and macrophages, activation of P2X7 via extracellular ATP leads to assembly of the NALP3 inflammasome, which consists of pro-caspase-1, ASC, and NALP3. Accordingly, caspase-1 is activated, cleaving gasdermin-D to its active form which allows the formation of a pore, which can lead to pyroptosis. Caspase-1 also cleaves and activates the pro-inflammatory cytokines IL-1 $\beta$  and IL-18, which are released into the extracellular space through the gasdermin pore.

Gating of P2X7 by either ATP or NAD<sup>+</sup>-dependent ADP-ribosylation leads to various downstream effects on the respective cell type, including changes in cell size and the membrane composition. A reduction of the cell volume leads to an externalization of PS to the outer leaflet of the cell membrane, which is a hallmark of apoptosis (Segawa and Nagata,

2015). If gating is caused by ATP, these effects can be reversed by degradation of ATP (CD39/CD73). Prolonged activation of P2X7 leads to blebbing and cell death, which can be shown by uptake of propidium iodide (PI) (Mackenzie et al., 2005; Roger, Pelegrin, and Surprenant, 2008) or 4,6-diamidino-2-phenylindole (DAPI). Cell death caused by P2X7 is impaired by the P451L mutation (Le Stunff et al., 2004). The dye uptake can be explained by the formation of a pore, which is another characteristic of P2X7 activation. This pore allows the passage of molecules up to a size of 900 Da. There are mainly two possible mechanisms discussed, which may cause this pore formation. On the one hand, P2X7 activates the dilation of pannexin-1 channels and on the other hand, the P2X7 receptor itself forms a pore, leading to a release of ATP. Furthermore, the C-terminus seems to be involved in the pore formation (Surprenant et al., 1996; Denlinger et al., 2003).

Truncated versions of panda P2X7 (without C- or N-termini) integrated into artificial liposomes show an uptake of dyes after gating via ATP, which seems solely dependent on the lipid composition of the used liposomes. In this study, sphingomyelin and phosphoglycerin caused the pore formation, whereas a higher amount of cholesterol in the liposomes seemed to inhibit this effect (Karasawa, Michalski, et al., 2017).

Since P2X7 is also widely expressed in hematopoietic cells, P2X7 is of great interest in the field of immunology. In T cells, the expression of P2X7 is dependent on their maturation and activation state. The expression level of P2X7 in CD4<sup>+</sup> or CD8<sup>+</sup> T cells is higher than in CD4<sup>+</sup>/8<sup>+</sup> double-positive cells (Haag, Freese, et al., 2002; Seman et al., 2003). Furthermore P2X7 expression is elevated in resting compared to activated T cells (Adriouch, Hubert, et al., 2007). Gating of P2X7 on T cells also leads to the activation of metalloproteases ADAM10 and ADAM17 (Garbers et al., 2011). These enzymes then cause a shedding of CD23 (Fcε-Rezeptor II), CD27, CD62L (L-selectin) and IL-6R (Garbers et al., 2011; Gu, Bendall, and Wiley, 1998; Moon et al., 2006). Interestingly, ARTC2.2 itself can be shed on activated T cells, which in turn protects T cells against the described downstream effects of P2X7 gating. Also, blocking ARTC2.2 via a nanobody (s+16) protects different T cell subtypes (e.g., Tregs) from ARTC2.2 mediated cell death during the preparation of organs from mice (Menzel et al., 2015; B. Rissiek, Lukowiak, et al., 2018).

Besides, in myeloid cells, P2X7 has an important role in inflammation, which will be further discussed in the following chapter.

#### 1.2.4 *Inflammation and P2X7*

Inflammation is an important mechanism against injuries and exogenous pathogens and facilitates a proper response for the organism. As already introduced, P2X7 on lymphocytes and macrophages plays a significant role in inflammation, which was investigated early on even before its gene was cloned (Di Virgilio, Bronte, et al., 1989; Surprenant et al., 1996). Gating of P2X7 in these cells is associated with the production and release of pro-inflammatory factors such as chemokines and cytokines. In macrophages, chemokines such as chemokine (C-C motif) ligand 3 (CCL3) or C-X-C motif chemokine 9 (CXCL9) are

produced and secreted after activation of P2X7 (Kataoka et al., 2009; Torre-Minguela et al., 2016). The primary role of P2X7 in inflammation is the activation of the inflammasome in microglia and macrophages. In these cells, the activation of P2X7, specifically the efflux of potassium, leads to assembly of the NACHT, LRR and PYD domains-containing protein 3 (NALP3) inflammasome. Consequently, caspase-1 is activated and cleaves the proIL-1 $\beta$  and proIL-18, leading to the release of the pro-inflammatory cytokines IL-1 $\beta$  and IL-18 through a gasdermin pore (Fig. 1.3) (Pelegrin, Barroso-Gutierrez, and Surprenant, 2008; Sakaki et al., 2013; Danquah et al., 2016). IL-1 $\beta$  is one of the major drivers of inflammation with a variety of effector functions on the innate and adaptive immune system. IL-1 $\beta$  acts on emergency hematopoiesis because it activates neutrophils and monocytes, and participates in B and T cell activation, Th17 differentiation. It can act synergistically with other cytokines (e.g., IL-23), as well as stimulating the production of interferon (INF) in innate lymphoid cells (ILC) e.g., natural killer cells (NK) (Mantovani et al., 2019; Proietti et al., 2014).

P2X7 also plays an important role in cancer, respectively in the tumor micro-environment. The tumor micro-environment is characterized by high levels of extracellular ATP compared to the basal level (see Section 1.2.5 “ATP release and metabolism”). Different studies have shown that the infiltration of e.g., DC and the growth of tumor cells are dependent on the expression of P2X7. Additionally, P2X7 is beneficial in immunogenic cell death (Hofman et al., 2015; Roger, Jelassi, et al., 2015)

How ATP, one of the major danger- or damage-associated molecular patterns (DAMPs) in the inflammation process, is released and metabolized will be discussed in more detail in the following chapter.

### 1.2.5 ATP release and metabolism

ATP is mainly produced through the respiratory chain in the mitochondria, which in turn is “fed” by metabolites of the glycolysis and fatty acid metabolism. Basal concentrations of intracellular ATP range from 1 mM to 10 mM (Forrester, 1972; Beis and Newsholme, 1975), whereas the extracellular concentration lies in the range of approximately 10 nM (Trautmann, 2009; Pellegatti, Raffaghello, et al., 2008; Milo et al., 2009). The ATP concentrations in the immediate vicinity of cell surfaces can be higher (pericellular cloud). To maintain this extracellular ATP halo, a continuous release is necessary (Campwala and Fountain, 2013). Next to the possible release of ATP through the P2X7 receptors and/or pannexin-1 hemichannels (Svobodova et al., 2018), there are other described pathways. These include injured and dying cells via necrosis and apoptosis, where ATP acts as a DAMP. Also, the vesicular release of ATP in monocytes and astrocytes was shown (Sivaramakrishnan et al., 2012; Z. Zhang et al., 2007). Additionally, other ATP release channels are described in the literature. These include the calcium homeostasis modulator 1 (CALHM1), volume-regulated anion channel (VRAC), and maxi-anion channel (Taruno et al., 2013; Gaitán-Peñas et al., 2016; Dutta et al., 2004).

The steep concentration gradient between extra- and intracellular ATP is regulated by ectoenzymes. These ectonucleotidases hydrolyze extracellular tri- and diphosphates (e.g., ATP

and ADP). Examples are the ecto-nucleoside triphosphate diphosphohydrolase (ENTPDase) CD39, the ecto-nucleoside pyrophosphatase/phosphodiesterase (E-NPP) CD203, and alkaline phosphatase gene families (Stefan, Jansen, and Bollen, 2005; Robson, Sévigny, and Zimmermann, 2006; Dwyer et al., 2007). CD39 belongs to the ENTPDase family and degrades ATP and ADP to AMP. It has two transmembrane domains at the C- and N-termini and a big extracellular loop. The extracellular loop consists of five conserved domains, the apyrase conserved regions. These regions are essential for the catalytic activity of the enzyme (Zimmermann, 1999). It is mainly expressed on endothelial cells and immune cells (e.g., dendritic cells, macrophages and Tregs).

The resulting product AMP can be further hydrolyzed to Ado by CD73, a 5'-ectonucleotidase. CD73 is a dimer where the C-terminus is covalently attached to the plasma membrane via a GPI anchor (Antonioli, Pacher, et al., 2013; Antonioli, Novitskiy, et al., 2017; Sträter, 2006). The AMP binding site is located in the C-terminal domain, and the N-terminal domain contains a binding site for two divalent metal ions,  $Zn^{2+}$  (zinc) and  $Co^{2+}$  (cobalt), that are important for the catalytic activity.

CD39 and CD73 are important regulators as they can change the proinflammatory activity, caused by ATP, to an immunosuppressive activity with Ado. One important example of this function is given by regulatory T cells (Tregs). In mouse Tregs CD39 and CD73 are highly upregulated (A. Rissiek et al., 2015). Activated Tregs can convert ATP that is released (for example, by cell damage) to Ado, which can act on A2A receptors on T effector cells to suppress the inflammatory activity (Vignali, Collison, and Workman, 2008; B. Rissiek, Haag, et al., 2015b).

### 1.3 ATP MEASUREMENT AND SENSORS

ATP is an important signaling molecule in inflammation and a good indicator for apoptosis, cytotoxicity, cell proliferation or bacterial contamination. To be able to measure and quantify the changes of intracellular ATP (iATP) and extracellular ATP (eATP) is thereby of utmost importance. Different approaches were developed in the last decades to solve this problem. A widely used approach is to use the luciferase/luciferin system (DeLuca and McElroy, 1974). Luciferase originates from different insects such as the *Lampyridae* family, commonly known as fireflies. The luciferase enzyme produces light in the presence of its substrate luciferin, as well as ATP and magnesium ions ( $Mg^{2+}$ ). Introduced in an organism with a gene of interest, it can act as a reporter gene (Ignowski and Schaffer, 2004). This system can also be used to measure the concentration of extracellular ATP in solutions (e.g., cell supernatants) in luminometers, for example plate readers. The advantage of this method is the high selectivity for ATP compared to other purine nucleotides such as UDP or UTP, AMP, or ADP. Furthermore, the method has a fast reaction time (in the range of milliseconds), a wide linear range, and a high sensitivity detection limit between  $10^{-18}$  –  $10^{-10}$  M because of its high signal-to-noise ratio (Wang, Haydon, and Yeung, 2000). Downsides of this method include inhibition through high salt concentration and anions e.g.  $I^-$  (Denburg and McElroy, 1970). Another problem is that bulk measurements of extracellular ATP do not reflect the

actual ATP concentrations around the cell. If luciferase is attached to the cell membrane via a membrane anchor, ATP concentrations are more accurate but used in a microscope system; it still lacks the time-spatial resolution (Praetorius and Leipziger, 2009).

The indirect measurement of ATP is also another alternative. In the case of the P2X receptors, the activation via ATP causes an influx of  $\text{Ca}^{2+}$ . The use of calcium dyes (e.g. Fluo-4, FuraRed or the ratiometric dye Fura-2) to measure the cytosolic calcium concentration can thus be used to detect relevant changes in the extracellular ATP concentration that are sufficient to activate P2X receptors.

### 1.3.1 Genetically encoded ATP sensors

In recent years different genetically encoded ATP sensors have been developed. Among them are Förster resonance energy transfer (FRET)-based sensors such as ATeam (Imamura et al., 2009), and ratiometric sensors such as QUEEN (Yaginuma et al., 2014). Given that ATP FRET sensors were used as a major tool in this study, the theoretical background of the FRET effect will be described and its application in biology.

#### *Förster Resonance Energy Transfer (FRET)*

The Förster Resonance Energy Transfer (FRET) was first described by Theodor Förster in 1948 (Förster, 1948). The effect describes the nonradiative energy (dipole-dipole coupling) transfer from an excited donor to an acceptor fluorophore in its proximity which in turn emits energy in the form of fluorescence of a specific wavelength (Shrestha et al., 2015; Bajar et al., 2016).

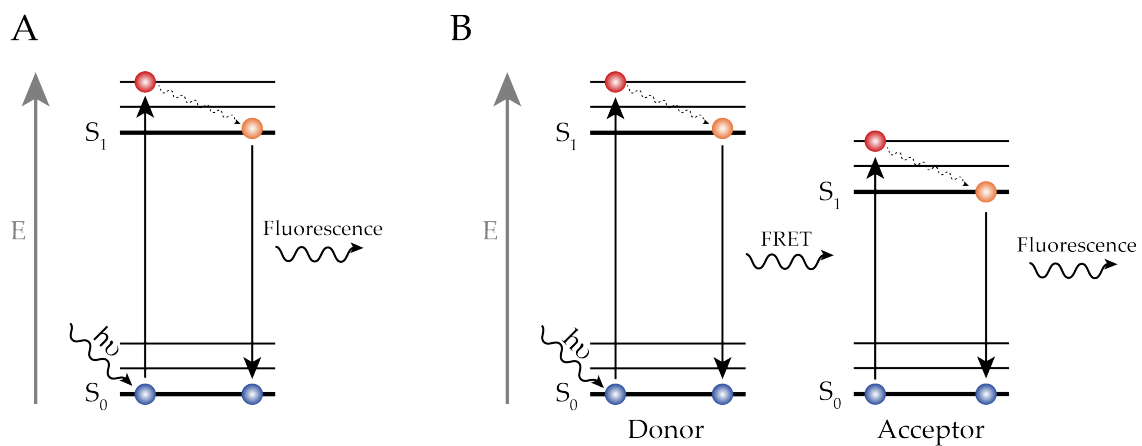


Figure 1.4: Fluorescence and FRET principle

**A** Shown is a Jablonski diagram and the absorption of energy in form of light by an electron which leads to energy increase and to the excited state  $S_1$ . After relaxation light is emitted at a lower wavelength, and the electron goes back to the ground state  $S_0$ . This mechanism is called fluorescence. In **B** the same principle is shown, but in this case there is a donor and an acceptor molecule. The emitted light of the donor is absorbed (FRET) by the acceptor, which leads to an emission of light from the acceptor.

Fluorescence and FRET process can be described in a Jablonski diagram (Figure 1.4), named after the polish physicist Aleksander Jabłoński (Jablonski, 1933). A fluorescent donor

molecule at the energy ground state  $S_0$  absorbs energy in form of light which brings the molecule into an excited state  $S_1$ . As the excited state is unstable, the molecule returns to the ground state  $S_0$  via vibrational relaxation by emitting light. This light is then absorbed by an acceptor fluorophore, which releases light after vibrational relaxation. This mechanism is only possible if the emission wavelength of the donor and the absorbance wavelength of the acceptor have a spectral overlap, and both molecules are in close proximity to each other (1 – 10 nm). The energy transfer  $E$  is dependent on the distance between donor and acceptor molecule and is described by the formula [Equation 1.1](#).

$$E(r) = \frac{1}{1 + \left(\frac{r}{r_0}\right)^6} \quad (1.1)$$

“ $r$ ” represents the distance between donor and acceptor, and “ $r_0$ ” is the distance between donor and acceptor where the probability of energy transfer (FRET) is 50%. Apart from the distance, the orientation  $\kappa$  between donor and acceptor is crucial for the FRET efficiency. In [Equation 1.1](#) the dependency of  $r_0$  on  $\kappa$  is shown.

$$r_0 = 0.02108 [\kappa^2 \times \Phi_D \times n^{-4} \times J]^{\frac{1}{6}} \text{ nm} \quad (1.2)$$

where “ $\Phi_D$ ” is the quantum yield of the donor in absence of the acceptor, “ $n$ ” is the refraction factor of the medium and “ $J$ ” is the overlap of donor emission and acceptor absorption.

Because FRET is highly dependent on the distance between donor and acceptor at  $\leq 10$  nm this system has a high sensitivity to measure protein-protein interactions *in vitro* and *in vivo*. An example of this approach would be to determine the interaction of an enzyme of interest with a possible interaction partner *in vitro* by co-expressing both molecules linked to fluorescent proteins capable of a FRET interaction (Margineanu et al., 2016; Schneckenburger et al., 2019). Apart from measuring protein-protein interactions, FRET biosensors are used. These sensors consist of a binding domain for a molecule of interest and two fluorescent proteins or molecules that can interact via FRET. The binding domain changes its conformation after it gets in contact with a ligand which, depending on the system, increases or reduces the distance between the two fluorescent proteins and thus the resulting signal. Suitable fluorescent proteins have been engineered and devolved from already existing fluorescent proteins, e.g. the green fluorescent protein (GFP), in the last decades. Some examples of FRET pairs are enhanced blue fluorescent protein (EBFP)/enhanced cyan fluorescent protein (ECFP) (Patterson, Piston, and Barisas, 2000), ECFP/Venus (Rizzo et al., 2006), or Clover/mRuby (Lam et al., 2012).

#### *FRET-based ATP sensors*

Until recently, there was no method to measure ATP concentrations or changes in ATP levels in live single cells. In 2009 the first ATP FRET sensor ATeam (Adenosine 5'-Triphosphate indicator based on Epsilon subunit for Analytical Measurements) was developed (Imamura

et al., 2009), which allows specific temporal and spatial measurement of ATP levels. As a FRET pair, they used monomeric super-enhanced CFP (mseCFP) and circularly permuted monomeric cp173-mVenus. mseCFP is a variant of the cyan fluorescent protein (CFP) where several amino acids were mutated to increase the brightness (T. Matsuda, Miyawaki, and Nagai, 2008). cp173-mVenus is a variant of the yellow fluorescent protein (YFP) that is more stable against changes in the pH (Nagai, Ibata, et al., 2002) and has a higher dynamic range gained through circular permutations than the latter (Nagai, Yamada, et al., 2004). The binding domain that connects the two fluorescent proteins is the  $\epsilon$  subunit of the  $F_0F_1$ -ATP synthase. This 14 kDa binding domain has an N-terminal  $\beta$  barrel domain and two  $\alpha$  helices at the C-terminal.

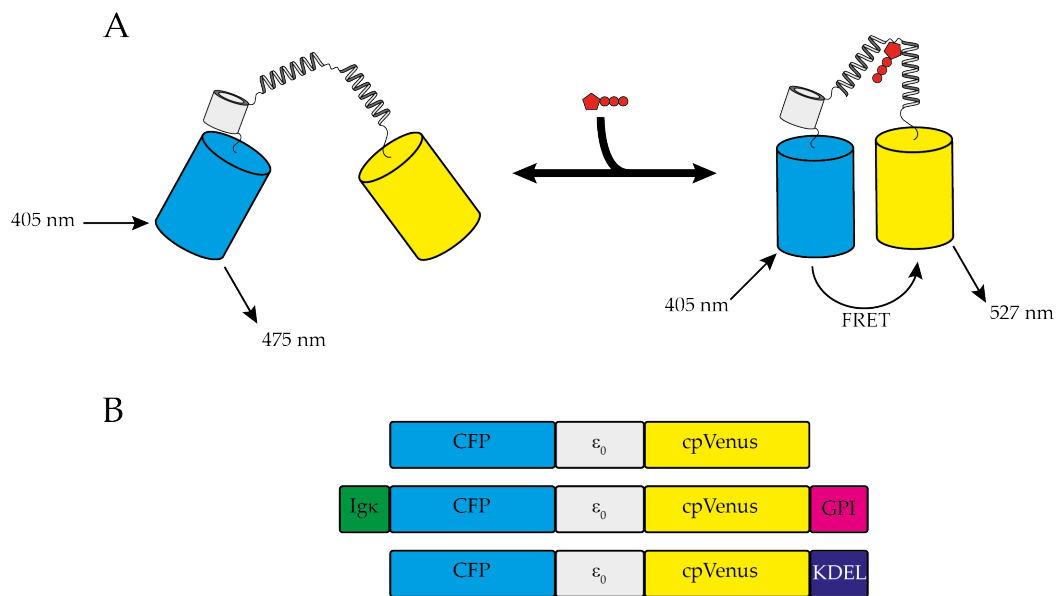


Figure 1.5: FRET ATP sensor ATeam

**A** Shown is a schematic view of the ATeam sensor (Imamura et al., 2009), which is based on the sensor used in this study. The FRET sensor consists of a CFP (blue) and a Venus (yellow) fluorescent protein that are connected by the  $\epsilon$  subunit of the  $F_0F_1$ -ATP synthase (grey). Upon binding of ATP to this subunit, a conformational change follows, which brings both fluorescent proteins close enough to each other so that the FRET effect can occur. The binding of ATP is reversible, and ATP is not hydrolyzed. **B** Shown are from top to down, schematic drawings of the cytosolic, membrane-bound (Ig $\kappa$  leader sequence and GPI anchor) and ER targeted (KDEL targeting sequence) ATP FRET sensor. In blue and yellow are the sequences of the CFP and YFP protein, respectively.  $\epsilon_0$  is the  $\epsilon$  subunit of the  $F_0F_1$ -ATP synthase. This can come from different *Bacillus* species with different affinities for ATP, e.g. Bs (lower mM range), PS3 (lower  $\mu$ M range) and RRKK (non-functional) variant (see text for details).

The binding site of ATP is located between these  $\alpha$  helices. Upon binding of ATP to the  $\alpha$  helices the binding domain undergoes a conformational change (Iino et al., 2005), which brings the fluorescent proteins into close proximity to each other, so that FRET occurs (Figure 1.5). The subunit is highly specific for ATP compared to other nucleotides (e.g., ADP, GTP, or UTP) and binds it reversibly (Kato-Yamada and Yoshida, 2003; Imamura et al., 2009).

The FRET-based ATP sensor used in this thesis is based on the above-described ATeam sensor. Similar to the work of Imamura et al., the binding domains of different bacterial

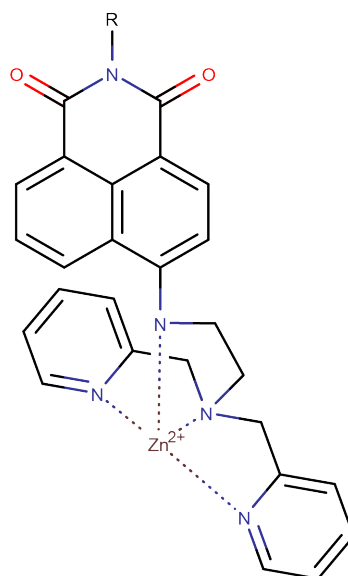


Figure 1.6: Small molecule ATP Sensor Zn-DPA

Shown is a Zn(II)-complexed dipicolylamine sensor coupled with a naphthalimide group for sensing ATP synthesized by Moro, Cywinski, et al. Upon binding of a ligand (e.g. ATP) there is an increase in the fluorescent intensity. The “R” on the naphthalimide group indicates a moiety for possible addition of different groups, such as azide, alkyne and maleimide.

strains were used. The subunit of *Bacillus* strain PS3 (abbrev. PS3) has an ATP sensitivity in the low micromolar range and is therefore suitable for measuring extracellular ATP. For intracellular measurement the binding domain of *Bacillus subtilis* (Bs) was used with an ATP sensitivity in the low millimolar range. As a control, two point mutations (arginine to lysine) were introduced into the binding domain to gain a nonfunctional sensor. For membrane expression of the sensors a GPI anchor and an I $\kappa$  leader sequence were introduced C- and N- terminally introduced, respectively. For expression in the endoplasmic reticulum (ER), a KDEL (Lysine, Aspartic acid, Glutamic acid, Leucine) targeting sequence was introduced at the C-terminus.

### 1.3.2 Small molecule ATP sensors

Apart from FRET-based ATP sensors, small molecule ATP sensors were also used in this study (Figure 1.6). These sensors were synthesized and provided by Alexander Laubach from the Department of Chemistry (University of Hamburg). The basis of these sensors is a Zn(II)-complexed dipicolylamine (DPA) receptor with a naphthalimide chromophore (referred to as Zn-DPA) (Moro, Cywinski, et al., 2010). This sensor is excited at a wavelength of 450 nm and emits light at 535 nm (maximum values), whereby the Zn(II) group is the fluorescent part of the molecule. This property could be shown in other publications e.g., using the Zn(II) labeling of cell organelles (Ojida, Takashima, et al., 2008; Ledderose, Bao, Lidicky, et al., 2014). Upon binding of a ligand, the fluorescence intensity increases in a dose-dependent manner, with a maximum of 100  $\mu$ M ATP (Ledderose, Bao, J. Zhang, et al., 2015). Other nucleotides such as GTP and pyrophosphate (PPi) show minor changes in

fluorescence intensity, but with ADP the sensor shows a similar sensitivity compared to ATP.

Additionally, the dipicolylamine of Zn-DPA allows the addition of functional groups, for example to label silica nano beads (Moro, Schmidt, et al., 2011) or cell membranes.

#### 1.4 AIM OF THIS WORK

ATP is the main carrier of energy in cells and has an important role as a signaling molecule in cells generally and in inflammation especially. The processes whereby ATP is released into the extracellular space are still not fully understood. P2X7 itself seems to be directly involved in the release of ATP.

The goals of this thesis were:

- to visualize extra- and intracellular ATP concentration in single cells using FRET-based sensors
- to use FRET-based ATP sensors to visualize ATP release in a physiological situation, e.g. through gating of P2X7 via  $\text{NAD}^+$  / ATP
- to specifically target small molecular ATP sensors to the cell membrane using nanobodies
- to evaluate the utility of small molecular ATP sensors for the measurement of extracellular ATP concentrations
- to establish an easy system for the measurement of bulk ATP concentrations using small molecular ATP sensors

# 2 | MATERIAL AND METHODS

## 2.1 MATERIALS

### 2.1.1 *Antibodies/nanobodies*

Table 2.1: Antibodies/nanobodies used for FACS and microscopy

ANTIGEN	CLONE	HOST	ISOTYPE	LABEL	MANUFACTURER
ART2.2	s-14	llama	VHH	unconjugated	Nolte Lab, UKE
ART2.2	s+16	llama	VHH	unconjugated	Nolte Lab, UKE
ART2.2	R8A9	rat	IgG2a	AF647	Nolte Lab, UKE
ART2.2	R8A106	rat	IgG2a	AF647	Nolte Lab, UKE
ART2.2	R8A9	rat	IgG2a	unconjugated	Nolte Lab, UKE
ART2.2	R8A106	rat	IgG2a	unconjugated	Nolte Lab, UKE
CD3	OKT3	mouse	IgG2a, $\kappa$	biotin	BioLegend
CD3	OKT3	mouse	IgG2a, $\kappa$	unconjugated	BioLegend
CD3epsilon	145-2C11	hamster	IgG1, $\kappa$	APC	BioLegend
CD4	RM4-5	rat	IgG2a	PE	BioLegend
CD4	RM4-5	rat	IgG2a, $\kappa$	APC	BioLegend
CD62L	MEL-14	rat	IgG2a, $\kappa$	AF647	eBioscience
GFP	7.1; 13.1	mouse	IgG1, $\kappa$	unconjugated	Roche
IgG(H+L)		goat		AF633	Invitrogen
IgG(H+L)		rabbit		HRP	Invitrogen
IgG(H+L)		goat		AF647	Invitrogen
P2X7	13A7	llama	VHH	unconjugated	Nolte Lab, UKE
P2X7	1c81	llama	VHH	unconjugated	Nolte Lab, UKE
P2X7	RH23A44	rat		AF647	Nolte Lab, UKE
P2X7	14D5	llama	VHH	unconjugated	Nolte Lab, UKE
P2X7	RH23A44	rat		AF488	Nolte Lab, UKE
P2X7	RH23A44	rat		PE	Nolte Lab, UKE

2.1.2 *Bacterial strains*

Table 2.2: Bacterial strains

NAME	TYPE	MANUFACTURER
<i>E.coli</i> BL21(DE3)pLysS	competent cells	Novagen
<i>E.coli</i> XL10-Gold <sup>®</sup>	competent cells	Stratagene
<i>E.coli</i> XL.1 blue	competent cells	Stratagene

2.1.3 *Buffers and solutions*

Table 2.3: Buffers and solutions

NAME	COMPOSITION
DMEM complete	500 mL DMEM (1x) 10 % (v/v) FCS 10 % (v/v) sodium pyruvate (100 mM) 1 % (v/v) L-glutamine (200 mM) 1 % (v/v) HEPES (1 M) 1 % (v/v) MEM non-essential amino acids
ECS <sup>-/-</sup>	15 mM HEPES 140 mM sodium chloride 5 mM potassium chloride 10 mM D(+)-glucose 0.1 % (m/v) BSA diH <sub>2</sub> O, pH 7.4
ECS <sup>+/-</sup>	ECS <sup>-/-</sup> 1 mM CaCl <sub>2</sub>
ECS <sup>+/+</sup>	ECS <sup>-/-</sup> 1 mM CaCl <sub>2</sub> 1 mM MgCl <sub>2</sub>
F17 transfection media	Gibco F17 4 mM L-glutamin 0.1 % (v/v) Pluronic

NAME	COMPOSITION
F17 complete	F17 transfection media 1 % (v/v) FCS 0.5 % (v/v) G418
F17 feeding media	F17 transfection media 20 % (m/v) trypton
Freezing Medium	75 % (v/v) FCS 15 % (v/v) DMEM or RPMI complete Medium 10 % (v/v) <b>DMSO!</b>
Maleimide Labeling Buffer (MLB)	100 mM potassium phosphate 150 mM sodium chloride 250 mM sucrose diH <sub>2</sub> O, pH 7.5
LB agar	40 g/L LB agar diH <sub>2</sub> O
LB broth	25 g/L diH <sub>2</sub> O
Lysing Buffer	5 mL BugBuster 50 µL AEBSF (100 mM) 0.5 µL Benzonase
RPMI complete	500 mL RPMI 10 % (v/v) FCS 1 % (v/v) sodium pyruvate (100 mM) 1 % (v/v) L-glutamine (200 mM)
SOC medium	0.5 % (m/v) yeast extract 2.0 % (m/v) trypton 10 mM NaCl 2.5 mM KCl 10 mM Ca <sub>2</sub> 10 mM MgSO <sub>4</sub> 20 mM D(+)-glucose diH <sub>2</sub> O

NAME	COMPOSITION
TBS Buffer	137 mM NaCl 2.7 mM KCl 25 mM TRIS diH <sub>2</sub> O, pH7.6

#### 2.1.4 Cell lines

Table 2.4: Cell lines

CELL LINE	CELL TYPE	ORIGIN	GROWTH
3T3	mouse fibroblasts	Nolte lab, UKE	adherent cells
4T1	mouse breast cancer cells	Loges lab, UKE	adherent cells
4T1 P2X7kp	mouse breast cancer cells, transfected with mouse P2X7, (k) splice variant	Haag lab, UKE	adherent cells
CHO	chinese hamster ovary cells	Nolte lab, UKE	adherent cells
DC27.10	mouse T cell lymphoma	Nolte lab, UKE	suspension cells
DC27.10 NOD	mouse T cell lymphoma	Nolte lab, UKE	suspension cells
DO11.10	mouse T cell lymphoma	Nolte lab, UKE	suspension cells
HEK-T	human embryonic kidney cells, transfected with SV40 T antigen	Nolte lab, UKE	adherent cells
HEK293 6E	human embryonic kidney cells, transfected with Epstein-Barr virus nuclear antigen	Nolte lab, UKE	adherent cells
Jurkat (JMP)	human T cell lymphoma	Guse lab, UKE	suspension cells
Yac-1	mouse T cell lymphoma	Habers lab, HPI	suspension cells

## 2.1.5 Chemicals and reagents

Table 2.5: Chemicals and reagents

CHEMICAL	MANUFACTURER	NUMBER
2x YT medium	Sigma-Aldrich	Y2377-250G
2-Mercaptoethanol	Gibco	31350010
Adenosin monophosphat (AMP)	Sigma-Aldrich	01930-5G
Adenosin triphosphate (ATP)	Sigma-Aldrich	A2383-1G
Adenosine diphosphate (ADP)	Sigma-Aldrich	A2754-1G
AEBSF	Sigma-Aldrich	532586
AF647 Maleimide	Jena Bioscience	APC-009-1
Antarctic Phosphatase Reaction Buffer, 10x	New England Biolabs	B0289S
Aqua ad	Braun	0082479E
Azide-PEG3-Biotin Conjugate	Jena Bioscience	CLK-AZ104P4-25
Blasticidin, 100 mg/mL	InvivoGen	ant-bl-1
Bovine Serum Albumin (BSA)	Sigma-Aldrich	9048-46-8
Bugbuster, 10x	Merck	70921
Calcium chloride (CaCl <sub>2</sub> )	Carl Roth	A119.1
Carbenicillin, 100 mg/mL	Carl Roth	6344.2
Carbonyl cyanide m-chlorophenyl hydrazone (CCCP)	Sigma-Aldrich	C2759
Centrifugal Filters, Amicon Ultra 30 kDa	Merck	UFC8033024
Chemical	Manufacturer	Number
CL-Xposure™ Film	Thermo Scientific	34089
Copper(II) sulfate (CuSO <sub>4</sub> )	Jena Bioscience	CLK-MI004-50.1
Cut Smart Buffer, 10x	New England Biolabs	B7204S
D-(+)-Glucose	Sigma-Aldrich	G8270-1KG
DAPI	Sigma-Aldrich	D9542-1MG
DBCO Maleimide	Jena Bioscience	CLK-A108-25
DBCO-PEG4-Biotin Conjugate	Jena Bioscience	CLK-A105P4-10.1
Dimethyl sulfoxide (DMSO)	Sigma-Aldrich	D2650-100ML
DMEM medium	Gibco	41965-039
DMEM, GlutaMAX medium	Gibco	10566016

CHEMICAL	MANUFACTURER	NUMBER
Drying-Solution	Invitrogen	LC4025-4
Ethanol	Carl Roth	K928.4
Ethanol, 99.8 %	Carl Roth	K928.4
FACS Lysing Solution	Becon Dickinson	349202
Fetal calf serum (FCS)	Gibco	16250078
Fluo-4 AM	Invitrogen	F14201
Fura-2 AM	Invitrogen	F1201
FuraRed AM	Invitrogen	F3021
Gel Loading Dye purple, 6x	New England Biolabs	B7024S
GeneRuler, 100 bp	Thermo Scientific	SM0243
GeneRuler, 1 kb	Thermo Scientific	SM0314
Geneticin, 50 mg/mL	Gibco	10131-019
Gentamicin, 50 mg/mL	Gibco	15750-045
HEPES, 1 M	Gibco	15630080
Hydrochloric acid (HCl), 30 %	VWR	28.226.293
Igepal	Sigma-Aldrich	I3021-100ML
Ionomycin	Invitrogen	I24222
IPTG	Roche	10724815001
jetPEI	Polyplus-transfection	101-40N
Kanamycin	Carl Roth	T832.2
LB Agar	Carl Roth	X969.2
LB Broth	Carl Roth	X968.2
LE Agarose	Biozym	652324
L-Glutamin, 200 mM	Gibco	25030081
Lysotracker Red	Invitrogen	L7528
Magnesium chloride (MgCl <sub>2</sub> )	Merck	7791-18-6
MEM NEAA, 100x	Gibco	11140-035
Methanol	Carl Roth	0082.3
Milk powder	Carl Roth	T145.2
Mitotracker Red CMXRos	Invitrogen	M7512
Mounting Medium, Vectashield H-1200	Vector Laboratories	H-1200-10
Mounting Medium, Vectashield H-1200	Vector Laboratories	H-1000-10

CHEMICAL	MANUFACTURER	NUMBER
Na-Ascorbate - click chemistry grade	Jena Bioscience	CLK-MI005-1G
N-Methyl-D-glucamine	Sigma-Aldrich	M2004-100G
Non essential amino acids, 10 mM	Gibco	1140-035
NuPAGE Antioxidant	Invitrogen	NP0005
NuPAGE MES SDS Running Buffer, 20x	Invitrogen	NP0002
NuPAGE Sample Reducing Agent, 10x	Invitrogen	NP0009
NuPage Transfere Buffer, 20x	Invitrogen	NP0006
Penicillin, 10000 U/mL	Gibco	15140122
Phosphate buffered saline (PBS <sup>-/-</sup> )	Gibco	14190-094
Phosphate buffered saline (PBS <sup>+/+</sup> ), with CaCl <sub>2</sub> /MgCl <sub>2</sub>	Gibco	14040-091
Platinum Blue PCR SuperMix	Invitrogen	12580-015
Pluronic	Gibco	24040032
Polyethylenimin (PEI), MW25000	Polysciences	23966-1
Poly-L-lysine 30 - 70 kDa , lyophilized	Sigma-Aldrich	P7280-5MG
Potassium chloride (KCl)	Merck	1.04936.1000
Propidium iodide	Sigma-Aldrich	537059
Puromycin, 10 mg/mL	InvivoGen	ant-pr-1
Roti-Safe Gel Stain	Carl Roth	3865.1
RPMI medium 1640	Gibco	21875-034
Sodium chloride (NaCl)	Carl Roth	P029.2
Sodium chloride (NaCl), 0.9 %	Braun	817403
Sodium hydroxide (NaOH), 30 %	VWR	28.226.293
Sodium pyruvate, 100 mM	Gibco	11360-039
Sulphuric acid, 1 N	Carl Roth	K027.1
Supermarker	Nolte lab, UKE	
Streptomycin, 10 mg/mL	Gibco	15140122
T4 DNA Ligase Buffer, 10x	New England Biolabs	B0202A
TAE, 50x	Invitrogen	24710030
Thapsigargin	Calbiochem	586005
Thapsigargin	Invitrogen	T7459

CHEMICAL	MANUFACTURER	NUMBER
Tris-HCl	Carl Roth	9090.3
Triton X-100	Serva	37240.01
Trypan blue	Carl Roth	1680.1
Trypsin-EDTA, 0.5 % (10x)	Gibco	15400054
Zeocin	Invitrogen	45-0430
$\beta$ -Nicotinamide adenine dinucleotide sodium salt (NAD <sup>+</sup> )	Sigma-Aldrich	N0632-1G

### 2.1.6 Consumables

Table 2.6: Consumables

DEVICES	MANUFACTURER	NUMBER
$\mu$ -Slide 8 well glass bottom	ibidi GmbH	80827
$\mu$ -Slide 8 well ibiTreat	ibidi GmbH	80826
6-well plate	Thermo Scientific	140675
12-well plate	Thermo Scientific	150628
24-well plate	Thermo Scientific	142475
96-well plate, flat	Thermo Scientific	167008
96-well plate, Maxisorp	Thermo Scientific	442404
96-well plate, round	Thermo Sientific	163320
96-well plate, v	Greiner bio-one	651161
96-well strip-plate, straptavidin	PolyAn	00681251
Amicon Ultra, 3 kDa cutoff	Sigma-Aldrich	UFC800324
Cell Strainer, 70 $\mu$ m	Falcon	352350
CellTrics, 30 $\mu$ m filter	Sysmex	04-004-2326
Cryo-tube, 1.8 mL	Thermo Scientific	375418PK
Dynabeads M-280 Streptavidin	invitrogen	11205D
Electroporation cuvette, 4 mm	Biozym	748040
Inoculation loop	Greiner bio-one	731170
MultiFlex Round tips, 200 $\mu$ L	Biozym	728204
NuPage 10 % Bis-Tris-Gel	invitrogen	NP0302BOX
Petri dish, 10 cm	Greiner bio-one	633180

DEVICES	MANUFACTURER	NUMBER
Petri dish, 15 cm	Greiner bio-one	639102
Pipette tips, 10 $\mu$ L	Sartstedt	70.1130.600
Pipette tips, 10 $\mu$ L, dualfilter	Eppendorf	022491211
Pipette tips, 100 $\mu$ L	Sartstedt	70.760.412
Pipette tips, 1000 $\mu$ L	Sartstedt	70.760.100
Pipette tips, 1000 $\mu$ L, dualfilter	Eppendorf	022491253
Pipette tips, 200 $\mu$ L	Sartstedt	70.760.002
Pipette tips, 200 $\mu$ L, dualfilter	Eppendorf	022491296
Pipette tips, 300 $\mu$ L, dualfilter	Eppendorf	022491245
PMMA Microparticles, Azid, 9 $\mu$ m	PolyAn	10835009
PMMA Microparticles, green, 9 $\mu$ m	PolyAn	10560009
PMMA Microparticles, Straptavidin, 5 $\mu$ m	PolyAn	10521005
PMMA Microparticles, Straptavidin, 9 $\mu$ m	PolyAn	10521009
Repeat dispenser Tips, 0.5 mL	Eppendorf	0030089421
Repeat dispenser Tips, 1 mL	Eppendorf	0030089430
Repeat dispenser Tips, 2.5 mL	Eppendorf	0030089448
Repeat dispenser Tips, 5 mL	Eppendorf	0030089456
Repeat dispenser Tips, 25 mL	Eppendorf	0030089839
Serological pipette, 1 mL	Sartstedt	86.1251.025
Serological pipette, 10 mL	Sartstedt	86.1254.025
Serological pipette, 2 mL	Sartstedt	86.1252.025
Serological pipette, 25 mL	Falcon	356525
Serological pipette 5 mL	Sartstedt	86.1253.025
Stericup, 150 mL	Millipore	S2GPU01RE
Stericup, 500 mL	Millipore	S2GPU05RE
Steriflip, 50 mL	Millipore	SCGP00525
T225 flask	Thermo Sientific	159933
T25 flask	Thermo Sientific	156340
T75 flask	Thermo Sientific	156472
Tube, 0.2 mL	Sarstedt	72.737.002
Tube, 0.5 mL	Sarstedt	72.704.200
Tube, 1.5 mL	Sarstedt	72.706.200
Tube, 1.5 mL SafeSeal, brown	Sarstedt	72.706.200
Tube, 12 mL	Greiner bio-one	163160

DEVICES	MANUFACTURER	NUMBER
Tube, 13 mL	Sarstedt	62.515.006
Tube, 5 mL	Greiner bio-one	188271
Tube, 2 mL	Sarstedt	72.695.200
Tube, 5 mL	Falcon	352052
Tube, 50 mL	Greiner bio-one	227261

### 2.1.7 Enzymes

Table 2.7: Used enzymes

NAME	MANUFACTURER	NUMBER
Antarctic Phosphatase	New England Biolabs	M0289S
Apyrase	Sigma-Aldrich	A6535-200UN
BamHI	New England Biolabs	R0136S
CD73	R&D Systems	5795-EN
EcoRI-HF	New England Biolabs	R3101S
HindIII	New England Biolabs	R0104S
HindIII-HF	New England Biolabs	R3104S
NcoI	New England Biolabs	R0193S
NotI-HF	New England Biolabs	R3189S
PacI	New England Biolabs	R0547S
ScaI-HF	New England Biolabs	R3122S
StuI	New England Biolabs	R0187S
T4 DNA Ligase	New England Biolabs	M0202L
XbaI	New England Biolabs	R0145S
XhoI	New England Biolabs	R0146S

## 2.1.8 Kits

Table 2.8: Kits

NAME	MANUFACTURER	NUMBER
BCA Protein Assay Kit	Life Technologies	23225
CellTiter-Glo Luminescent Cell Viability Assay	Promega	G7570
Colloidal Blue Stain Kit	Invitrogen	LC6025
EasySep Mouse CD4 <sup>+</sup> T cell Isolation Kit	Stemcell	19852
EasySepMouse CD4 <sup>+</sup> CD25 <sup>+</sup> Regulatory T Cell Isolation Kit	Stemcell	18783
Nucelospin gel and PCR clean-up	Macherey-Nagel	750.609.250
Pierce LDH Cytotoxicity	Thermo Scientific	88953
Plasmid Maxi Kit	Qiagen	12362
Plasmid Mini Kit	Qiagen	27149

## 2.1.9 Laboratory equipment

Table 2.9: Laboratory equipment

NAME	MANUFACTURER
Analytical balance, 1412	Sartorius AG
Balance, Scout Pro	Ohaus
Biological Safety Cabinet, Herasafe KS12	Thermo Scientific
Centrifuge, 5417R	Eppendorf AG
Centrifuge, Galaxy Mini	VWR
Centrifuge, Heraeus Pico 17	Thermo Scientific
Centrifuge, Mikro 20	Hettich GmbH
Centrifuge, Rotanta 460R	Hettich GmbH
Centrifuge, Sorvall RC-26+	DuPont
Counting chamber, Neubauer improved	Brand GmbH
EasySep Magnet	Stemcell
Flow cytometer, Calibur	Becton Dickinson
Flow cytometer, Canto II	Becton Dickinson
Freezer	Liebherr
Freezer, -20 °C	Liebherr

NAME	MANUFACTURER
Freezer, 4 °C	Liebherr
Gel electrophoresis chamber	Peqlab biotechnology
Heat block, thermomixer compact	Eppendorf
Incubator, Biotherm 37	julabo
Incubator, MCO-20AIC	Sanyo
Infrared lamp, HP3616	Phillips
Microscope, Apotome	Zeiss
Microscope, Axiovert 200M	Zeiss
Microscope, Evos fl	Advanced Microscopy Group
Microscope, TCS SP5	Leica
Multichannel Finnpipette 5 -50 µL	ThermoLabsystems
Multichannel Finnpipette 50 -300 µL	ThermoLabsystems
Nanodrop, 2000c	Peqlab biotechnology
PCR Thermal Cycler, T3	Biometra
pH meter, HI2211	Hanna Instruments
pH meter, MP220	Mettler toledo
Pipette, 10 µL	Eppendorf
Pipette, 100 µL	Eppendorf
Pipette, 1000 µL	Eppendorf
Pipette, 2.5 µL	Eppendorf
Pipette, 20 µL	Eppendorf
Pipette, 200 µL	Eppendorf
Pipette Filler, accu-jet pro	Brand GmbH & Co KG
Plate reader, Infinite 200	TECAN
Plate reader, Victor	PerkinElmer
Power supply, 250/2,5	Bio-Rad
Power supply, PowerPac 200	Bio-Rad
Precision balance, Analytical Plus	Ohaus
Roller mixer, SRT6	Stuart
Shaker	Medgenix Diagnostics
UV table, TI 1	Biometra
Vortex mixer	Heidolph
Water bath	Gesellschaft für Labortechnik
Water bath, WTE var 3185	Lauda

2.1.10 *Mouse lines*

Table 2.10: Mouse lines used for T cell preparation

LINE	GENOTYPE	MANUFACTURER
C57BL/6	wt	Charles River
C57BL/6	P2X7 <sup>-/-</sup>	Nolte lab, UKE
Balb/c	wt	Charles River
Balb/c	P2X7 <sup>-/-</sup>	Nolte lab, UKE

2.1.11 *Plasmids*

Table 2.11: Plasmids

INSERT	VECTOR	RESISTANCE	MANUFACTURER
Anti-GFP nanobody Enhancer PDB 3K1K	pQE80	Kan	Görlich lab
ARTC2.2	pCSE2.5	Amp	Nolte lab, UKE
ATPFS1_Bs.Cyt	pCDNA3.1	Amp/Zeo	Haag lab, UKE
ATPFS1_Bs.GPI	pCSE2.5	Amp	Haag lab, UKE
ATPFS1_PS3.cyt	pCDNA3.1	Amp/Zeo	Haag lab, UKE
ATPFS1_PS3.GPI	pCSE2.5	Amp	Haag lab, UKE
ATPFS1_PS3.ProtG	pCSE2.5	Amp	Haag lab, UKE
ATPFS1_PS3.SEKDEL	pCSE2.5	Amp	Haag lab, UKE
ATPFS1_RRKK.Cyt	pCSE2.5	Amp	Haag lab, UKE
ATPFS1_RRKK.Cyt	pCDNA3.1	Amp/Zeo	Haag lab, UKE
ATPFS1_RRKK.GPI	pCSE2.5	Amp	Haag lab, UKE
ECFP	pECFP-N1	Kann/Neo	Clontech
EGFP-dnLKLF	pCDNA3.1	Amp/Zeo	Nolte lab, UKE
EYFP	pEYFP-N1	Kann/Neo	Clontech
iATPSnFR1.0	pdisplay	Amp/Neo	Khakh
iATPSnFR1.0	pRSET	Amp	Khakh
iATPSnFR1.1	pRSET	Amp	Khakh
iATPSnFR1.1	pdisplay	Amp/Neo	Khakh

INSERT	VECTOR	RESISTANCE	MANUFACTURER
mP2X4	pCDNA3.1	Amp/Zeo	Nolte lab, UKE
mP2X7kP	pMXs-IP	Pur	Haag lab, UKE
mP2X7-Strep-His-eGFP (451L)	pCDNA3.1	Amp/Zeo	Nicke
mP2X7-Strep-His-eGFP (451P)	pCDNA3.1	Amp/Zeo	Nicke
NEDD8-specific protease 1 (NEDP1)	pQE80	Kan	Görlich
Ruby3-iATPSnFR1.0	pdisplay	Amp/Neo	Khakh
TP1170 (1xCysteine)	pQE80	Kan	Görlich
TP1170 (3xCysteine)	pQE80	Kan	Görlich

### 2.1.12 Primers

Table 2.12: Primers used for sequencing and genotyping

NAME	SEQUENCE 5' → 3'	MANUFACTURER
CMV.fw	CGCAAATGGGCGGTAGGCGTG	Sigma-Aldrich
BGH.rv	TAGAAGGCACAGTCGAGG	Sigma-Aldrich
P2X7.fw	GGAAAATTTGACATCATCCAGC	Sigma-Aldrich
ε <sub>0</sub> PS3.fw	CCGCCCTCGAGATGAAGACC	Eurofins
ε <sub>0</sub> PS3.rv	GCCGTCAAGCTTCATCTCGG	Eurofins
ε <sub>0</sub> Bs.fw	TGAAAGTGAACATCACGACC	Eurofins
ε <sub>0</sub> Bs.fw	GCTCTCTCTTTGTCGATTCC	Eurofins

### 2.1.13 Software

Table 2.13: Software

SOFTWARE	VERSION	MANUFACTURER
Adobe Illustrator	CS5	Adobe Inc.
Adobe Photoshop	CS5	Adobe Inc.
AxioVision	4.7	Zeiss
BioEdit	7.0.5.3	Tom Hall

SOFTWARE	VERSION	MANUFACTURER
Excel	Office 2016	Microsoft
FACS Diva	8.0	Becton Dickinson
Fiji	1.52t	Wayne Rasband (NIH)
FlowJo (Mac)	9.6	Becon Dickinson
FlowJo (Windows)	10.06.1	Becon Dickinson
Prism	8.4.3	GraphPad
Imaris	8.1.2	Oxford Intruments
JabRef	4.3.1	MIT License
Leica LAS AF	2.6.0.7266	Leica
LyX	2.3.4.4	Matthias Ettrich
MarvinSketch	20.3	ChemAxon Ltd.
Micro Manager	1.43	Open Imaging
Nanodrop 2000/2000C	1.2.	Peqlab
PowerPoint	Office 2016	Microsoft
Snap Gene Viewer	5.0.7	GSL Biotech LLC
TeXLive	2020	TeX Users Group
VisionCapt	15.08	analis

## 2.2 METHODS

### 2.2.1 *Methods in cell biology*

#### 2.2.1.1 *Culture and passage of adherent cells*

Adherent cells were cultivated in Dulbecco's modified eagle medium (DMEM) complete in cell culture flasks at 37 °C and 5% carbon dioxide (CO<sub>2</sub>). Cells were split three times a week (Mondays, Wednesdays, and Fridays). For the passage of cells, DMEM complete and phosphate buffered saline (PBS<sup>-/-</sup>) were preheated in a water bath for 30 min to reach approximately 37 °C. The culture medium was removed from the flasks and the cells were washed with an equal amount of PBS<sup>-/-</sup>. PBS<sup>-/-</sup> was removed and an adequate volume (e.g., 0.5 mL for a T25 flask) of Trypsin-EDTA solution was added. After approximately 5 min, the cells detached and were resuspended in medium to stop the enzymatic activity of trypsin. Subsequently, the cell solution was centrifuged for 5 min at 300 x g. The supernatant was discarded, and the cells were resuspended in DMEM complete and diluted in a new flask in the desired concentration.

#### 2.2.1.2 *Culture and passage of suspension cells*

Suspension cells were cultivated in Roswell Park Memorial Institute (RPMI) complete in Petri dishes at 37 °C and 5% CO<sub>2</sub>. Cells were split three times a week (Mondays, Wednesdays, and Fridays). These cells were diluted with fresh medium in a new Petri dish (10 or 20 cm in diameter).

#### 2.2.1.3 *Counting of cells*

The number of cells per milliliter was determined by diluting a cell suspension 1:10 with trypan blue. Trypan blue stains dead cells, as it can pass through the cell membrane when the latter is not intact anymore (Strober, 2015). 10 µL of this solution was then pipetted between a hemocytometer and a cover glass. The hemocytometer contains four squares, each of which are divided into sixteen smaller squares; four diagonal small squares from every large square were counted, summed, and multiplied with 10<sup>5</sup>, to obtain the cell number per milliliter (or with 10<sup>4</sup> in case the cells were not pre-diluted with trypan blue). The multiplier (10<sup>4</sup>) is defined by the area of each large square (1 mm<sup>2</sup>) multiplied with the depth of the chamber (0.1 mm), which is 0.1 mm<sup>3</sup> or 0.0001 mL .

#### 2.2.1.4 *Transfection of cells with jetPEI<sup>®</sup>*

Transfection is a method to transfer foreign DNA (often in the form of a plasmid) into eukaryotic cells with the help of a transfection agent in order to express a gene of interest. Here, jetPEI<sup>®</sup>, a linear polyethyleneimine (PEI) derivative was used, which is positively charged and can bind to negatively charged deoxyribonucleic acid (DNA), and allows the passage of this complex through the cell membrane via endocytosis (Boussif et al., 1995; Sonawane, Szoka, and Verkman, 2003).

Before transfection, the cells were split to reach approximately 50% confluency on the day of transfection. Directly before transfection, the cell culture medium was exchanged with fresh medium. The jetPEI<sup>®</sup> and DNA solutions were prepared in 150 mM sodium chloride (NaCl), vortexed, and briefly centrifuged in a table centrifuge. The DNA solution was added to the jetPEI<sup>®</sup> solution, vortexed, centrifuged, and subsequently incubated for 30 min at room temperature. After incubation, the solution was added to the prepared cell lines (see [Table 2.14](#) for volumes). After approximately 6 h the cell medium was exchanged for fresh medium.

Table 2.14: Reagents needed for transfections using jetPEI<sup>®</sup>

REAGENT	T 25	T 75
jetPEI <sup>®</sup>	10 $\mu$ L	20 $\mu$ L
Plasmid	5 $\mu$ g	10 $\mu$ g
150 mM NaCl	ad 250 $\mu$ L	ad 500 $\mu$ L

#### 2.2.1.5 Production of proteins in HEK293 6E cells

For the production of proteins such as nanobodies or ATP sensors linked to a nanobody, the corresponding sequences were cloned into the pCSE vector and subsequently used to transfect HEK293 6E cells. The transfection of HEK293 6E is similar to [Section 2.2.1.4](#), with the following differences. The cells were split 1 : 8 on the day before transfection. The following day, the cell culture medium was exchanged with F17 transfection medium. The DNA and PEI solution were prepared according to [Table 2.15](#) and vortexed (addition of the PEI to the DNA solution). The mixture was incubated for 30 min at room temperature (RT) and afterward added to the cells. 24 h after transfection, 500  $\mu$ L of F17 feeding medium was added to the cells. The supernatant was collected after additional 5 days, centrifuged at 4600  $\times$  g, filtered using a 50 mL steriflip cup, and stored at 4 °C.

Table 2.15: Reagents needed for transfections using PEI

	REAGENT	T 75	T 225
DNA solution	diH <sub>2</sub> O	ad 250 $\mu$ L	ad 750 $\mu$ L
	Plasmid	10 $\mu$ g	20 $\mu$ g
	300 mM NaCl	250 $\mu$ L	750 $\mu$ L
PEI solution	diH <sub>2</sub> O	126 $\mu$ L	502 $\mu$ L
	PEI	124 $\mu$ L	248 $\mu$ L
	300 mM NaCl	250 $\mu$ L	750 $\mu$ L

#### 2.2.1.6 Electroporation of cells

Electroporation is another method for the transfection of cells, that does not require a transfection reagent. This method was used to transfect suspension cells in this thesis. In

the case of electroporation, an electrical field is used to induce pores in the membrane of cells, allowing the passage of plasmid DNA (Neumann et al., 1982).

First, cells (e.g., Jurkat) were counted as described before and adjusted to a cell number of  $2.5 \times 10^6$  cells/mL. After centrifugation, the cell pellet was resuspended in 500  $\mu$ L RPMI without phenol red, containing 7.5% fetal calf serum (FCS) and penicillin/streptomycin (diluted 1:100). 30  $\mu$ g of plasmid DNA was first placed in an electroporation cuvette. For stable transfection, half of the plasmid DNA was previously linearized, in most cases with the restriction enzyme ScaI and then pipetted into the cuvette with the rest of the plasmid DNA. Then, the cell solution was added to the DNA, mixed gently, and incubated for 5 min at 37 °C. The DNA cell solution was then electroporated (960  $\mu$ F and 0.24 kV), and again incubated at 37 °C for 10 min. The DNA cell solution was then pipetted in a pre-warmed 10 cm Petri dish containing 10 mL RPMI medium.

#### 2.2.1.7 *Sorting of transfected cells*

Cells were sorted after transfection, to separate transfected from non-transfected cells or to separate cells with different expression levels of the gene of interest. The sorting was performed on an AriaIIIu fluorescence activated cell sorting (FACS) after labeling of the protein of interest with a fluorochrome-conjugated antibody or reporter gene. Cells were prepared in PBS<sup>-/-</sup>, counted, and adjusted to  $1 \times 10^7$  cells/mL. The cell solution was then filtered with cell strainers to remove aggregated cells to avoid clogging of the FACS needle. The prepared cells were then gated according to the desired expression level and collected in a 15 mL tube with 1 mL of RPMI and penicillin/streptomycin (1:100).

#### 2.2.1.8 *Limited dilution and selection of transfected cells*

After the transfection or sorting of cells, they were diluted to get single clones. After several dilution steps cells were seeded in 96-well plates at calculated densities of 10, 1, and 0.3 cells per well. After a week of incubation, the wells were screened for clones (and weeks/days after that). Clones were picked and grown in increasingly bigger dishes and aliquots were frozen.

#### 2.2.1.9 *Cryopreservation of cells*

Freezing in nitrogen tanks (-196 °C) allows the storage of e.g., cell lines for long periods of time. Enzyme activity is nearly stopped at these temperatures, and any change of the cells is prevented.

For the cryopreservation of cells, freezing medium (75% FCS, 15% cell culture medium, and 10% DMSO) was prepared and stored on ice. Adherent or suspension cells were prepared as described above and centrifuged at 300 x g. The cell pellet was then resuspended in freezing medium, pipetted in cryo-tubes, and first transferred to a -80 °C refrigerator. After 24 h the cells were transferred into a nitrogen tank for long-term preservation.

#### 2.2.1.10 *Thawing of cells*

To thaw frozen cells, a water bath and cell culture medium in Petri dishes or cell culture flasks were prepared and preheated for 30 min at 37 °C. The cells were taken out of the nitrogen tank, transported on dry ice, quickly thawed in a water bath, and transferred into the prepared cell culture dishes.

#### 2.2.1.11 *Preparation of CD4<sup>+</sup> T cells from mice*

Mice were narcotized with CO<sub>2</sub>/oxygen (O<sub>2</sub>), euthanized with CO<sub>2</sub>, and additionally a cervical dislocation was performed. Spleens were removed from mice and passed through a cell strainer (70 µm). The erythrocytes were lysed using the “BD FACS Lysing Solution” according to the manufacturer’s instructions. CD4<sup>+</sup> cells were isolated by negative selection using “EasySep™ Mouse CD4<sup>+</sup> T Cell Isolation Kit”, which removes all unwanted cell subsets are removed with streptavidin magnetic beads and biotinylated antibodies.

#### 2.2.1.12 *Labeling of mitochondria in cells*

Mitochondria were stained with MitroTracker™ Red CMXRos for live-cell imaging. The mitochondrial dye can pass the cell membrane and intercalate into the intermembrane space of mitochondria of living cells (Poot, Gibson, and Singer, 1997). Cells were stained with 150 nM MitroTracker for 30 min at 37 °C in conditioned (used) cell culture medium. After incubation, the labeled cells were washed once with PBS with calcium and magnesium (PBS<sup>+/+</sup>) and prepared for live-cell imaging.

#### 2.2.1.13 *Labeling of Lysosomes in cells*

Labeling of lysosomes was performed similar to the staining of mitochondria, but with 75 nM of LysoTracker Red.

#### 2.2.1.14 *Labeling of cells with the calcium dyes FuraRed, Fluo-4 and Fura-2*

For the measurement of cytosolic Ca<sup>2+</sup>, cells were labeled with the acetoxymethyl (AM) esters Fura-2 (for global imaging of Ca<sup>2+</sup>) or with Fluo-4 combined with FuraRed (for local imaging of Ca<sup>2+</sup>) or just Fluo-4 for Ca<sup>2+</sup> using FACS. The AM esters give the dyes a neutral charge and allow the passage of the dyes through the cell membrane. Inside the cell, the AM ester is cleaved by esterases (Bass et al., 1983). For Ca<sup>2+</sup> measurements, either CD4<sup>+</sup> T cells or suspension cell lines (e.g., Jurkat) were used. Cells were counted and adjusted to 1 × 10<sup>6</sup> cells/mL (5 mL), washed in extracellular solution (ECS<sup>-/-</sup>) and centrifuged at 300 × g for 5 min. Ca<sup>2+</sup> dyes were prepared in 50 µL complete medium (10 µM Fluo-4, 20 µM FuraRed and 10 µM Fura-2). The cells were then resuspended in the dye solution, incubated for 20 min at RT and protected from light. 2 mL of cell culture medium was then added to the solution and incubated for 30 min, followed by a centrifugation step for 5 min. Cells were washed once with ECS<sup>-/-</sup> with Ca<sup>2+</sup> and Mg<sup>2+</sup> (ECS<sup>+/+</sup>) and centrifuged. The cells were then resuspended in 500 µL (for primary cells e.g., CD4<sup>+</sup>) or 2 mL (for cell lines e.g., Jurkat)

of ECS<sup>+/+</sup>, and incubated for an additional 20 min at RT , to permit the de-esterification of the dyes.

## 2.2.2 Immunological methods

### 2.2.2.1 Flow cytometry

Flow cytometry allows the characterization of cells by measurement of fluorescent surface or intracellular molecules/proteins. Essentially, flow cytometry measures the fluorescence intensity of targets (e.g., proteins), that were previously labeled by fluorescently conjugated antibodies, or structures such as DNA, stained with e.g., DAPI. Cells suspended in a FACS tube are sucked into a flow chamber where they are focused so that only one cell at a time passes a light source (laser). The emitted light is then recorded by detectors specific for certain wavelengths or positioned at certain angles to capture forward scatter (FSC) and side scatter (SSC) signals (McKinnon, 2018).

For FACS measurement, a tube with  $1 \times 10^6$  cells was prepared (for kinetic measurements,  $1 \times 10^7$  cells were used). Cells were stained with fluorescent-labeled antibodies in 100  $\mu$ L FACS buffer (PBS<sup>-/-</sup> + 0.1 % bovine serum albumin (BSA)) for 30 min at 4 °C. Cells were washed once, centrifuged at 300 x g, and resuspended in 200  $\mu$ L FACS buffer (or 500  $\mu$ L ECS<sup>-/-</sup> with Ca<sup>2+</sup> (ECS<sup>+/-</sup>) for kinetic measurements) and recorded.

#### 2.2.2.2 Shedding of CD62L after P2X7 stimulation

Yac-1 cells were stained for CD62L according to [Section 2.2.2.1](#) with CD62L-APC in ECS<sup>+/+</sup>. Cells were then either incubated with 250  $\mu$ M ATP or 20  $\mu$ M NAD<sup>+</sup> for 45 min at 37 °C to induce the P2X7-mediated shedding of CD62L. Cells were washed once with ECS<sup>+/+</sup>, centrifuged at 300 x g, resuspended in 200  $\mu$ L ECS<sup>+/+</sup>, then measured with the FACS Canto II and gated for CD62L expression (ex.: 633 nm; em.: 660/20 nm).

#### 2.2.2.3 PI and DAPI uptake after P2X7 stimulation

Yac-1 cells were prepared as described in [Section 2.2.2.2](#). Shortly before the measurement, 2  $\mu$ L PI or 2  $\mu$ L DAPI was added to the cells. Cells were then gated for PI or DAPI expression.

#### 2.2.2.4 Measurement of calcium uptake after gating of P2X7 using flow cytometry

For the measurement of Ca<sup>2+</sup> uptake after gating of P2X7  $1 \times 10^7$  DO11.10 or Yac-1 per tube were labeled with Fluo-4 or FuraRed according to [Section 2.2.1.14](#). A 30 sec baseline was recorded, a stimulus (e.g., ATP) was added to the cells and the cells were measured for an additional 90 sec. An infrared lamp was used to keep the cell-solution temperature at approximately 37 °C.

#### 2.2.2.5 *Measurement of cytosolic ATP after gating of P2X7 using flow cytometry*

Cells (3T3 or Yac-1) expressing the cytosolic FRET sensors Bs.cyt or RRKK.cyt were used to measure ATP secretion by following the loss of ATP from the cytosol over time after P2X7 stimulation. The measurement was performed according to [Section 2.2.2.4](#). For excitation, a 405 nm laser was used, donor emission (CFP) was detected with a 450/50 nm and acceptor emission (YFP) with a 510/50 nm filter. Cells were treated with 250  $\mu$ M ATP, 20  $\mu$ M NAD<sup>+</sup>, or 10  $\mu$ M carbonyl cyanide m-chlorophenyl hydrazone (CCCP).

#### 2.2.2.6 *Inducing complement-dependent cytotoxicity (CDC) in Yac-1 cells*

Complement-dependent cytotoxicity CDC is the lysis of cells following activation of the classical complement pathway. In this pathway the complement component 1q (C1q) binds to Fc portions of immunoglobulins bound to antigens on the cell surface, resulting in the formation of a membrane attack complex (MAC) and lysis of the cell (Park, Yoon, and Jung, 2016). For an end-point assay,  $5 \times 10^4$  Yac-1 cells were resuspended in 175  $\mu$ L PBS<sup>-/-</sup> containing 0.2% BSA. 25  $\mu$ L pooled human serum (untreated or inactivated by heating to 56 °C for 20 min) was added to the cells and incubated for 30 min at 37 °C. Cells were washed twice with PBS<sup>-/-</sup> and resuspended in 100  $\mu$ L PBS<sup>-/-</sup>.

For kinetic measurements of CDC Yac-1 cells expressing either the cytosolic FRET-based ATP sensor Bs.cyt or RRKK.cyt were used and prepared according to [Section 2.2.2.4](#) and [Section 2.2.2.5](#). Cells were treated with 12.5% pooled human serum, inactivated serum, 250  $\mu$ M ATP, or 20  $\mu$ M NAD<sup>+</sup>.

#### 2.2.2.7 *Measurement of ATP release after gating of P2X7 using luciferase*

For NAD<sup>+</sup> mediated ATP release YAC-1 cells were used, which express both P2X7 and ARTCs 2.2. Extracellular ATP was measured in 96-well microtiter plates with the Victor3<sup>TM</sup> luminometer and the CellTiter-Glow (Luciferase) assay kit. The basis of the luciferase assay was already explained in [Section 1.3](#).

For every experiment, an ATP standard curve was measured (0 - 2  $\mu$ M). Yac-1 cells were adjusted to  $2 \times 10^6$  cells/mL in ECS<sup>+/+</sup> and per condition/well  $3 \times 10^5$  cells were used and pre-incubated with P2X7 (13A7, 14D5, A43, KN62) or ARTC2.2 (s+16, s-14) inhibitors for 30 min at RT. Additionally, 20  $\mu$ M NAD<sup>+</sup> was added to the cells and incubated for 45 min at 37 °C. Lastly, the CellTiter-Glow solution was added to the wells and incubated for 10 min at 37 °C inside the luminometer. Wells were then measured for 1 sec.

For kinetic measurements, the CellTiter-Glow solution was added to the wells, and plates were directly measured for 5 min to record a baseline. Then 20  $\mu$ M NAD<sup>+</sup> was added and plates were measured every 2.5 min for 30 min.

### 2.2.3 Microscopy and image processing

#### 2.2.3.1 Immune fluorescence microscopy

For immune fluorescence staining, cells were incubated with antibodies specific for a certain target protein on cells in order to make it visible under the microscope. The staining was performed directly with antibodies conjugated to a fluorescent dye/protein, or indirectly with an unlabeled primary and a labeled secondary antibody, which binds specifically to the first antibody.

For extracellular staining of cells (e.g., cell surface proteins), 10 mm coverslips were coated with a 0.1 mg/mL poly-L-lysine (PLL) solution for 30 min in a 24-well microtiter plate and washed with PBS<sup>-/-</sup>. The cells were then seeded with  $4 \times 10^4$  cells per well 24 h before staining. The medium was then removed, and the cells were washed once with PBS<sup>+/+</sup> and fixed with 2% paraformaldehyde (PFA) for 20 min. The coverslips were then removed and put on parafilm in a staining chamber and incubated with the first antibody (diluted in antibody solution) for 1 - 3 h at RT. Coverslips were washed twice for 10 min with PBS<sup>+/+</sup>. The coverslips were then incubated with a secondary antibody for 1 h and washed twice for 10 min with PBS<sup>+/+</sup>. The coverslips were then put on a microscope slide with 5  $\mu$ L mounting medium (Vectashield<sup>®</sup> with or without DAPI depending on the staining) and sealed with nail polish.

#### 2.2.3.2 Live cell imaging of Ca<sup>2+</sup>

Either cell lines or CD4<sup>+</sup> T cells (see [Section 2.2.1.11](#)) were labeled with Fura-2 for the measurement of global Ca<sup>2+</sup> signals (see [Section 2.2.1.14](#)). For this measurement, thin glass slides were coated with 0.1% BSA and 0.1 mg/mL PLL and subsequently, a rubber ring was placed in the middle of it with Vaseline. 10  $\mu$ L of cell suspension was placed inside the ring and incubated for 20 min at room temperature in a humid chamber to permit the attachment of the cells to the surface of the glass slide. An inverted fluorescence microscope (Nikon Eclipse TE300) was used for the measurements with excitation wavelengths at 340 and 380 nm, a 40x objective, and the software Volocity for recording. Every 10 sec images were taken, and the ratio between the two wavelengths was visualized. Each measurement was performed over 20 min. First, a 2 min baseline was recorded, followed by the addition of a stimulant (e.g., ATP) for 10 min and the addition of 5  $\mu$ M of thapsigargin for the last 5 min of the recording. Thapsigargin is a blocker for the sarco/endoplasmic reticulum Ca<sup>2+</sup> ATPase (SERCA) channels located on the ER membrane. Blocking these channels results in an accumulation of Ca<sup>2+</sup> in the cytosol and a maximum Fura-2 signal.

#### 2.2.3.3 Evaluation of Ca<sup>2+</sup> imaging

The recorded data was imported into the OpenLab software. OpenLab allows calculating of the ratio of the images recorded at the extinction wavelengths of 340 and 380 nm. In these generated ratios every cell was marked as a region of interest (ROI). Every value of the

selected ROIs was then measured and exported as a .txt file for each cell and time point. For further evaluation, exclusion of outliers and statistics the data was imported into Prism.

#### 2.2.3.4 *Live cell FRET imaging and evaluation of ATP*

For ATP live-cell imaging, a Leica inverted fluorescence microscope equipped with a 40x objective and a dual-view system consisting of a filter-cube with a dichroic mirror and two filters at 480/30 nm (CFP channel) and 535/40 nm (YFP channel) was used. As a light source, a 435 nm LED was used. For recording and evaluation, the software Micromanager 1.4.5 (based on ImageJ) was used (Nikolaev, Gambaryan, and Lohse 2006; Kraft and Nikolaev 2017). 24 h before measurement, 25 mm coverslips were prepared according to 2.2.3.2 in 6-well microtiter plates, and  $1 \times 10^5$  cells per well were seeded. For measurement, the coverslip was put into a cell chamber, washed once with ECS<sup>+/+</sup>, and covered with 300  $\mu$ L ECS<sup>+/+</sup>. For suspension cells,  $4 \times 10^6$  cells/mL were used. 20  $\mu$ L of cell suspension was then added on a coverslip and incubated for 20 min for the attachment of the cells to the surface and washed twice with ECS<sup>+/+</sup>. For the measurement, every 5 sec a picture was taken. First a 2 min baseline was recorded before a stimulus (300  $\mu$ L of e.g., ATP in ECS<sup>+/+</sup>) was added, and the measurement was continued for another 8 min.

Because of the spectral overlap of the CFP and YFP emissions, a correction factor was determined. For this purpose HEK293 cells were transfected (according to Section 2.2.1.4) with pECFP-N1 (a plasmid encoding for CFP) and prepared and measured as described above. The correction factor b (see equation Equation 2.1) was determined as the mean of the acquired FRET ratios .

$$\text{FRET}_{\text{corr}} = \text{FRET} - b \quad (2.1)$$

The recorded data were evaluated with Micromanager and Excel. First, the CFP and YFP channels were recorded separately, and a FRET ratio (YFP/CFP) image was created using the “FREToffline” plugin. Serial images were analyzed using the “Time Series Analyzer” plugin, and the mean FRET values were displayed in a table and a graph (Sprenger et al., 2012). The values were then imported into Excel and corrected according to Equation 2.1 and normalized to the mean values of the recorded baseline.

#### 2.2.3.5 *Live cell imaging and evaluation of ATP (confocal)*

For confocal live-cell imaging of ATP, a Leica TCS SP5 microscope with a 63x oil objective was used. Additionally, the microscope was equipped with an incubation chamber (including temperature and CO<sub>2</sub> control), which was switched on 30 min before measurement to reach 37 °C and 5 % CO<sub>2</sub> concentration. For the excitation of CFP, a 405 nm laser was used. Detection of the donor channel CFP was done at 472 - 482 nm, and the acceptor channel YFP was measured at 522 - 532 nm. Ibidi slides (glass bottom and 8 wells) were used for imaging and coated with 0.1 mg/mL PLL for 30 min at RT.  $4 \times 10^4$  adherent cells were seeded per well 24 h before imaging. The cells were then washed twice with ECS<sup>+/+</sup> and subsequently covered with 200  $\mu$ L ECS<sup>+/+</sup>. The imaging protocol was performed according

to [Section 2.2.3.4](#) (baseline recording and the addition of the stimulus). For the overlap correction of CFP and YFP HEK293 cell were transfected (according to [Section 2.2.1.4](#)) either with pECFP-N1 or pEYFP-N1 and the correction factor ( $k = 0.59$ ) was calculated. The corrected FRET (FRET<sub>corr</sub>) was then calculated with [Equation 2.1](#).

$$\text{FRET}_{\text{corr}} = 255 \times \left( \frac{\text{ch3}}{\text{ch1} + \text{ch3}} \right) \quad (2.2)$$

Where ch3 is defined by:

$$\text{ch3} = \text{ch2} - k \times \text{ch1} \quad (2.3)$$

in which ch1 stands for CFP, ch2 for YFP and the coefficient 255 gives FRET<sub>corr</sub> a range between 0 and 255 (8 bit scale). [Equation 2.2](#) and [Equation 2.3](#) gives:

$$\text{FRET}_{\text{corr}} = 255 \times \left( \frac{\text{YFP} - 0.59 \times \text{CFP}}{\text{CFP} + (\text{YFP} - 0.59 \times \text{CFP})} \right) \quad (2.4)$$

The analysis software Imaris in combination with Matlab was used for evaluation. First, the recorded images were smoothed with a median filter of 3x3 pixels. Then the ratio of the YFP and CFP channels was calculated, using equation [Equation 2.4](#). The calculated ratios were then saved as .tiff files and further evaluated with Fiji is just ImageJ (Fiji) software, where ROIs were defined, and the mean fluorescent was calculated according to [Section 2.2.3.4](#).

#### 2.2.3.6 Pseudo color staining of imaged cells

Cells recorded via live-cell imaging of ATP using FRET sensors, were assigned to specific colors with the look up table (LUT) plugin “Blue Green Red”, where “Blue” is the lowest signal ranging to “Red” with the highest signal, according to Hou et al. [2011](#)

### 2.2.4 Methods in molecular biology

#### 2.2.4.1 Genotyping of transgenic mice using PCR

To verify the presence of foreign DNA in mice after pronuclear injection, the genomic DNA of these mice was analyzed by polymerase chain reaction (PCR) genotyping. The PCR reaction allows the multiplication of small amounts of DNA using specific primers, polymerases, and a thermocycler. Biopsies from mice (tail or ear) were digested with 600  $\mu\text{L}$  lysis buffer containing 100  $\mu\text{g}$  proteinase K in a thermal shaker for 3 h or overnight at 55  $^{\circ}\text{C}$ , and 350 rpm. Samples were then vortexed and centrifuged for 10 min at 14000  $\times g$ . 600  $\mu\text{L}$  of isopropanol was added to the supernatant and centrifuged for 1 min at 6600  $\times g$ . The pellet was then resuspended in 100  $\mu\text{L}$  TE buffer for 3 h at 55  $^{\circ}\text{C}$ . With the isolated genomic DNA a PCR screening was performed. [Table 2.17](#) shows the PCR mixture and program used.

Table 2.16: PCR mixture

REAGENT	VOLUME [ $\mu\text{L}$ ]
Platinum Blue PCR SuperMix	18 $\mu\text{L}$
Forward primer $\mu\text{M}$	1 $\mu\text{L}$
Reverse primer $\mu\text{M}$	1 $\mu\text{L}$
Genomic DNA	1 $\mu\text{L}$

Table 2.17: PCR program

STEP	TEMPERATURE [ $^{\circ}\text{C}$ ]	TIME [MIN]	CYCLES
Initial denaturation	95	9	1
Denaturation	95	1	30
Annealing	56	30	
Elongation	72	1	
Final elongation	72	5	1
Stop	4	$\infty$	1

#### 2.2.4.2 Digestion of DNA

For the digestion of DNA (plasmids or DNA fragments), specific restriction enzymes were used. The total reaction volume was 20  $\mu\text{L}$ , including 1  $\mu\text{g}$  of DNA, 1  $\mu\text{L}$  of 10 mM concentrated restriction enzymes, and a specific buffer, which was added as a 10x concentrate. The buffer providing the best reaction conditions for each enzyme activity was selected using the NEBcloner tool (New England BioLabs, <https://nebcloner.neb.com>). The digestion was performed for 1 h at 37  $^{\circ}\text{C}$ , followed by inactivation of the enzymes at 80  $^{\circ}\text{C}$  for 20 min. Depending on the used enzymes, different inactivation temperatures were required.

#### 2.2.4.3 Agarose gel electrophoresis

Agarose gel electrophoresis allows the separation of DNA fragments of different sizes, using an electrical field, which forces the negatively charged DNA fragments to move. Inside the agarose matrix smaller DNA fragments travel faster than bigger fragments. 1 to 1.5 % (m/v) agarose gels were prepared. The agarose was dissolved in TAE buffer using a microwave. Afterward, Rotisafe was added as a staining agent, and the solution was poured into a casting tray. After polymerization (app. 30 min) of the gel the well comb was removed, the gel was placed in the gel box filled with TAE buffer. 6x Loading-dye was added to the samples and pipetted into the wells alongside molecular weight ladders (100 bp or 1 kb). The gel was run at 100 V for 45 to 90 min. Analysis of the gel was performed with "Gel Documentation System". Afterward, the gel was put on an UV-transilluminator to cut out the DNA fragments of interest.

#### 2.2.4.4 *Measurement of DNA concentration*

For the measurement of DNA concentrations (e.g., plasmid preparations), a NanoDrop fluorospectrometer was used. The sample size was 1  $\mu\text{L}$  and the absorption of the sample was measured at 260 (DNA) and 280 nm (proteins). The ratio of A260/A280 indicates the purity of the sample, where approximately 1.8 is considered “pure” (Gallagher and Desjardins, 2006). First, a “blank” was measured, which was the buffer in which the DNA was dissolved. Afterward, the samples were measured to determine the DNA concentration in  $\mu\text{g}/\mu\text{L}$ .

#### 2.2.4.5 *Transformation*

Transformation is a method to deliver foreign DNA (plasmids) into bacteria using heat to induce pores into the membrane of the bacteria (Pope and Kent, 1996). 50  $\mu\text{L}$  of competent bacteria (XL1 blue) were thawed on ice, and afterward, 1  $\mu\text{L}$  plasmid DNA or 2  $\mu\text{L}$  of a ligation mixture was added and incubated for 30 min on ice. The bacteria were heat-shocked for 30 sec at 42 °C in a water bath and incubated on ice for 2 min. 37 °C warm Super optimal broth with catabolite repression (SOC) medium was added and incubated for 1 h at 37 °C and 250 rpm in an incubator. Two dilutions of the bacterial solution were added on Petri dishes containing antibiotics corresponding to the plasmid and incubated overnight at 37 °C. Additionally, un-transformed bacteria or a re-ligation control (bacteria transformed with digested plasmid) were put on other Petri dishes as controls.

#### 2.2.4.6 *Plasmid preparation (mini- and maxi kit)*

The plasmid preparation method is based on the adsorption of plasmid DNA to a matrix (silica gel) of a column under acidic and chaotropic conditions. Multiple clones were picked after transformation and incubated overnight in 5 mL LB medium on a rotary shaker at 37 °C and 250 rpm. Afterward, the bacterial culture was centrifuged at 4600  $\times$  g for 15 min and the supernatant was discarded. For maxi plasmid preparation, the 5 mL overnight culture was used to inoculate 250 mL of LB medium, which was incubated under the same conditions as described above. The overnight culture was centrifuged at 4600  $\times$  g, and the plasmid preparation was then performed as described by the manufacturer. The resulting DNA pellet was either resuspended in ddH<sub>2</sub>O (mini kit) or TE Buffer (maxi kit), and the concentration was measured (see [Section 2.2.4.4](#)).

#### 2.2.4.7 *Dephosphorylation*

Dephosphorylation of digested plasmids prevents the re-circulation of the plasmid during ligation, by removing phosphate residues on the 5' ends. 1  $\mu\text{L}$  Antarctic Phosphatase and 2.5  $\mu\text{L}$  phosphatase buffer (10x) were added to the digested plasmid, incubated for 1 h at 37 °C and 20 min at 80 °C to inactivate the enzyme.

#### 2.2.4.8 *Ligation*

To ligate DNA fragments, e.g., to introduce a gene of interest in a plasmid, ligases are used. For a successful ligation a molar ratio of 1 : 3 between plasmid and insert is required. The reaction volume was adjusted to 20  $\mu$ L, including 1  $\mu$ L of T4 ligase and 2  $\mu$ L T4 ligase buffer (10x). The ligation was carried out at 4 °C for 16 h. As a control, samples without inserts were used.

#### 2.2.4.9 *Isolation and purification of DNA*

For the isolation of DNA fragments from gels, a DNA purification kit from Qiagen was used. The bands of the gel were made visible using a UV-transilluminator and the desired band(s) were cut out with a scalpel and weighed. DNA purification was then performed following the manufacturer's protocol.

#### 2.2.4.10 *Sequencing of DNA*

For the sequencing of DNA (Sanger sequencing), the mix2seq kit from Eurofins was used. Depending on the size of the gene one or two primers (forward and reverse primer) were used. A total volume of 17  $\mu$ L was needed per sequencing reaction, including 1.2  $\mu$ g of DNA and 3  $\mu$ L of 10 mM primer and double-distilled water (ddH<sub>2</sub>O). The sequencing reactions were performed by the company Eurofins. After approximately one day, the results of the sequencing could be downloaded and analyzed further.

### 2.2.5 *Methods in protein chemistry*

#### 2.2.5.1 *SDS gel electrophoresis*

The sodium dodecyl sulfate (SDS) gel electrophoresis is a method to separate proteins by mass. The negatively charged SDS molecules bind to the proteins giving them a negative charge proportional to their molecular mass. In an electrical field, these proteins migrate in the direction of the cathode. The migration time through the matrix of the gel is proportional to the mass of the proteins, leading to their separation (Laemmli, 1970). The samples were denatured at 70 °C with sample buffer for 10 min and loaded onto a gel (12% Bis-Tris Gel; Invitrogen) together with a molecular weight marker. Electrophoresis was performed in a gel chamber for 45 min at 200 V.

#### 2.2.5.2 *Coomassie staining of SDS gels*

SDS gels were stained using the "colloidal Blue Stain Kit". Gels were stained overnight and washed for 8 h or overnight in deionized water (diH<sub>2</sub>O). After washing, the gel was transferred to gel drying solution for 5 min, and dried overnight in cellophane inside a plastic frame. The gel was then scanned for documentation.

### 2.2.5.3 *Western blotting*

Western blotting allows the (indirect) detection of specific proteins with primary and secondary antibodies. The primary antibody (often poly clonal) binds specifically to the target protein, whereas the secondary antibody targets the primary antibody's Fc region. Additionally, the secondary antibody is labeled with horseradish peroxidase (HRP). HRP induces the oxidation of a substrate, resulting in the emission of that can be captured on films to visualize the bands detected by the primary antibodies, a process known as enhanced chemiluminescence (Mishra, Tiwari, and Gomes, 2017).

In a first step, the proteins were transferred from the SDS gel to a nitrocellulose membrane using a blotting chamber. The membrane was blotted for 90 min at 30 V and 300 mA. If pre-stained markers were contained on the gel, these could be visualized on the blotting membrane to determine the molecular size of individual bands. Otherwise, the membrane was stained with Ponceau Red to verify the successful blotting. The dye was removed by briefly washing with diH<sub>2</sub>O. The membrane was blocked overnight with 5 % milk powder in TBS and afterward incubated with a primary antibody (1 : 4000 in 5 % milk powder) for 2 h at RT or overnight at 4 °C. After washing with 0.05 % Tween20 (in PBS<sup>-/-</sup>), the membrane was incubated with the secondary antibody (1 : 4000 in 5 % milk powder) for 60 min at RT. The membrane was then washed three times with the same buffer, followed by the addition of ECL solution to the membrane and its exposure to a film (10 sec and 10 min).

### 2.2.5.4 *Production of nanobodies and single-wavelength ATP sensors in bacteria*

The TP1170 nanobody and the ATP sensors iATPSnFR1.0 (called HHM1.0)/iATPSnFR1.1 (called HHM1.0) were produced in BL21(DE3)pLysS competent cells. The bacteria were first transformed with the corresponding plasmids, according to [Section 2.2.4.5](#). Colonies were picked and used to inoculate 10 mL 2x YT medium containing carbenicillin (1:1000) in a 50 mL tube and incubated overnight at 37 °C and 250 rpm on a rotary shaker. The pre-culture was then centrifuged at 4600 x g for 10 min, and the pellet was resuspended in 10 mL 2x YT medium. 4 mL of the suspension was used to inoculate 200 mL 2x YT medium containing carbenicillin (1:1000) and incubated at 37 °C and 250 rpm for 2 – 4 h until a OD<sub>600</sub> of 0.3 – 0.6 was measured. Subsequently, protein production was induced by the addition of 0.1 mM isopropyl-β-D-thiogalactoside (IPTG), and the suspension was incubated for a further 3 h. The suspension was then centrifuged at 4600 x g for 15 min, and the pellet was then stored at –80 °C until further use.

For protein isolation, the pellet was resuspended in lysis buffer with 5 mL buffer per 1 g of pellet, and incubated for 30 min at RT on a roller mixer. The suspension was then centrifuged at 43.000 x g for 1 h at 4 °C. The supernatant was used for further purification steps and the pellet was discarded.

### 2.2.5.5 Protein purification with affinity chromatography (Ni-NTA)

The nanobody TP1170 and the single-wavelength sensors HHM1.0 and 1.1 were purified using a nickel-nitrilotriacetic acid (Ni-NTA) column. The column was prepared by filling 2 mL of Ni-NTA matrix into a 15 mL column between two frits. The matrix was then washed with 20 column volumes of PBS<sup>-/-</sup>. The bacterial lysate was then added onto the column and washed with 10 mL wash buffer (10 mM in PBS<sup>-/-</sup>). Then 0.5 mL of 250 mM elution buffer, and in three additional steps, 1 mL elution buffer was added, and 1 mL samples were collected. The buffer was exchanged for maleimide labeling buffer (MLB) using a PD10 column. For this, the PD10 column was first washed with 5 × 5 mL MLB buffer, the samples were loaded onto the column, and washed with MLB buffer, and the flow-through was collected. To estimate the purity and concentration of the samples, a SDS gel was performed according to [Section 2.2.5.1](#) and [Section 2.2.5.2](#).

### 2.2.5.6 Determination of protein concentrations using the BCA assay

With the bicinchoninic acid (BCA) assay, concentrations of protein solution can be determined. It is based on the formation of Cu<sup>2+</sup>-protein complexes under alkaline conditions followed by a reduction from Cu<sup>2+</sup> to Cu<sup>1+</sup>. BCA then forms a purple complex with Cu<sup>1+</sup>, which can be measured with a plate reader photometer (Smith et al., 1985). The measurement was performed according to the manufacturer's instructions using a Victor plate reader and absorption at 562 nm was measured. For every sample, the mean value of triplicate measurements was calculated. To calculate the protein concentration a calibration curve with BSA (triplicates with 2 - 0.0039 mg/mL was also measured. With linear regression the protein concentrations of the samples were calculated with [Equation 2.5](#)

$$A = m \times C \quad (2.5)$$

where "A" is the absorption, "m" the steepness of the linear regression and "C" the protein concentration.

### 2.2.6 Labeling of proteins, beads and other surfaces using click chemistry

For coupling of the Zn-DPA-azide sensor to streptavidin (SA)-coated solid-phase substrates such as beads or the wells of microtiter plates, a dibenzocyclooctyne (DBCO)-biotin linker was used. For coupling of the Zn-DPA-azide sensor to the TP1170 nanobody a DBCO-maleimide linker were used. The azide and DBCO groups form a stable bond under physiological conditions; this reaction is called strain-promoted azide-alkyne cycloaddition (SPAAC).

In case of the biotin variant of this linker, 66.7 μM DBCO-biotin was incubated either with 1 × 10<sup>6</sup> SA beads or with SA microtiter plates for 30 min at RT in ECS<sup>+/-</sup>. After incubation, the beads/microtiter plates were washed once with ECS<sup>+/-</sup> and 10 μM Zn-DPA-azide in ECS<sup>+/-</sup> was added and incubated for 4 h. Beads were incubated in a tube rotator to ensure an even labeling of the beads.

For labeling TP1170 with Zn-DPA-azide a DBCO-maleimide linker was used, since TP1170 harbors a free cysteine residue. TP1170 was mixed with DBCO-maleimide in a molar ratio of 1 to 1.2 in MLB buffer and incubated overnight at 4 °C. The mixture was then separated from unbound DBCO-maleimide, and the buffer was exchanged to ECS<sup>+/-</sup>, using an Amicon column with a cutoff of 3000 MW at 4 °C and 4600 x g. Additionally, the labeled nanobody was incubated with 10 µM Zn-DPA-azide in ECS<sup>+/-</sup> and incubated for 4 h.

# 3 | RESULTS

The results are divided into four parts. In the first part the hallmarks of P2X7 activation are discussed. These include the uptake of calcium ions ( $\text{Ca}^{2+}$ ) and the shedding of different membrane proteins, the release of adenosine triphosphate (ATP) after nicotinamide adenine dinucleotide ( $\text{NAD}^+$ ) –dependent ADP-ribosylation, as well as the differential potency of nanobodies and a small-molecule inhibitor to specifically block different P2X7 effects. The following four parts describe methods to determine ATP concentrations inside and outside of cells after P2X7 activation.

Part two focuses on FRET-based ATP sensors used in microscopy and flow cytometry. In these experiments the FRET sensors were targeted to different parts of the cells. In addition, as a proof of principle, the sensor proteins were expressed as fusion proteins with the ARTC2.2 specific nanobody s+16 to target the surface of ARTC2.2-expressing cells.

In part three small-molecule sensors for detecting ATP and other purines were investigated. Zinc (Zn)- DPA sensors with different functional groups for coupling to partners were provided by the Department of Chemistry at the University of Hamburg. Specificity tests for different purines, labeling of cells as well as coating of surfaces and labeling of a nanobody using click chemistry are shown. Furthermore, a change in the relative sensitivity against AMP over ATP dependent on the functional group of the sensor could be observed.

Part four shows results using single-wavelength ATP sensors based on the same ATP-binding unit as in the FRET sensor. Their expression in different cell lines, their production as soluble molecules in a prokaryotic expression system, as well as their validation as ATP sensors by measuring bulk ATP concentrations in solution could be shown. Finally, a system to detect ATP release during stimulation of T cells was devised by co-coating beads with the sensor and an anti-CD3 antibody.

## 3.1 HALLMARKS OF P2X7 ACTIVITY

P2X7 activity is accompanied by a variety of downstream effects on cells expressing P2X7 directly as well as cells in close proximity. Briefly, gating of P2X7 is caused by ATP concentrations in the higher micromolar range as well as by low micromolar  $\text{NAD}^+$  concentrations in the presence of ARTs. Gating of P2X7 leads to an influx of  $\text{Ca}^{2+}$ , the shedding of different cell surface proteins, and pore formation, which in turn can lead to cell death. This chapter shows these P2X7 hallmarks using P2X7-specific nanobodies and small-molecule inhibitors to show that the observed effects are P2X7 specific. Furthermore, it is shown that P2X7 activation itself leads to a release of ATP. Therefore, activation of P2X7 via  $\text{NAD}^+$ -dependent ADP-ribosylation was used and ATP release into the supernatant was measured in bulk with a luciferase-luciferin assay.

### 3.1.1 Shedding of CD62L and PI uptake

A good marker for activation of the P2X7 receptor is the measurement of the shedding of L-selectin (CD62L), a molecule mediating T-cell homing to lymph nodes. Yac-1 cells showed a decrease in CD62L expression after 45 min incubation with either 20  $\mu$ M NAD<sup>+</sup> or 250  $\mu$ M ATP, indicated by the median fluorescence intensity (MFI) of CD62L compared to the untreated control (Figure 3.1 A). In cells that were pre-treated with either an inhibitory nanobody (13A7) or a small-molecule inhibitor (A438079), expression of CD62L after treatment remained approximately at the same level as in untreated cells.

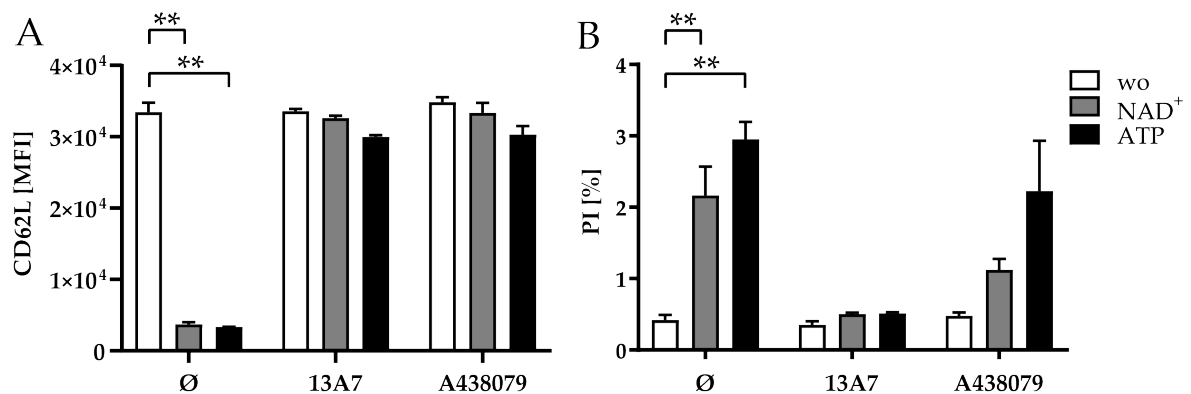


Figure 3.1: Shedding of CD62L and PI uptake after gating of P2X7

Yac-1 cells were either pre-treated or not with the inhibitory P2X7 nanobody 13A7 or the small-molecule inhibitor A438079 for 30 min at RT. Subsequently, the cells were either left untreated or treated with 20  $\mu$ M NAD<sup>+</sup> or 250  $\mu$ M ATP for an additional 45 min at 37 °C. Propidium iodide (10  $\mu$ g/mL) was added directly before analysis on a FACS CantoII. **A** shows the shedding of CD62L as MFI. **B** shows the percentage of YAC-1 cells stained with PI. Statistical significance was calculated using 2way ANOVA and Tukey's multiple comparison test.  $P > 0.05$  ns,  $P \leq 0.05$  \*,  $P < 0.01$  \*\*.

Pore formation is another indicator of P2X7 activation. It allows the passage of molecules up to a size of 900 Da, such as PI. PI can move through that pore and then stains the DNA via intercalation. The uptake of PI was measured parallel to the CD62L shedding and is indicated as the percentage of positively stained cells (Figure 3.1 B). Untreated cells showed no or only a low percentage of labeled cells. Cells treated with NAD<sup>+</sup> or ATP had an elevated level of PI-positive cells compared to the control, whereby ATP had a higher impact on the pore formation compared to NAD<sup>+</sup>. When the cells were pre-treated with 13A7, the percentage of PI-positive cells was at the same level as in the untreated control. The inhibitory effect of A438079 was lower than that of 13A7 as the level of PI-positive cells after treatment with ATP or NAD<sup>+</sup> was higher than in cells that had been pre-treated with 13A7 but lower than in cells that had not been pre-treated with 13A7 a P2X7 inhibitor. Furthermore, the inhibitor A438079 seemed to protect better from ADP-ribosylation than from ATP stimulation.

### 3.1.2 Calcium uptake after P2X7 activation

One main function of the P2X7 receptor is to permit the influx of  $\text{Ca}^{2+}$  after activation by either ATP or ADP-ribosylation. To investigate this consequence of P2X7 activation, cell lines or primary mouse  $\text{CD4}^{+}$  T cells were labeled with the ratiometric  $\text{Ca}^{2+}$  dye Fura-2, and stimulated with ATP. **Figure 3.2 A** shows a representative measurement of Yac-1 cells over a time course of 20 min. The lines in **Figure 3.2 A** represent the mean course of 53 cells treated with ATP (black) and 64 cells additionally pre-treated with 1c81 (dashed), each contained in one field of view. The ratio of 340/380 nm is plotted against the time (seconds). After recording a baseline for 2 min, the cells were stimulated (ST) by the addition of 500  $\mu\text{M}$  ATP. At  $t=15$  min, 2  $\mu\text{M}$  thapsigargin (THG) was added to visualize the maximum signal. THG is an inhibitor for SERCA, which transports  $\text{Ca}^{2+}$  from the cytosol to the ER/SR (Thastrup, 1990; Thomas and Hanley, 1994). When SERCA is blocked, the cytosolic  $\text{Ca}^{2+}$  levels rises, which results in a maximum signal for the  $\text{Ca}^{2+}$  sensor Fura-2 and thus can be used as a positive control.

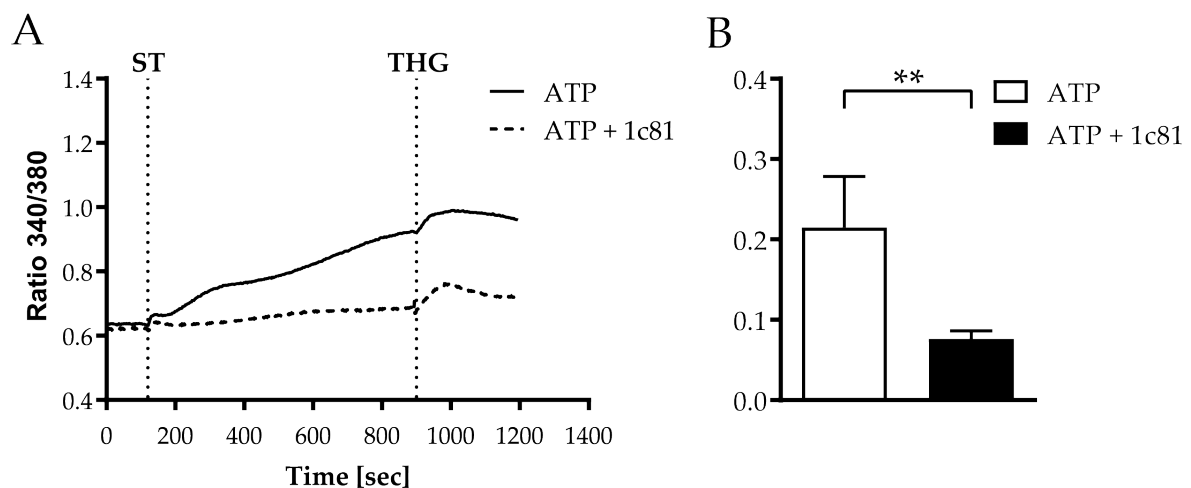


Figure 3.2: Calcium release after gating of P2X7 in Yac-1 cells

Yac-1 cells were loaded with the  $\text{Ca}^{2+}$  dye Fura-2 and stimulated with 500  $\mu\text{M}$  ATP after pre-treatment with or without the inhibitory nanobody 1c81. Cells were measured at a Nikon Eclipse TE300 microscope with excitation at 340 nm and 380 nm. A 10x objective was used, and pictures were taken every 10 sec **A** shows the cytosolic calcium concentration (340/380 nm ratio) against time (seconds). A baseline of 2 min was recorded before addition of ATP (ST). After 13 min THG was added, and recording was continued for an additional 5 min. Each curve represents the mean signal of the cells measured in one field of view. The black curve ( $n=53$ ) represents the cells which received no pre-treatment, and the dashed curve ( $n=64$ ) the cells which were pre-treated with 1c81. **B** shows the collective data of 3 independent experiments with  $n=213$  for cells without pre-treatment (white column) and  $n=152$  for 1c81-treated cells (black column). The bars represent the maximal increase over baseline of the signal after stimulation with ATP. Statistical significance was calculated using the Shapiro-Wilk normality and the paired Student's  $t$  test.  $P > 0.05$  ns,  $P \leq 0.05$  \*,  $P < 0.01$  \*\*.

Cells that were pre-treated with the inhibitory nanobody 1c81 show significant less  $\text{Ca}^{2+}$  influx after ATP than non-pre-treated cells (**Figure 3.2 B**). The figure shows the calcium signal after stimulation but before the addition of THG.

The  $\text{Ca}^{2+}$  influx was also tested in primary  $\text{CD4}^+$  T cells from C57BL/6 mice. The  $\text{CD4}^+$  cells were negatively selected from the spleen of wild type (WT) and P2X7-knock-out (KO) mice and analyzed the same day and the day after preparation. Figure 3.3 A shows the time curve of a representative measurement. The lines represent the mean course of 36 WT cells (black) and 66 P2X7-KO cells (dashed), each measured in one field of view. The ratio of 340/380 nm is plotted against the time in seconds. After recording a baseline for 2 min, the cells were stimulated (ST) by the addition of 500  $\mu\text{M}$  ATP. At  $t=15$  min, 2  $\mu\text{M}$  THG was added to visualize the maximal signal. After the addition of ATP, there was a steep increase of the 340/380 nm ratio that was further increased after addition of THG for the WT  $\text{CD4}^+$  cells. The P2X7-KO  $\text{CD4}^+$  cells showed no increase in the 340/380 nm ratio after stimulation with ATP but increased to a similar level as the WT cells after stimulation with THG. Quantification of the data as the maximal increase in signal over the baseline after the addition of ATP revealed that the increase in signal was significantly higher in WT than in P2X7-KO  $\text{CD4}^+$  cells (Figure 3.3).

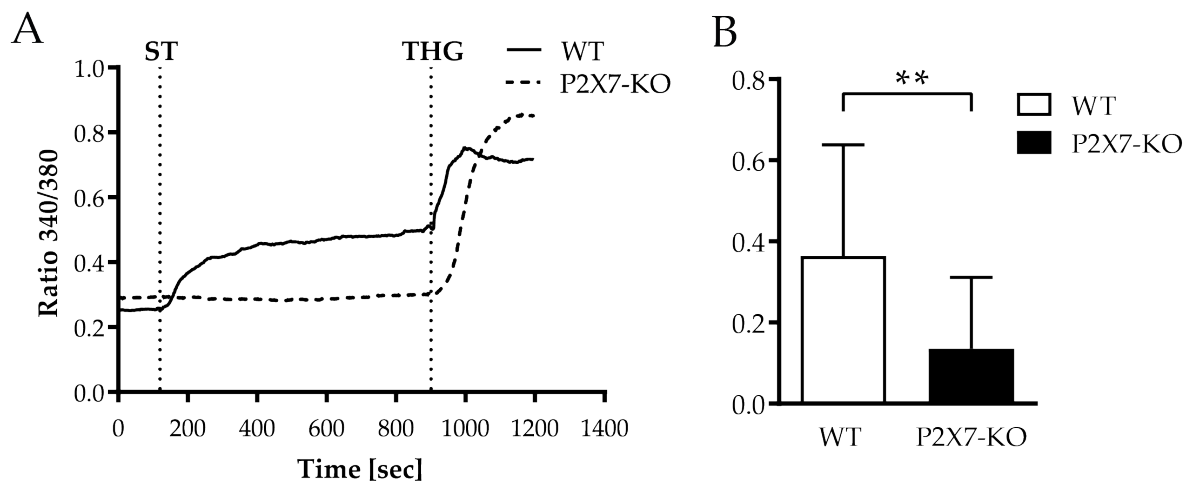


Figure 3.3: Calcium release after gating of P2X7 in primary  $\text{CD4}^+$ T cells

$\text{CD4}^+$  cells from WT C57BL/6 and P2X7 KO mice were loaded with the  $\text{Ca}^{2+}$  dye Fura-2 and stimulated with 500  $\mu\text{M}$  ATP. Cells were measured with a Nikon Eclipse TE300 microscope with excitation at 340 nm and 380 nm. A 10x objective was used, and pictures were taken every 10 sec. **A** shows the cytosolic calcium concentration (340/380 nm ratio) against time (seconds). A baseline of 2 min was recorded before addition of ATP (ST). After 13 min THG was added and recording was continued for 5 min. Each curve represents the mean 340/380 nm ratio of the cells measured in one field of view. The black curve represents  $\text{CD4}^+$ WT cells ( $n=36$ ), the dashed curve represents  $\text{CD4}^+$ P2X7-KO cells ( $n=66$ ). **B** shows the collective data of 5 measurements with 467 WT (white column) and 220 P2X7-KO cells (black column). The bars represent the maximal increase over baseline of the signal after stimulation with ATP. Statistical significance was calculated using the Shapiro-Wilk normality and the paired Student's  $t$  test.  $P < 0.05$  ns,  $P \leq 0.05$  \*,  $P < 0.01$  \*\*.

### 3.1.3 ATP release after gating of P2X7 by $\text{NAD}^+$ -dependent ADP-ribosylation

Measurement of ATP release caused by the gating of P2X7 in cells is difficult because ATP is also the ligand that activates the receptor. To circumvent this issue, P2X7 was gated by  $\text{NAD}^+$ -dependent ADP-ribosylation in a cell line (Yac-1), which expresses both P2X7 and

ARTC2.2. Furthermore, Yac-1 cells do not express CD39, which would hydrolyze the released ATP, which in turn would hamper the measurement of extracellular ATP (Figure 3.4 A). A chemiluminescent assay was used based on the emission of photons by luciferase when it cleaves its substrate luciferin in the presence of ATP. To achieve gating of P2X7, YAC-1 cells were treated with 20  $\mu\text{M}$   $\text{NAD}^+$  for 45 min at 37  $^{\circ}\text{C}$  and measured in a plate reader (Figure 3.4 B). The bars show the ATP concentration in the supernatants of unstimulated (white) or  $\text{NAD}^+$ -stimulated cells (black) that were either pre-treated with inhibitors of P2X7 (nanobody 13A7 and A438079) or ARTC2.2 (nanobody s+16) or not pre-treated. The ATP concentration in the supernatant increased by approximately 15 fold after stimulation with  $\text{NAD}^+$  and without an inhibitory treatment of P2X7. When P2X7 inhibitors were used, the extracellular ATP levels were reduced to the levels of the unstimulated cells. Additionally, all inhibitors seemed to have a similar inhibitory effect on the activation of P2X7.

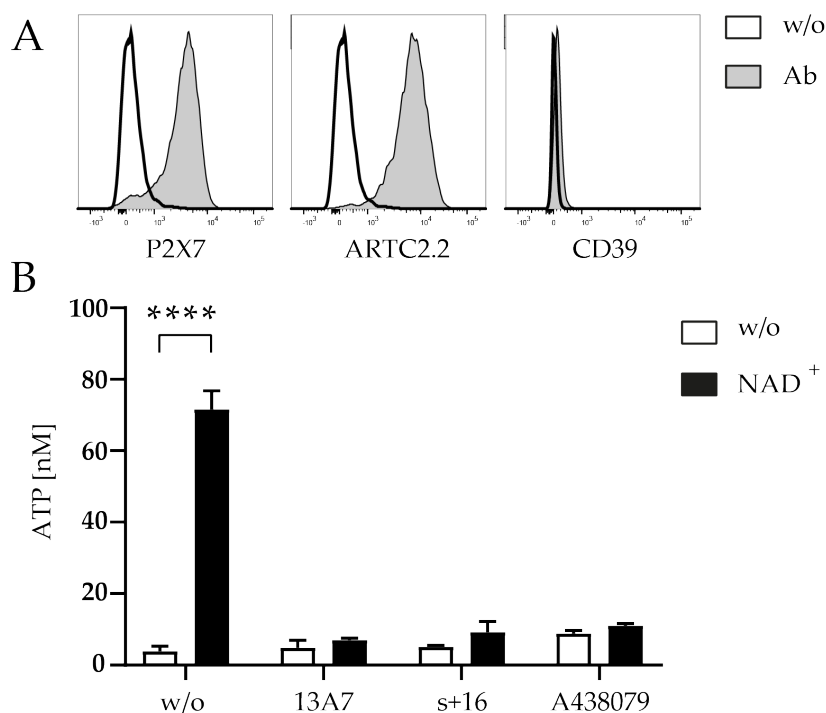


Figure 3.4: Bulk measurement of ATP release after ADP-ribosylation of P2X7

**A** shows the expression levels of P2X7, ARTC2.2, and CD39 on Yac-1 cells. Cells were stained with the corresponding antibodies and measured on a flow cytometer (CantoII). Histograms show unstained (white) against stained cells (gray). **B** shows the release of ATP concentrations in nM in the supernatants of Yac-1 cells after gating of P2X7. Yac-1 were left untreated (white) or were treated for 30 min with 20  $\mu\text{M}$   $\text{NAD}^+$  (black). Additionally cells were pre-treated with inhibitory nanobodies against ARTC2.2 (s+16), or P2X7 (13A7), or with the small-molecule inhibitor A438079 for 30 min. After addition of luciferase/luciferin solution (CellTiter-Glo<sup>®</sup> reagent, Promega), bioluminescence was measured on a plate reader photometer (Victor). Statistical significance was calculated using 2way ANOVA and Tukey's multiple comparison test.  $P > 0.05$  ns,  $P \leq 0.05$  \*,  $P < 0.01$  \*\*,  $P < 0.001$  \*\*\*,  $P < 0.0001$  \*\*\*\*

The results presented in this chapter show the commonly known hallmarks of P2X7 activation. These include the requirement of P2X7 for high ATP concentrations compared to other P2X channels, and the possibility of gating via  $\text{NAD}^+$ /ARTC2.2-dependent ADP

ribosylation. Measured effects of P2X7 activation include shedding of CD62L, the pore formation, and  $\text{Ca}^{2+}$  influx. Additionally, by bulk measurements of ATP in cell supernatants, it could be shown that gating of P2X7 via ADP-ribosylation leads to an efflux of ATP. This provides the basis to look further into the mechanism of local ATP release and its visualization using different approaches such as FRET-based ATP sensors. The next chapters will address this problem.

### 3.2 FRET-BASED ATP SENSORS FOR MEASUREMENT OF CYTOSOLIC AND EXTRACELLULAR ATP

After showing P2X7 related effects on cells upon its activation, visualizations of the P2X7-dependent release of ATP are shown. In the previous section, the  $\text{NAD}^+$ -dependent gating of P2X7 and its resulting release of ATP were shown in bulk measurements using a luciferase/luciferin assay. In this section, local release of ATP will be shown using FRET-based ATP sensors derived from the ATeam sensor (see [Figure 1.5](#)) (Imamura et al., 2009) that were targeted to different compartments of cells. In accord with the different ATP concentrations present at different cellular locations, ranging from low millimolar in the cytosol to low micromolar at the cell surface, these sensors also differ in their sensitivity to ATP. Accordingly, the cytosolic sensor (Bs.cyt) has its maximum sensitivity in the low millimolar range, while the cell surface- and ER-targeted variants (PS3.GPI and PS3.SEKDEL, respectively) show maximal sensitivity in the low micromolar range. As a control, a non-functional variant of the sensors (designated RRKK) was constructed that carries two point mutations that prevent the binding of ATP.

The first part will focus on ATP sensors localized to the cytosol, subsequent parts will deal with FRET-based ATP sensors located to the cell membrane and the ER, and the final part will address the problem of expressing these sensors in primary cells.

#### 3.2.1 *Generation of cell lines expressing FRET-based ATP sensors*

The FRET-based ATP sensors used in this study were all derived from the original cytosolic sensor ATeam (see [Figure 1.5](#)) (Imamura et al., 2009), but modified in order to target them to different cellular compartments. In essence, variants were targeted to the cell surface by introducing a N-terminal leader sequence and a C-terminal GPI membrane anchor or to the ER by introduction of the C-terminal ER-targeting sequence SEKDEL. The variants targeted to the cytosol also carry slight modifications compared to the original ATeam sequences to facilitate cloning of the other variants.

In accord with the different ATP concentrations present at different cellular locations (ranging from low millimolar in the cytosol to low micromolar at the cell surface), these sensors also differ in their sensitivity to ATP. Accordingly, the cytosolic sensor (Bs.cyt) has its maximum sensitivity in the low millimolar range, while the cell surface- and ER-targeted variants (PS3.GPI and PS3.SEKDEL, respectively) show maximal sensitivity in the low

micromolar range. As a control, a non-functional variant of the sensors (designated RRKK) was constructed that carries two point mutations that prevent the binding of ATP.

In this study, the sensors were expressed in the 3T3 mouse fibroblast or the Yac-1 mouse lymphoma cell lines. Stable transfectants were obtained for the cytoplasmic variants in 3T3 cells, and cytoplasmic and cell-surface variants in Yac-1 cells. Stably expressing cell lines were generated by transfection using a cationic polymer (Section 2.2.1.4), and long-term expressing cells were isolated by FACS sorting and limiting dilution culture (Section 2.2.1.8). For studies of P2X7-mediated changes in the distribution of ATP in 3T3 cells, which do not endogenously express P2X7, cell lines co-expressing the kp variant of mouse P2X7 and the sensors were generated by super-transfection of the sensor into previously existing stable P2X7 transfectants (3T3-P2X7kp).

### 3.2.2 Functional validation of the sensor and visualization of cytosolic ATP

#### 3.2.2.1 Visualization of cytosolic ATP by flow cytometry

To manipulate cytosolic ATP levels, the cells were either treated with the mitochondrial uncoupling agent CCCP in order to inhibit ATP production, or with ATP to induce P2X7-mediated ATP release. A 30 sec baseline was recorded before the addition of either buffer alone (ECS<sup>+/-</sup>), 10  $\mu$ M CCCP, or 500  $\mu$ M ATP, and further measurement for 3 min.

3T3 cells stably transfected with the cytosolic variants Bs.cyt and RRKK.cyt of the FRET-based ATP sensor are shown in Figure 3.5 A, with bright-field and fluorescent (GFP channel) images. Both sensors show a high level of expression. To test the functionality of these sensors, the FRET signals of these cells as well as their P2X7-expressing counterparts, were measured by flow cytometry using a FACS Canto II under conditions suspected to affect the cytosolic ATP content. To manipulate cytosolic ATP levels, the cells were either treated with the mitochondrial uncoupling agent CCCP in order to inhibit ATP production, or with ATP to induce P2X7-mediated ATP release (Figure 3.5 B). A 30 sec baseline was recorded before the cells were treated with either buffer alone (solid black line), CCCP (dashed black line), or 500  $\mu$ M ATP (grey line) and measured for a further 3 min. Cells expressing Bs.cyt, regardless of whether they co-express P2X7 or not, show a steep initial decrease in the FRET signal after treatment with the uncoupling agent CCCP with a recovery of the FRET signal after reaching a minimum of 94 % or 96 %, compared to the baseline. Treatment with ATP induces a steady linear decrease of the FRET signal only in cells co-expressing Bs.cyt and P2X7kp. 3T3 cells expressing the non-functional variant of the FRET sensor RRKK.cyt do not show a change of the FRET signal after treatment with either CCCP or ATP (Figure 3.5 C). The data from three independent experiments are summarized in Figure 3.5 D and E. The functionality of these sensors was demonstrated by treating the cells with agents known or suspected to cause depletion of cytosolic ATP. Furthermore, this section shows that the FRET signals from these sensors can be conveniently measured by flow cytometry. In addition to validating the functional Bs.cyt sensor as a suitable tool for reporting intracellular ATP concentrations, the experiments performed in this section also validated the non-functional sensor RRKK.cyt as a negative control, since it did not show any change in

FRET under conditions that caused FRET changes in Bs.cyt. The section also shows that the change in intracellular ATP observed in 3T3 cells co-expressing P2X7kp after addition of exogenous ATP is mediated by P2X7, since it did not occur in cells that did not express P2X7. To investigate the utility of these sensors in a microscopic setup, the sensor-expressing cells were studied in imaging experiments in the following chapters.

Taken together, this section shows the generation of stable 3T3-derived cell lines expressing either the FRET-based ATP sensors alone or co-expressing them with P2X7, with expression levels close to 100 %. The functionality of these sensors was demonstrated by treating the cells with agents known or suspected to cause depletion of cytosolic ATP. Furthermore, this section shows that the FRET signals from these sensors can be conveniently measured by flow cytometry. In addition to validating the functional Bs.cyt sensor as a suitable tool for reporting intracellular ATP concentrations, the experiments performed in this section also validated the non-functional sensor RRKK.cyt as a negative control since it did not show any change in FRET under conditions that caused FRET changes in Bs.cyt. The section also shows that the change in intracellular ATP observed in 3T3 cells co-expressing P2X7kp after the addition of exogenous ATP is mediated by P2X7 since it did not occur in cells that did not express P2X7. To investigate the utility of these sensors in a microscopic setup, the sensor-expressing cells were studied in imaging experiments in the following chapters.

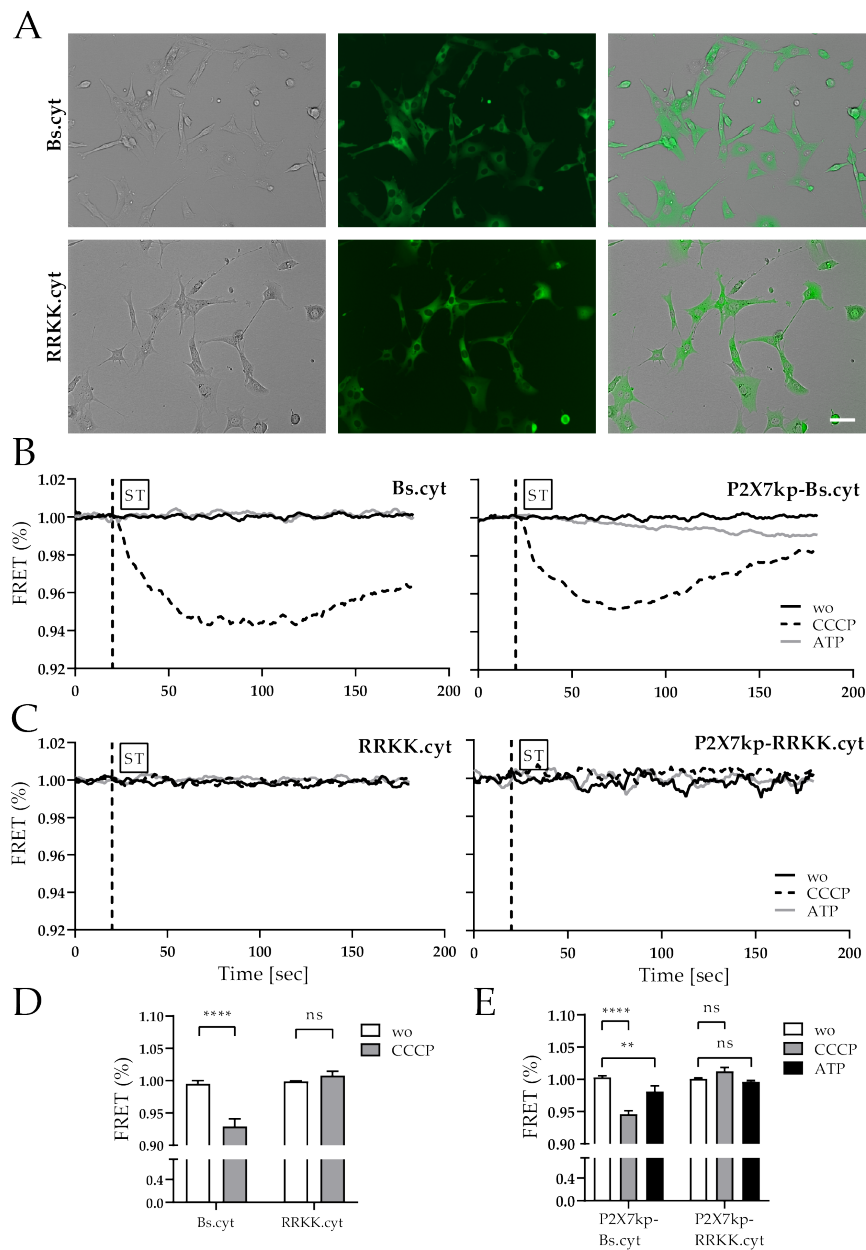


Figure 3.5: Expression and function of cytosolic FRET sensors

**A** Shown are fluorescent and bright-field images of 3T3 cells stably transfected with either the cytosolic variants of either the functional FRET-based ATP sensor Bs.cyt (first row) or the non-functional variant RRKK.cyt (second row). Panels on the left show bright-field, middle panels show fluorescent (GFP channel) images, and panels on the right show an overlay of both. The scale bar is 50  $\mu\text{m}$ . **B** shows kinetic measurements of the FRET signal of 3T3-Bs.cyt cells as measured by flow cytometry on a FACS Canto II. FRET was calculated as the ratio of the signals from the 450/50 nm and 510/50 nm channels excited by the 405 nm laser. The FRET signal is displayed in % (normalized to the baseline) against the time. ST shows the time point (20 sec) at which a stimulus was added consisting of either 10  $\mu\text{M}$  CCCP (black, dashed), 500  $\mu\text{M}$  ATP (grey), or the ECS<sup>+/−</sup> buffer control (black). The right panel shows cells that were additionally transfected with the kp variant of mouse P2X7. **C** shows the same as in **B**, but for cells expressing the non-functional variant RRKK.cyt. **D** and **E** show the complete data of three FACS experiments with cells expressing the sensor alone (**D**) or in combination with P2X7 (**E**). Statistical significance was calculated using 2way ANOVA and Tukey's multiple comparison test.  $P > 0.5$  ns,  $P \leq 0.5$  \*,  $P < 0.1$  \*\*,  $P < 0.01$  \*\*\*,  $P < 0.001$  \*\*\*\*.

### 3.2.2.2 Visualization of cytosolic ATP by live cell imaging

The cells described in the previous section were used to visualize changes in the intracellular ATP concentration by live-cell imaging. Figure 3.6 shows an image series of 3T3 cells stably transfected with the FRET-based ATP sensor variants Bs.cyt and RRKK.cyt recorded on a fluorescent microscope. Shown are recorded images at the time points 0, 200, 400, and 600 sec with a pseudocolor “staining” generated with the Fiji software. The color scale indicates the relative ATP concentration with blue (low ATP concentration), yellow (intermediate ATP concentration), and red (high ATP concentration). After recording a baseline for 2 min, the uncoupling agent CCCP was added to the cells. This agent causes the uncoupling (inhibition of oxidative phosphorylation) of the electron transport chain and thus inhibits the ATP synthase function, which leads to a decrease of the ATP concentration in the cell. In contrast to cells carrying the non-functional RRKK.cyt variant, cells expressing the Bs.cyt variant show a decrease in their FRET signal upon addition of CCCP. Figure 3.6 B shows the corresponding traces of the FRET signals over time. The traces represent the mean FRET signal of all cells within a field of view at a given time point. The kinetic shows what is already visible in the fluorescent images: the decrease of the FRET signal point. The kinetic shows what is already visible in the fluorescent images; the decrease of the FRET signal following administration of CCCP in the functional variant Bs.cyt and no or only a minor change in FRET of the RRKK.cyt variant.

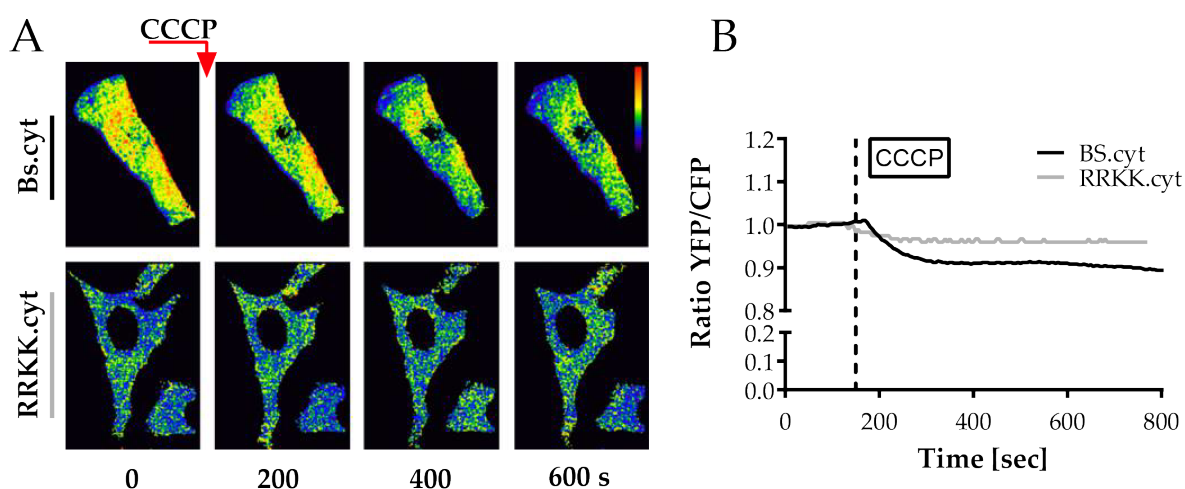


Figure 3.6: Visualization of cytosolic ATP concentrations by live cell imaging

A Shown are fluorescent images from live cell imaging of 3T3 cells transfected with the Bs.cyt and RRKK.cyt variants of the FRET-based ATP sensor. Cells were recorded for 10 min, and after recording a 2 min baseline the cells were treated with 10  $\mu$ M CCCP. Ever 10 sec a picture was taken of the CFP (donor) and YFP (acceptor) channel. The FRET ratio (YFP/CFP) was calculated, and the cells were pseudocolor-stained using the imaging software Fiji. B. The corresponding traces of the FRET ratio from cells expressing RRKK.cyt (grey, n=4 cells) or Bs.cyt (black, n=7 cells) over time are shown. Every curve is the mean FRET signal of all cells in the field of view of the recording.

### 3.2.3 Use of FRET-based ATP sensors to monitor cytosolic depletion of ATP following complement-dependent cytotoxicity (CDC)

To get an idea of how the kinetics of P2X7-mediated depletion of ATP from the cytosol, as visualized in the previous section by kinetic FACS measurements and live-cell imaging, compare with ATP loss through other types of pores, complement-dependent cytotoxicity (CDC) was induced in Yac-1 cells expressing Bs.cct and RRKK.cyt. For the CDC assay, serum as a source of complement, and antibodies targeting specific antigens on the membrane of the cells of interest (such as CD62L), generally required.

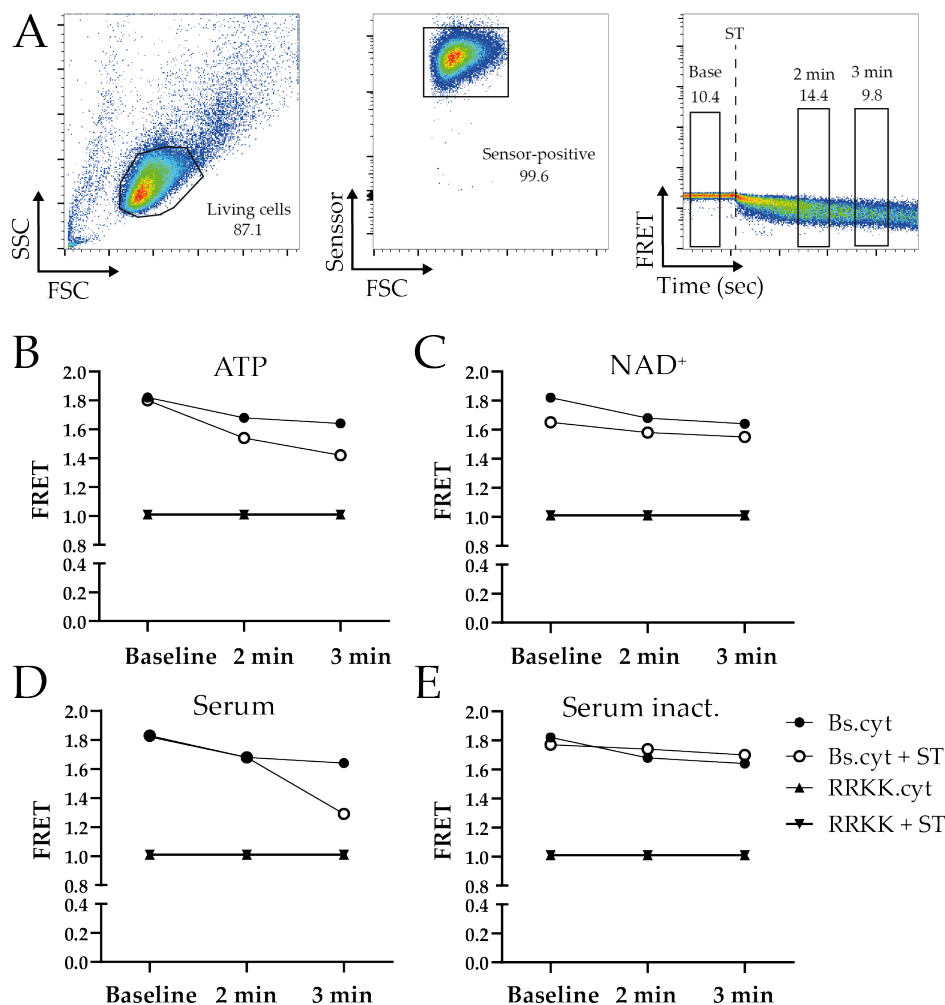


Figure 3.7: Monitoring intracellular ATP depletion after CDC in Yac-1 cells with FRET-based ATP sensors

A shows the gating strategy for the kinetic measurement of ATP release from Yac-1 cells expressing Bs.cyt or RRKK.cyt, after treatment with a stimulus (ST). A baseline was recorded for 60 sec, then a stimulus was added and recording was continued for an additional 3 min. Sensor-positive Yac-1 cells were gated and used for the graphs in B - E. Graphs in B - E show the FRET values of the Yac-1 cells expressing Bs.cyt or RRKK.cyt, at the baseline, 2 min, and 3 min. Cells were stimulated with 500  $\mu$ M ATP (B), 20  $\mu$ M NAD<sup>+</sup> (C), 12.5% pooled human serum (D), and 12.5% inactivated human serum (E).

However, when using human serum on Yac-1 cells, antibodies targeting specific antigens were not needed because human serum alone was sufficient to trigger CDC in these cells (Data not shown). Therefore, online human serum was used to induce CDC in Yac-1 cells, and measured the subsequent loss of ATP by kinetic flow cytometry (Figure 3.7). Figure 3.7 A shows the gating strategy used in these experiments. Yac-1 cells were first gated for “Living cells” and of these cells, only sensor-positive cells were used for the analysis. For quantification, three time points were taken from the kinetic measurement (Baseline, 2 min, and 3 min). Measurements at each time-point included all cells within a 30 sec period. Figure 3.7 B to E shows the levels of FRET signals for these time points in Yac-1 cells expressing Bs.cyt or RRKK.cyt, which were treated with 500  $\mu$ M ATP (B), 20  $\mu$ M NAD<sup>+</sup> (C), 12.5 % serum (D), or 12.5 % heat-inactivated serum (E). The non-functional variant RRKK showed no change in FRET with any stimulus present. In cells expressing Bs.cyt, ATP reduced the FRET signal in a manner similar to Figure 3.5 B. Cells treated with serum showed a delay of approximately 2 min before beginning to lose ATP, but then responded with a relatively steep decrease in the FRET signal. On the other hand, the inactivated serum did not cause any loss of ATP from the cells, supporting the notion that the effect of the non-inactivated serum was indeed due to complement. Yac-1 cells treated with NAD<sup>+</sup> showed only a minimal change in FRET in this experiment.

#### 3.2.4 Use of FRET-based ATP sensors to monitor cytosolic depletion of ATP following gating of P2X7

After demonstrating their functionality, the cytosolic FRET-based ATP sensors were used to investigate changes in the cytosolic ATP concentration caused by gating of P2X7. Therefore, 3T3 cells stably expressing either Bs.cyt alone or together with P2X7kp were treated with 500  $\mu$ M ATP. Figure 3.8 shows pseudocolor images of the FRET signals in the described cells at 0, 200, 400, and 600 sec. After the addition of ATP (at time point 2 min), the FRET signal inside the cells decreased, as indicated by the color change from red to green (Figure 3.8 A). Cells expressing only the Bs.cyt variant of the FRET sensor showed only a minor change in the FRET signal. The corresponding traces show an estimated 20 % reduction of the FRET signal (Figure 3.8 B).

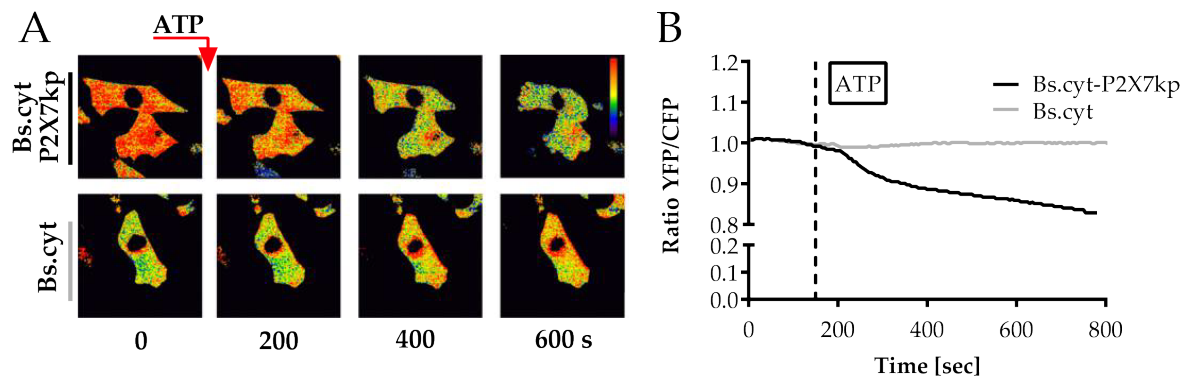


Figure 3.8: Gating of P2X7 is associated with a depletion of cytosolic ATP

**A** Shown are fluorescent images from live cell imaging of 3T3 cells transfected with Bs.cyt alone or in combination with the P2X7kp receptor. Cells were recorded for 10 min and after recording a 2 min baseline the cells were treated with 500  $\mu$ M ATP. Every 10 sec a picture was taken of the CFP (donor) and YFP (acceptor) channel. The FRET ratio (YFP/CFP) was calculated, and the cells were pseudocolor-stained using the imaging software Fiji. **B** shows the corresponding traces of the FRET ratio from cells expressing Bs.cyt (grey, n=10 cells) or Bs.cyt/mP2X7 (black, n=7 cells) over time. Every curve represents the mean FRET signal of all cells in the field of view of the recording.

A similar experiment, as shown in [Figure 3.8](#), was performed using Yac-1 cells ([Figure 3.9](#)). Yac-1 cell endogenously express P2X7 and ARTC2.2, and thus only needed to be transfected with the FRET sensor (the Bs.cyt variant in this case). As in the previous experiment, the cells were treated with 500  $\mu$ M ATP after recording a 2 min baseline. To demonstrate that observed changes in the intracellular ATP concentration after adding exogenous ATP in these cells were indeed mediated by P2X7, an aliquot of the cells was pre-treated with the inhibitory P2X7 nanobody 13A7 for 30 min. After stimulation with ATP the Yac-1 cells showed a decrease in the FRET signal over time (color change from yellow/green to blue), whereas the cells treated with the 13A7 nanobody showed almost no change in the FRET signal ([Figure 3.9 A](#)). The kinetic graph of the FRET signal indicates a decrease of 20 % in the FRET signal after gating of P2X7 ([Figure 3.9 B](#)). Additionally, after gating of P2X7 “blebbing” was observed on untreated Yac-1 cells but not on the cells pre-treated with 13A7 ([Figure 3.9 A](#)).

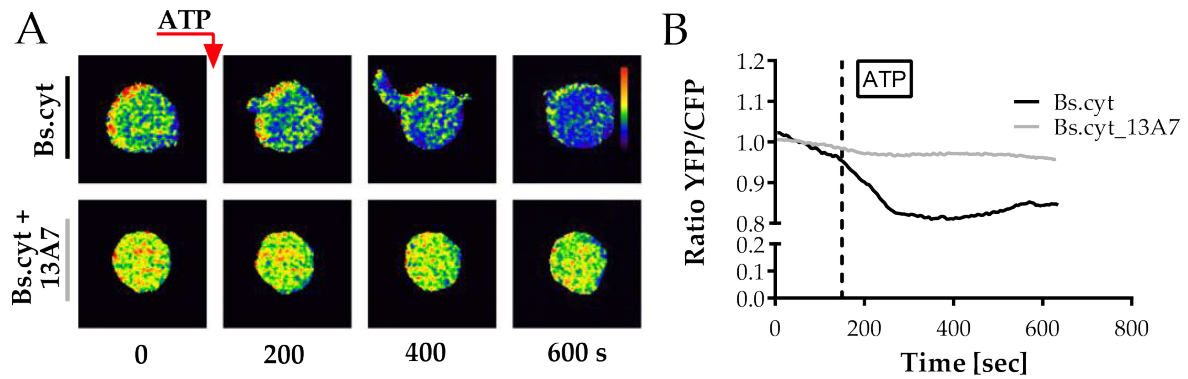


Figure 3.9: Visualization of P2X7-dependent cytosolic ATP depletion in Yac-1 lymphoma cells  
**A** Shown are fluorescent images from live cell imaging of Yac-1 cells transfected with the Bs.cyt variants of the ATP FRET sensor and pre-treated or not with the P2X7 inhibitory nanobody 13A7. Cells were recorded for 10 min, and after recording a 2 min baseline the cells were treated with 500  $\mu$ M ATP. Every 10 sec a picture was taken of the CFP (donor) and YFP (acceptor) channel. The FRET ratio (YFP/CFP) was calculated, and the cells were pseudocolor-stained using the imaging software Fiji. **B** shows the corresponding traces of Yac-1 cells pre-treated in the absence (black, n=8 cells) or presence (grey, n=9 cells) of 13A7. Every curve represents the mean FRET signal of all cells in the field of view of the recording.

### 3.2.5 Use of FRET-based ATP sensors to visualize extracellular ATP

After using FRET-based ATP sensors to visualize and measure changes in ATP concentrations inside of cells, these sensors were targeted to the cell membrane of 3T3 cells to measure released ATP after gating of P2X7. As was done for the cytosolic sensors, 3T3 cells (that do not express P2X7) were transfected with the PS3.GPI and the RRKK.GPI variants of the sensor (Figure 3.10). These constructs contain an Ig leader sequence that mediates transport of the sensor proteins to the cell membrane, as well as a GPI anchor sequence that mediates covalent attachment to the membrane. In accord with the low ATP concentrations in the extracellular space, these sensors carry a sensing unit (PS3) with a maximum sensitivity in the micromolar range. The same inactivating mutations in the cytosolic sensors were incorporated into the PS3 constructs to create non-functional RRKK variants to be used as a negative control. Figure 3.10 A shows fluorescent images taken at 0, 200, 400, and 600 sec that were pseudocolor stained using Fiji software. After recording a 2 min baseline, 500  $\mu$ M ATP was added to the cells. Immediately after addition of ATP there was a steep increase in the FRET signal in cells expressing the PS3.GPI variant, which is indicated by the color change from yellow to orange/red. The cells expressing the RRKK.GPI on the other hand showed no or little change in the FRET signal (Figure 3.10 A).

Figure 3.10B shows the corresponding traces of the recorded cells. Here, the differences in the FRET signal over time between the cells expressing the PS3.GPI and the RRKK.GPI become apparent. The traces demonstrate an increase of approximately 15 % in the FRET signal after the addition of ATP as compared to the control (Figure 3.10 B).

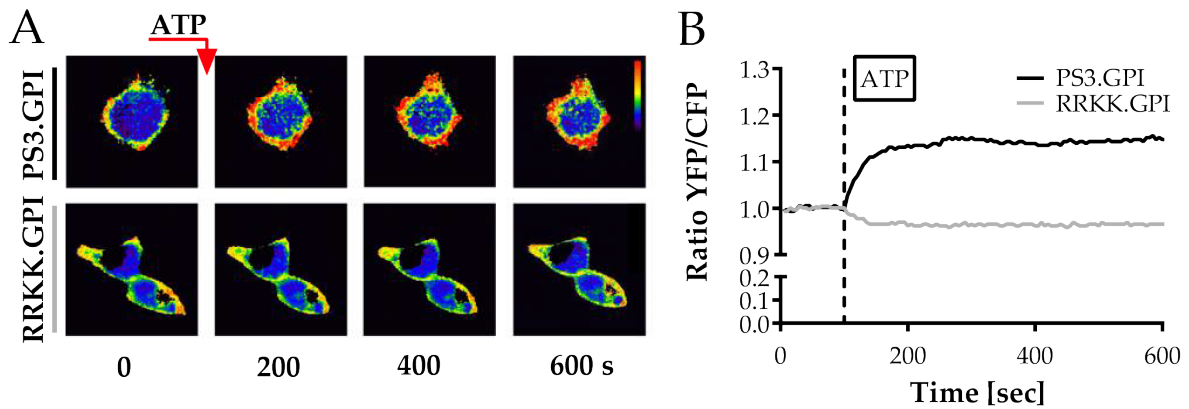


Figure 3.10: Validation of the membrane bound ATP FRET sensor

**A** Shown are fluorescent images from live cell imaging of 3T3 cells transfected with the PS3.GPI and RRKK.GPI membrane bound variants of the FRET-based ATP sensor. Cells were recorded for 10 min and after recording a 2 min baseline the cells were treated with 500  $\mu$ M ATP. Every 10 sec a picture was taken of the CFP (donor) and YFP (acceptor) channel. The FRET ratio (YFP/CFP) was calculated, and the cells were pseudocolor-stained using the imaging software Fiji. **B** shows the corresponding traces of cells expressing the non-functional sensor RRKK.GPI (grey line, n=3 cells) or functional PS3.GPI (black line, n=3 cells). Every curve is the mean FRET signal of all cells in the field of view of the recording.

After demonstrating the functionality of the FRET-based ATP Sensors targeted to the cell membrane, the next step was to test whether these sensors can detect ATP released from the cytosol at the cell surface. This question is difficult to address using the model of P2X7-mediated ATP release, since gating of P2X7 usually requires administration of exogenous ATP precisely at the location where ATP released from the cell should be detected. Therefore it was made use of the fact that mouse P2X7 can also be activated unconventionally by NAD<sup>+</sup>-dependent ADP-ribosylation in the presence of the ecto-ADP-ribosyltransferase ARTC2.2. Hence, 3T3 cells expressing P2X7kp were co-transfected with ARTC2.2 and PS3.GPI. These cells were then treated with 20  $\mu$ M NAD<sup>+</sup> to induce gating of P2X7 through ADP-ribosylation, which then should lead to an efflux of cytosolic ATP.

**Figure 3.11 A** shows pseudocolor-stained images (generated using Fiji) of the FRET signal from the triple-transfected cells at time points 0, 200, 400 and 600 sec. Double-transfected cells expressing PS3.GPI and ARTC2.2, but lacking P2X7, were used as a control. After the addition of NAD<sup>+</sup>, the triple-transfected cells showed an increase in the FRET intensity, which is indicated by the color change of the membrane from blue/green to yellow (**Figure 3.11 A**).

Compared to **Figure 3.10**, this signal is weaker, as the amount of released ATP is lower than the added concentration of ATP added from the outside in that experiment (500  $\mu$ M). 3T3 cells which do not express P2X7kp showed an initial increase of the FRET signal, but then returned to the level of the baseline after approximately 80 sec. The corresponding kinetic of this experiment shows this behavior more precisely (**Figure 3.11 B**). After stimulation with NAD<sup>+</sup>, there was a linear increase of the FRET signal until it reached a maximum of approximately 11.5% compared to the baseline that remained stable until the end of the measurement. The FRET signal of the cells lacking P2X7 returned to the baseline level after

a short increase and stayed at that level for the rest of the measurement.

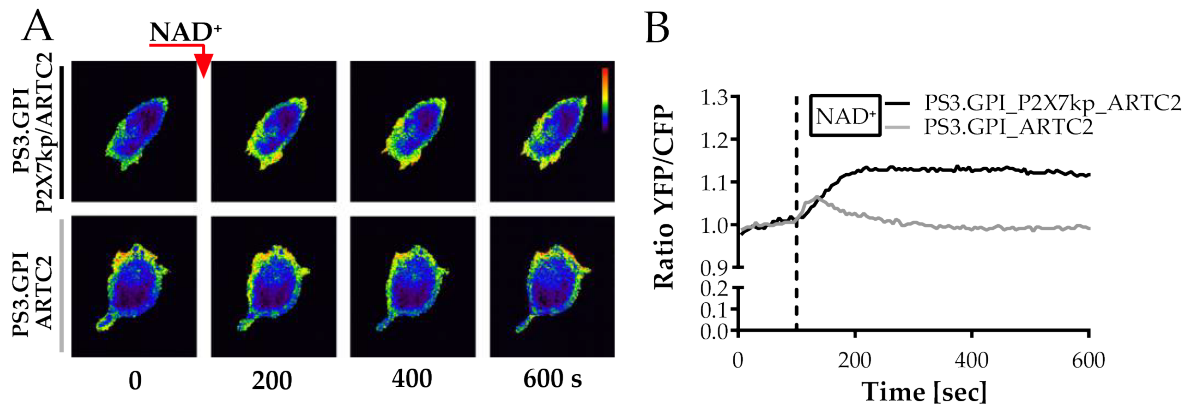


Figure 3.11: Release of ATP after ADP-ribosylation of P2X7

**A** Shown are fluorescent images from live cell imaging of 3T3 cells co-transfected with the membrane bound FRET-based ATP sensor PS3.GPI and ARTC2.2 alone or in combination with P2X7kp. Cells were recorded for 10 min, and after recording a 2 min baseline the cells were treated with 20  $\mu$ M NAD<sup>+</sup>. Every 10 sec a picture was taken of the CFP (donor) and YFP (acceptor) channel. The FRET ratio (YFP/CFP) was calculated, and the cells were pseudo color stained using the imaging software Fiji. **B** The right panel shows the corresponding traces of the triple-transfected cells (black line, n=4 cells) compared to double-transfected cells lacking P2X7 (grey line, n=2 cells) over time. Every curve is the mean FRET signal of all cells in the field of view of the recording.

### 3.2.6 Transgenic mice, AAV and lentiviral production of FRET-based ATP sensors

Another goal of this thesis was to generate transgenic mice that express the different variants of the FRET-based ATP sensors. Therefore the sequence of the Bs.cyt and PS3.GPI variants under the control of a CMV promotor was introduced via pronuclear injection into three- to four-week-old C57BL/6 embryos. The blood and tissue samples of the F1 generation were subsequently analyzed. The erythrocytes in the blood samples were lysed and the remaining cells were then analyzed for FRET-based ATP sensor expression in the FACS. Genomic DNA was isolated from the tissue samples and genotyped with specific primers for the  $\epsilon_0$  ATP binding domain of these sensors. While the inserted sequence of the FRET sensor could be verified via genotyping, the sensors were not expressed, as there was no fluorescence detected in the blood samples (data not shown).

A subsequent goal was to generate adeno-associated virus (AAV) carrying the sequence for the FRET sensors in order to transduce primary human and mouse T cells. A potential problem with this approach is the homologous recombination by the virus of the two chromophore regions of the FRET sensor (Komatsubara, M. Matsuda, and Aoki, 2015). The CFP and Venus fluorescent proteins in the sensor both originate from GFP and therefore have a high homology of approximately 95%. To circumvent this problem, the sequence of the CFP in the FRET sensor was codon-modified to reduce homology between the two regions on the nucleotide level while retaining the coding sequence. The codon modification of CFP reduced the homology of these fluorescent proteins to 72%. It could be demonstrated

that the FRET sensors with the modified CFP were still functional, but the cloning of the FRET sensors into the viral vectors could not be completed within the time-frame of the project.

In the following chapter, small-molecule Zn-DPA sensors, first described by Moro, Cywinski, et al. (2010), will be analyzed, to detect ATP.

### 3.3 SMALL-MOLECULE SENSORS FOR DETECTION OF EXTRACELLULAR ATP

Another approach for the measurement of ATP on the cell surface is the use of small-molecule ATP Sensors. In this work, these sensors are based on a Zn-DPA backbone with a moiety that allows the attachment of different groups, such as azide, alkyls, or carbon chains of different lengths. Here, sensors with azide (Zn-DPA-azide), cholesterol groups, and carbon chains (Zn-DPA-C(n)) are tested. For the labeling of e.g., cells with Zn-DPA-azide a click-chemistry approach was necessary, whereas the Zn-DPA-C(n) and cholesterol variants were designed to be directly attached to the cell membrane due to their lipophilic properties.

In the following chapters, these sensors are first tested in solution and then attached to different surfaces such as the membrane of cells or SA-coated beads microtiter plates.

#### 3.3.1 Soluble Zn-DPA sensors

The first goal was to find out whether these small-molecule sensors function as intended. These sensors are based on Moro, Cywinski, et al. (2010) and show an increased “green” fluorescence in the presence of nucleotides with a preference for adenine nucleotides such as ATP and ADP. To verify the functionality of these Zn-DPA sensors, they were measured in solution in the presence of different nucleotides. Figure 3.12 A<sup>1</sup> shows the fluorescent emission changes of 10  $\mu\text{M}$  Zn-DPA in the presence of 20  $\mu\text{M}$  of different nucleotides, such as ATP, ADP, AMP, and GTP. Zn-DPA has an emission maximum at 535 nm and shows the strongest emission in the presence of ADP and ATP, with a reduction of fluorescence in the presence of e.g., pyrophosphate (PPi) compared to the absence of any nucleotide (blank). The goal was to measure ATP with this sensor. Therefore a dose-response curve with ATP concentrations of 1, 3, 10, 30, 100, 300, 1000, and 3000  $\mu\text{M}$  in the presence of 10  $\mu\text{M}$  Zn-DPA was measured (Figure 3.12 B). The dose-response curve shows an ATP concentration-dependent fluorescent signal (sigmoidal curve) reaching saturation at around 1000  $\mu\text{M}$  ATP. To investigate if the increase of the fluorescent signal of Zn-DPA in presence of ATP can be reversed, the sensor was measured alone, with 100  $\mu\text{M}$  ATP, and with 1 U of apyrase in combination with 100  $\mu\text{M}$  ATP, every 2.5 min for 30 min (Figure 3.12 . C). Zn-DPA with ATP shows an increase of approximately 20% in the fluorescence compared to the control (Zn-DPA without ATP). In the presence of apyrase, the fluorescence shows a steep decline and reaches the fluorescence level of the control after 15 min.

<sup>1</sup> This measurement was performed by Alexander Laubach, Department of Chemistry, University of Hamburg

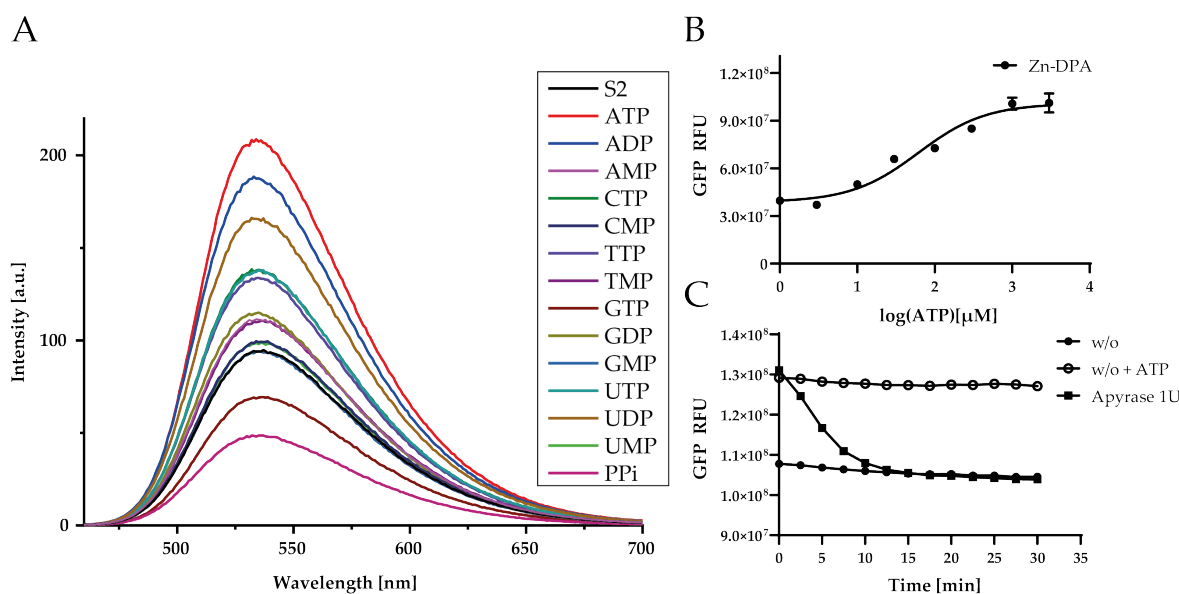


Figure 3.12: Functionality testing of Zn-DPA sensors

**A** Zn-DPA fluorescence in the presence of different nucleotides (data from A. Laubach)  $10 \mu\text{M}$  sensor was tested with  $20 \mu\text{M}$  of the different nucleotides. **B** Dose-response curve of Zn-DPA with ATP concentrations from  $1 \mu\text{M}$  to  $3 \text{mM}$ . **C** Reversibility of the Zn-DPA fluorescence signal in the presence or absence of  $1 \text{U}$  apyrase. Measurements were made every  $2.5 \text{min}$  for  $30 \text{min}$ .

After testing the reactivity of Zn-DPA against ATP, the azide variant of this sensor was also tested. To test whether the azide modification influenced the sensitivity or selectivity of the sensor, additional dose-response curves were recorded with Zn-DPA-azide. Surprisingly, the addition of the azide group changed the rank order of sensitivity towards nucleotides compared to the unmodified sensor. A particular change was noted in the sensitivity to AMP. Whereas the Zn-DPA sensor showed a higher sensitivity for ATP and ADP compared to AMP (Figure 3.12 A), the Zn-DPA-azide sensor showed the highest emission in the presence AMP and other monophosphates (Figure 3.13 A<sup>2</sup>). Additionally, Zn-DPA-azide was measured with different ATP (Figure 3.13 B) and AMP (Figure 3.13 C) concentrations ( $1, 3, 10, 30, 100, 300, 1000,$  and  $3000 \mu\text{M}$ ) to generate dose-response curves. A dose-dependent increase of the fluorescence signal was observed for both sensors. Interestingly, for both sensors, the EC<sub>50</sub> values for AMP were lower than those for ATP.

This chapter shows the general functionality of the small-molecule sensors Zn-DPA and Zn-DPA-azide to respond to nucleotides such as ATP and AMP in a dose-dependent manner in solution. The next chapter will focus on the feasibility of attaching these sensors to different surfaces such as SA beads using a click-chemistry approach.

### 3.3.2 Targeting of Zn-DPA-azide sensor variants to cell membranes

To target the Zn-DPA-azide sensor to different surfaces, a click-chemistry approach was used. Here, the SPAAC reaction was applied, where DBCO-biotin was used as a reaction partner for Zn-DPA-azide (Figure 3.14). The SPAAC reaction can be performed under physiological

<sup>2</sup> This measurement was performed by Alexander Laubach, Department of Chemistry, University of Hamburg

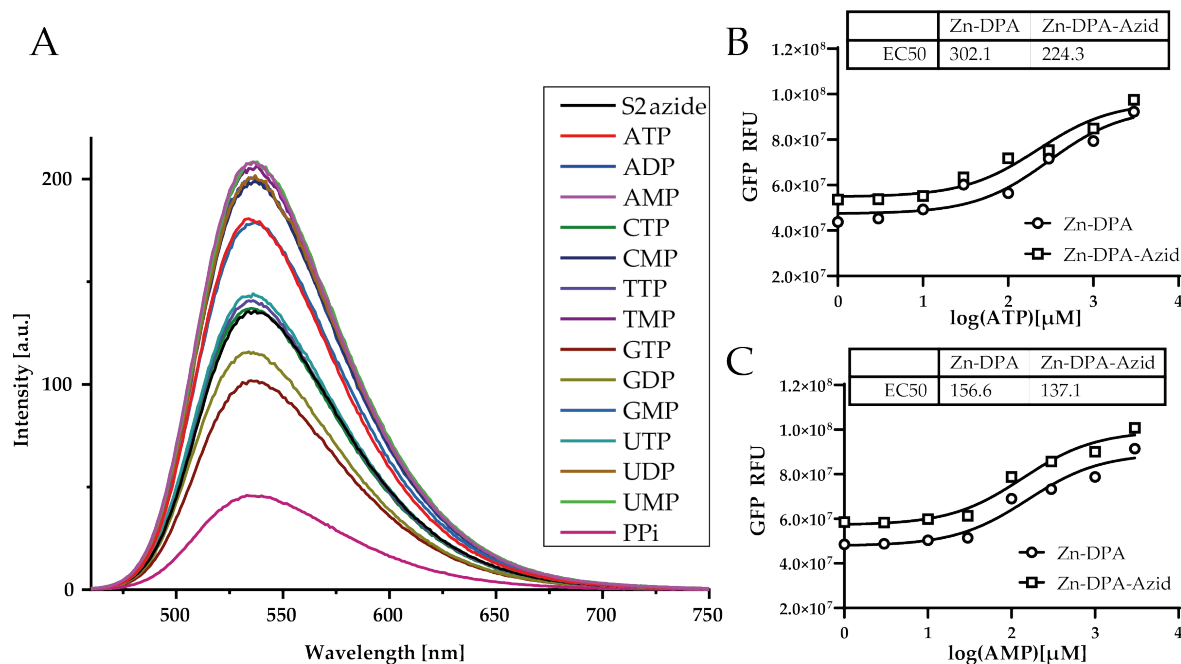


Figure 3.13: The Zn-DPA-azide variant of the small-molecule ATP sensor shows an altered specificity for ATP

**A** Zn-DPA-azide fluorescence in the presence of different nucleotides (A. Laubach). 10 μM sensor was tested with 20 μM of the different nucleotides. **B** and **C** Dose-response-curves of Zn-DPA/Zn-DPA-azide with ATP and AMP concentrations from 1 μM to 3 mM.

conditions (ECS<sup>-/-</sup>) with a two-fold molar excess of the azide molecule compared to the DBCO molecule. The subsequent labeling of the SA-coated surfaces (beads or a microtiter plate) with the sensor/DBCO-biotin complex was also performed under physiological conditions. After washing the labeled beads/96-well plates, the actual measurements can be done.

As previously shown in Section 3.3.1, the Zn-DPA-azide sensor had an altered specificity for specific nucleotides compared to the original Zn-DPA sensor. Here it was tested whether the Zn-DPA-azide sensor still functioned and whether it retained its altered nucleotide specificity when it was attached to a surface. Figure 3.15 A shows a fluorescence measurement of a labeled 96-well SA-plate. Wells containing only the buffer and wells that were only labeled with DBCO-biotin show a similar low level of fluorescence. Wells, also labeled with the Zn-DPA-azide sensor, show an approximately 2.5 × fold change in fluorescence compared to the controls. In the presence of 10, 100, and 1000 μM ATP, there is a slight increase in the fluorescence signal, where 1000 μM ATP shows the highest increase compared to the absence of ATP.

Figure 3.15 B shows the fluorescence of Zn-DPA-azide bound to a SA-plate in combination with 10, 100, and 1000 μM ATP, ADP, or AMP. Here AMP shows the lowest fluorescence compared to ATP and ADP. Furthermore, the sensitivity to AMP is shifted compared to the measurements performed in solution with this sensor (Figure 3.13). SA-Beads were also labeled with the Zn-DPA-azide sensor, but they did not show a detectable change in the

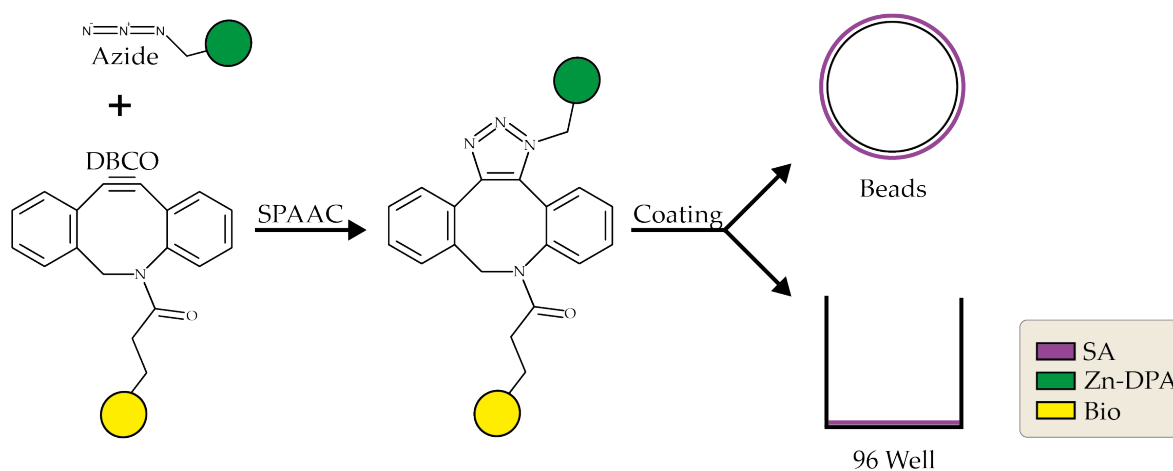


Figure 3.14: Labeling of SA surfaces with Zn-DPA-azide  
 Scheme showing the SPAAC reaction of DBCO-biotin (yellow) and Zn-DPA (green) -azide, as well as the coating of SA (purple) -beads and 96-well plates with the SPAAC product.

fluorescence signal measured in a 96-well plate or under the microscope, even though the labeling of the beads was successful (Figure 3.14 C).

Another strategy to target the sensor to cell surfaces is to co-label SA-beads with the Zn-DPA-azide sensor and biotinylated antibodies that can be directed against any cell surface protein. Here, SA-beads were co-labeled with Zn-DPA-azide and biotinylated CD62L or ARTC2.2 antibodies to attach these beads to the cell surface of Yac-1 cells (Figure 3.15 D). Figure 3.15 D shows FACS measurements of Yac-1 cells with these beads. Beads only labeled only with Zn-DPA-azide were used as a control. 25 % of the Yac-1 cells incubated with ARTC2.2-labeled SA-beads and 33 % of the cells incubated with CD62L-labeled SA-beads were marked.

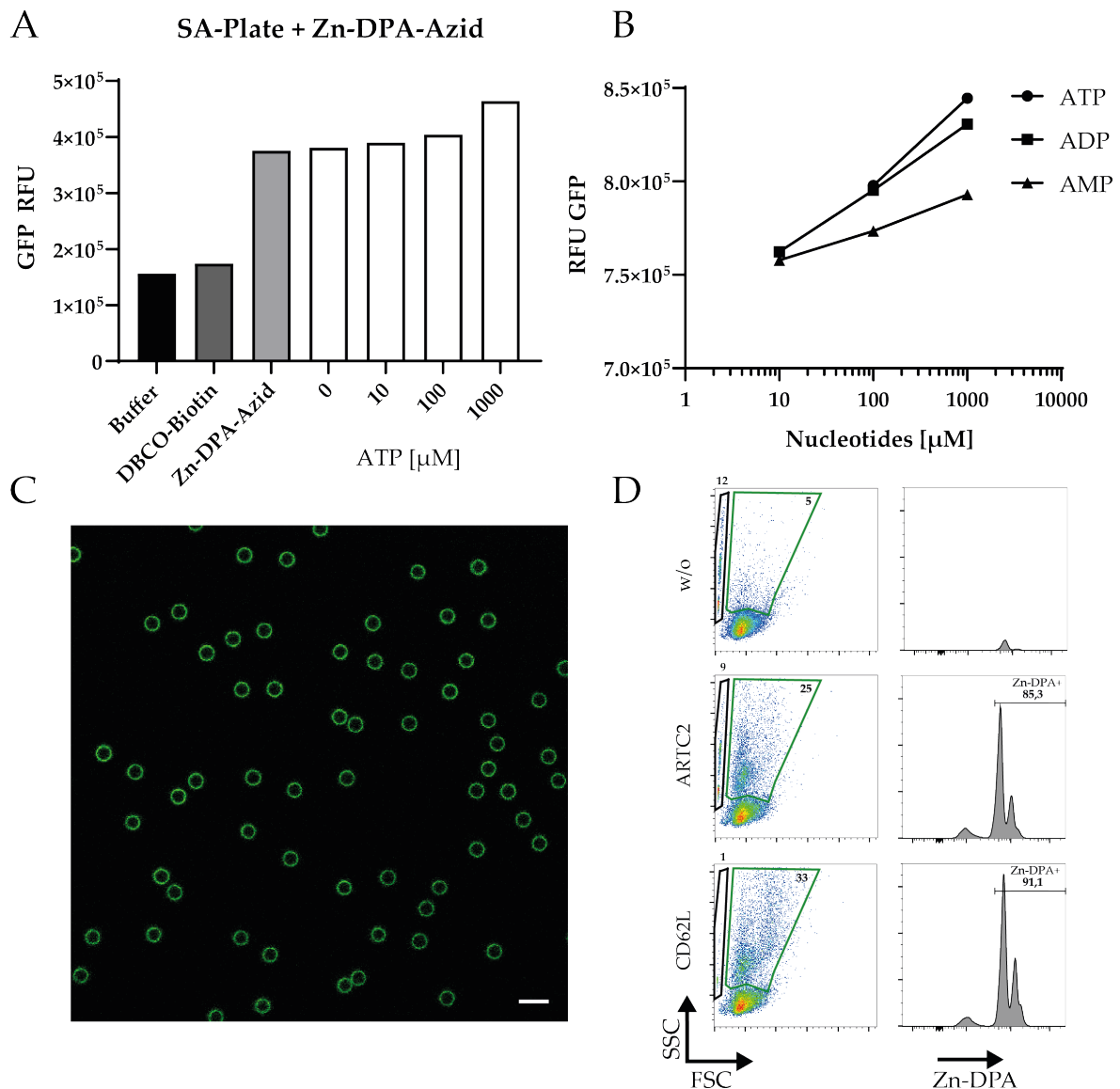


Figure 3.15: Labeling of SA beads/plates with Zn-DPA-C-azide variants

**A** SA microtiter plates were labeled with Zn-DPA-azide via a DBCO-biotin linker and the fluorescence was measured in the presence of increasing amounts of ATP. **B** Zn-DPA-azide-coated SA-Plates were measured in the presence of different concentrations of ATP, ADP, or AMP. **C** Fluorescent image of SA-Beads labeled with Zn-DPA-azide **D** SA-Beads co-labeled with Zn-DPA-azide and biotinylated antibodies against ARTC2.2 or CD62L to target the beads to Yac-1 cells. Black gate = free beads; green gate = beads+cells.

A further approach to label cell surfaces with the Zn-DPA sensors was developed, making use of the TP1170 nanobody specific for the mouse kappa light chain (Pleiner, Bates, and Görlich, 2018). This nanobody was produced in a variant containing a free cysteine residue at its C-terminus. This residue was used to link the nanobody to the Zn-DPA-azide sensor following a similar approach, as described in Figure 3.14, but with a DBCO-maleimide (instead of a DBCO-biotin) linker. DBCO-maleimide binds the free cysteine of the nanobody and thus can link Zn-DPA-azide with TP1170. Figure 3.16 A shows a schematic image of the Zn-DPA-azide nanobody complex, which binds to a cell surface. Here LP1 cells (a human myeloma cell line) were labeled with a BV785 (blue) conjugated human

leukocyte antigen (HLA)-DR antibody, which then can be recognized by TP1170 (orange). [Figure 3.16 B](#) shows a FACS measurement of labeled LP1 cells and their MFI for HLA-DR (black circles) and Zn-DPA (white circles). Different amounts of TP1170 were used to identify the concentration of TP1170 needed to achieve a sufficient signal. In fact, increasing concentrations of TP1170 resulted in higher signals of Zn-DPA (linear growth), showing that binding of the sensor was not yet saturated with the given concentration of the HLA-DR antibody.

The following chapter will investigate the properties and usability of lipophilic Zn-DPA variants which, can be used directly to label cell surfaces.

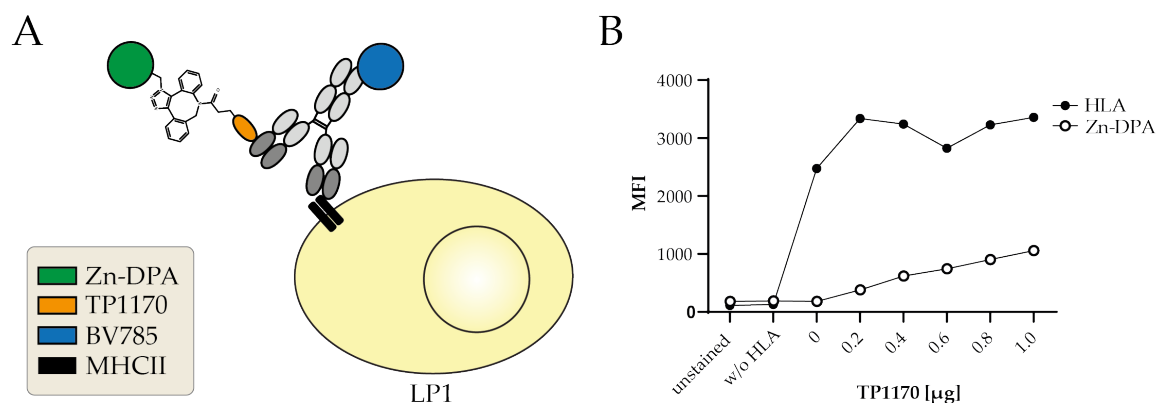


Figure 3.16: Targeting TP1170-Zn-DPA to LP1 cells via an anti-HLA-DR antibody

**A** Schematic image of the anti-mouse kappa light chain nanobody TP1170 (orange) bound to Zn-DPA-DBCO (green) used to label an anti-HLA-DR antibody bound to the MHCII (black) complex of LP1 human myeloma cells. **B** shows the MFI of the TP1170-Zn-DPA complex (white circles) and of HLA (black circles) with different concentrations of TP1170 (0.2 - 1.0 µg).

### 3.3.3 Direct membrane anchors of Zn-DPA-C(n) variants

Besides targeting specific structures on cell surfaces by using antibodies described in [Section 3.3.2](#), a non-specific approach to label cell surfaces with Zn-DPA sensors was investigated. For this purpose, carbon chains or lipids (e.g., cholesterol and tocopherol) that are already part of cell membranes were attached to the Zn-DPA sensor. These residues provide lipophilic properties to the sensors and enable them to integrate into cell membranes without an additional reaction, such as click chemistry. In the following chapters, these modifications of the Zn-DPA sensors were investigated to test their usability for staining cell surfaces.

#### 3.3.3.1 Long carbon chains

Zn-DPA sensors with a carbon chain length of 16 were tested to label YAC-1 cells. Zn-DPA-C16 was used, as it had shown the best signal to noise ratio in solution in comparison to other chain lengths in measurements performed by A. Laubach (data not shown). Yac-1 cells were stained with 2, 4, 6, 8, and 10 µM Zn-DPA-C16 for 10 min and measured on a

FACS for the fluorescence intensity of the sensor. In addition, fluorescent pictures of these cells were taken. Both, the FACS measurement and the fluorescence images showed an increase of the Zn-DPA-C16 signal with increased concentration (data not shown). These cells were then used for further experiments to investigate whether these sensors are still active when attached to the cell surface. Measurements of labeled cells in 96-well plates did not show a change in fluorescence signal after the addition of different concentrations of ATP or treatment of the cells with  $\text{NAD}^+$  to induce P2X7-dependent ATP release, as shown in [Figure 3.4](#).

To investigate if the Zn-DPA-C(n) variants integrate in the cell membrane or other parts of the cell, Yac-1 cells were again labeled with the Zn-DPA-C16 sensor and additionally with the C18 variant and imaged with a confocal microscope. The cells were co-stained with MitotrackerRed to identify mitochondria. [Figure 3.17](#) shows fluorescence images of these Yac-1 cells with Zn-DPA-C(n) in green, MitotrackerRed in red, and a merged image of both channels. Zn-DPA-C16 is in the top row and Zn-DPA-C18 below. The results show a co-localization of the Mitotracker signal and the sensor for both sensor variants. Zn-DPA-C16 shows weak labeling of the cell membrane and seems to additionally label different compartments of the cells including mitochondria. Compared to the C16 variant, Zn-DPA-C18 seems to penetrate the cell membrane less (higher sensor signal at the cell surface), but also labels cell organelles such as mitochondria. Both sensor variants, when incorporated into Yac-1 cells, did not show a difference in the fluorescence signal after the addition of 500  $\mu\text{M}$  ATP (data not shown).

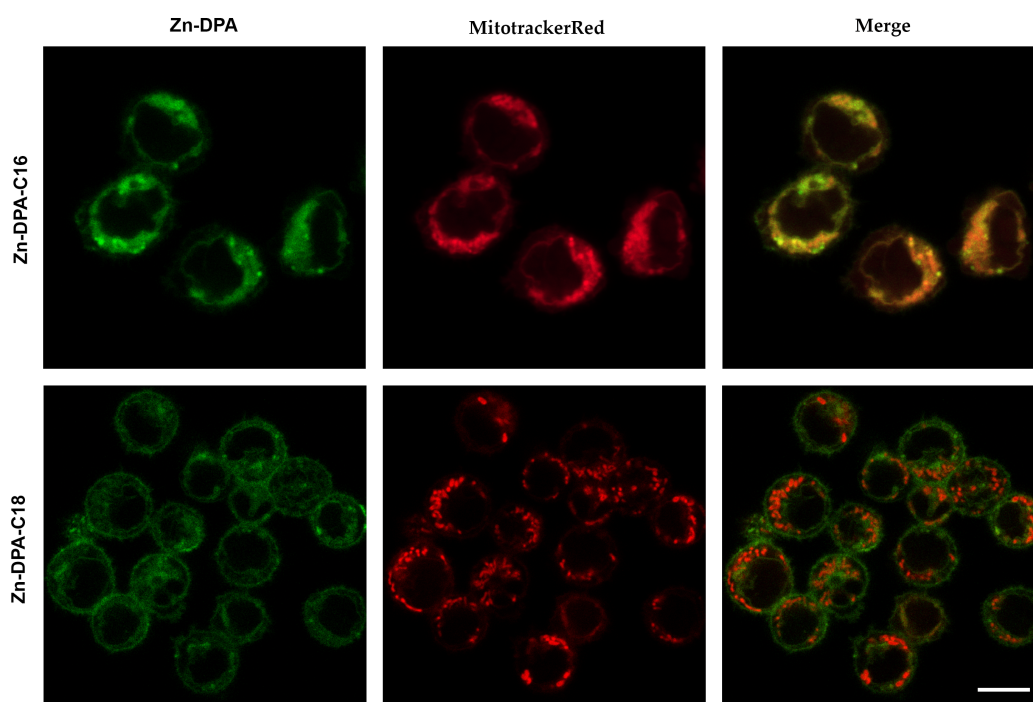


Figure 3.17: Localization of the Zn-DPA-C(n) sensor in Yac-1 cells

Yac-1 cells labeled with Zn-DPA-C16 (upper row) or C18 (lower row) and co-stained with MitotrackerRed. Fluorescence images of the individual channels are shown as well as a merge of both channels. Images were taken with a SP5 confocal microscope with a 63x objective and the scale bar is 10  $\mu\text{m}$ .

To circumvent the apparent penetration of cell surface membranes by the Zn-DPA-C(n) sensors, other residues were introduced into the Zn-DPA sensor to improve the labeling of cell membranes. These new sensor variants are tested in the following chapter.

### 3.3.3.2 Cholesterol and tocopherol Zn-DPA variants label cell surface membranes

Other residues were introduced into the Zn-DPA sensor with additional polyethylene glycol (PEG) spacers in different lengths to prevent the penetration of cell surface membranes and to improve their surface labeling. In a preliminary experiment, Yac-1 cells were incubated with different lipophilic Zn-DPA variants and imaged to ascertain the Zn-DPA variants best suited to label the cell membrane (data not shown). From these Zn-DPA variants, three were used for further experiments: NE26 (PEG2 tocopherol), AL386 (PEG2 cholesterol), and AL338 (PEG5 cholesterol).

First, the sensors were tested in solution. Therefore dose-response curves with 1, 3, 10, 30, 100, 300, 1000, and 3000  $\mu\text{M}$  ATP and 10  $\mu\text{M}$  respectively were recorded as previously described (Section 2.2.6). All three sensors showed an increase in fluorescence with increasing concentrations of ATP. NE26 had the lowest fluorescence intensity, and AL338 showed a lower increase in fluorescence compared to AL386 variant. Compared to the Zn-DPA and Zn-DPA-azide variants, the total fluorescence intensity was higher than of the tocopherol and cholesterol variants (Figure 3.18).

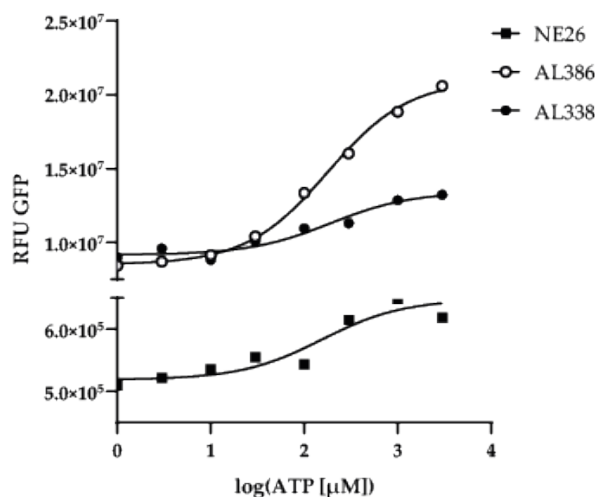


Figure 3.18: Functionality testing of cholesterol- and tocopherol-modified Zn-DPA sensors  
Dose-response curves of 10  $\mu\text{M}$  Zn-DPA in solution with ATP concentrations from 1  $\mu\text{M}$  to 3 mM. Modifications are NE26:PEG2 Tocopherol AL386:PEG2 Cholesterol AL338: PEG5 Cholesterol

Following the testing of these Zn-DPA variants in solution, they were used to label the cell surface of Yac-1 cells. Figure 3.19 A shows confocal images of Yac-1 cells labeled with AL338, AL386, and NE26 and co-stained with MitotrackerRed. The AL338 sensor showed a weak signal (dots in different sizes) on the cell membrane and minimal labeling of cell organelles. The signal of NE26 was even weaker than the signal of AL338 and showed almost no difference compared to the negative control (w/o). AL386 showed the highest signal of the three sensors; it was evenly distributed on the cell membrane and showed only a minor signal inside the cells.

Live-cell imaging of Yac-1 cells labeled with AL338 and AL386 was performed to test the functionality of these sensors when bound to the cell surface. Figure 3.19 B shows one of these experiments where images were taken before and 10 min after the addition of 500  $\mu\text{M}$  ATP. In these images, the cells were pseudocolor-stained using the Fiji software.

Additional labeled Yac-1 cells were also measured in a plate reader with 10, 100, and 1000  $\mu\text{M}$  ATP. For AL338 and AL386, there seems to be a tendency to an increased fluorescence signal with higher ATP concentrations, but it is not as clear as the measurement in solution with the same sensors. Taken together, the introduction of a cholesterol group with a PEG5 linker improves the labeling of cell membranes without or with a weaker penetration of the cell membrane and the labeling of cell organelles. Measurements in solution provides a dose-response with increased concentration of ATP, but as of now, bound to a cell membrane no reliable results can be generated.

### 3.4 SINGLE WAVELENGTH SENSORS FOR MEASUREMENT OF CYTOSOLIC AND EXTRACELLULAR ATP

Genetically encoded single-wavelength sensors (iATPSnFr) were described recently by Lobas et al. (2019). These sensors use the same ATP binding domain as the FRET-based ATP

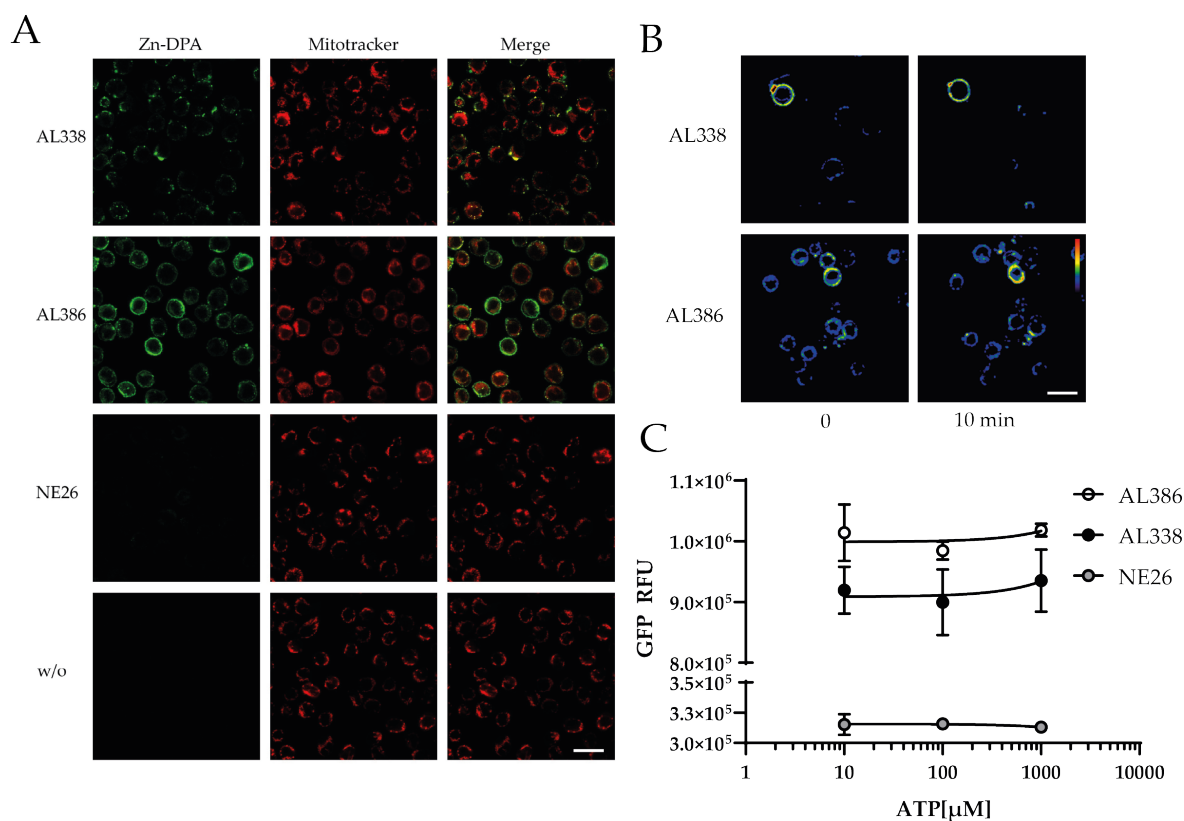


Figure 3.19: Cholesterol and tocopherol Zn-DPA variants label cell membranes

**A** Yac-1 cells were co-stained with MitotrackerRed and Zn-DPA (cholesterol and tocopherol variants). Shown are the individual channels (sensor in green and MitotrackerRed in red) and a merge of both. The lower row (w/o) shows Yac-1 cells not labeled with any sensor. **B** Yac-1 cells labeled with AL386 (lower row) and AL338 (upper row) at 0 and 10 min. A baseline was recorded for 2 min, then the cells were treated with 500 μM ATP and additionally measured for 8 min. The images were pseudocolor-stained using the Fiji software **C** The fluorescence of Yac-1 cells treated with the same Zn-DPA sensors as in **A** in the presence of 10, 100 and 1000 μM ATP was recorded. Graphs represent the means +/- standard deviations of three measurements. Modifications are NE26:PEG2 tocopherol AL386:PEG2 cholesterol AL338: PEG5 cholesterol. Pictures were taken with a SP5 confocal microscope with a 63x objective and the scale bar is 20 μm.

sensors originally described by Imamura et al. (2009) and used in this thesis. A modified version of GFP (circularly permuted superfolder GFP) was used and cloned between the ATP binding domain. Upon binding of ATP a conformational change occurs, which leads to an increased fluorescence of the GFP protein. Here, some preliminary data of these sensors used in different approaches are shown.

Plasmids coding for the sensor variants iATPSnFr<sup>1.0</sup> (called HHM1.0) and iATPSnFr<sup>1.1</sup> (called HHM1.1), fused to a combined 6x histidine/cmyc-tag were obtained from Addgene. The respective proteins were produced in E.coli and purified by immobilized metal affinity chromatography using a nickel-nitrilotriacetic acid (Ni-NTA) column. SDS gel and western blot analyzes confirmed the expression and purity of these sensors (Data not shown). The responsiveness of the sensors to ATP was first tested in solution, and then bound to different surfaces such as streptavidin-(SA)-coated beads or microtiter plates. HHM 1.0 was described to have a lower affinity for ATP than HHM1.1 (EC<sub>50</sub> of 120 μM vs. 50 μM, respectively) Lobas

et al. (2019). Here, an increase of the fluorescence could be observed with up to  $\sim 250 \mu\text{M}$  of ATP for the 1.1 variant and up to  $\sim 500 \mu\text{M}$  of ATP for the 1.0. At higher concentrations of ATP, the fluorescence signal was reduced, presumably by quenching (Data not shown). The HHM1.1 sensor was thus used for further experiments.

In order to use the sensor to detect local ATP concentrations at the plasma membrane it was necessary to devise a strategy to bring it into contact with cell surfaces. For this purpose, the cmc-tag of the sensor was used to couple it to SA beads coated with a biotinylated anti-cmyc antibody. To target the beads to the surface of Yac-1 cells, they were co-coated with a biotinylated antibody against the  $\alpha\text{L}$  integrin (CD11a, LFA-1) which is expressed at a high density on the surface of Yac-1 cells. Additionally, a PE-conjugated anti-rat IgG antibody was used to label the beads with a fluorescent dye to allow their detection when attached to the Yac-1 cells. The labeling is schematically shown in [Figure 3.20 A](#). [Figure 3.20 B](#) shows the gating strategy, where Pacific Orange (general low-level staining of the Yac-1 cells) is plotted against PE (beads) to show the formation of Yac-1 SA beads complexes. Measurements of Yac-1 cells alone were compared to a measurement where beads and Yac-1 cells were previously incubated together. Approximately 13% of recorded events were complexes. The MFI shows an increase in fluorescence of the complexes compared to the free beads and cells, suggesting that of the fluorescence of the sensor increases when it is in close contact to a Yac-1 cell.

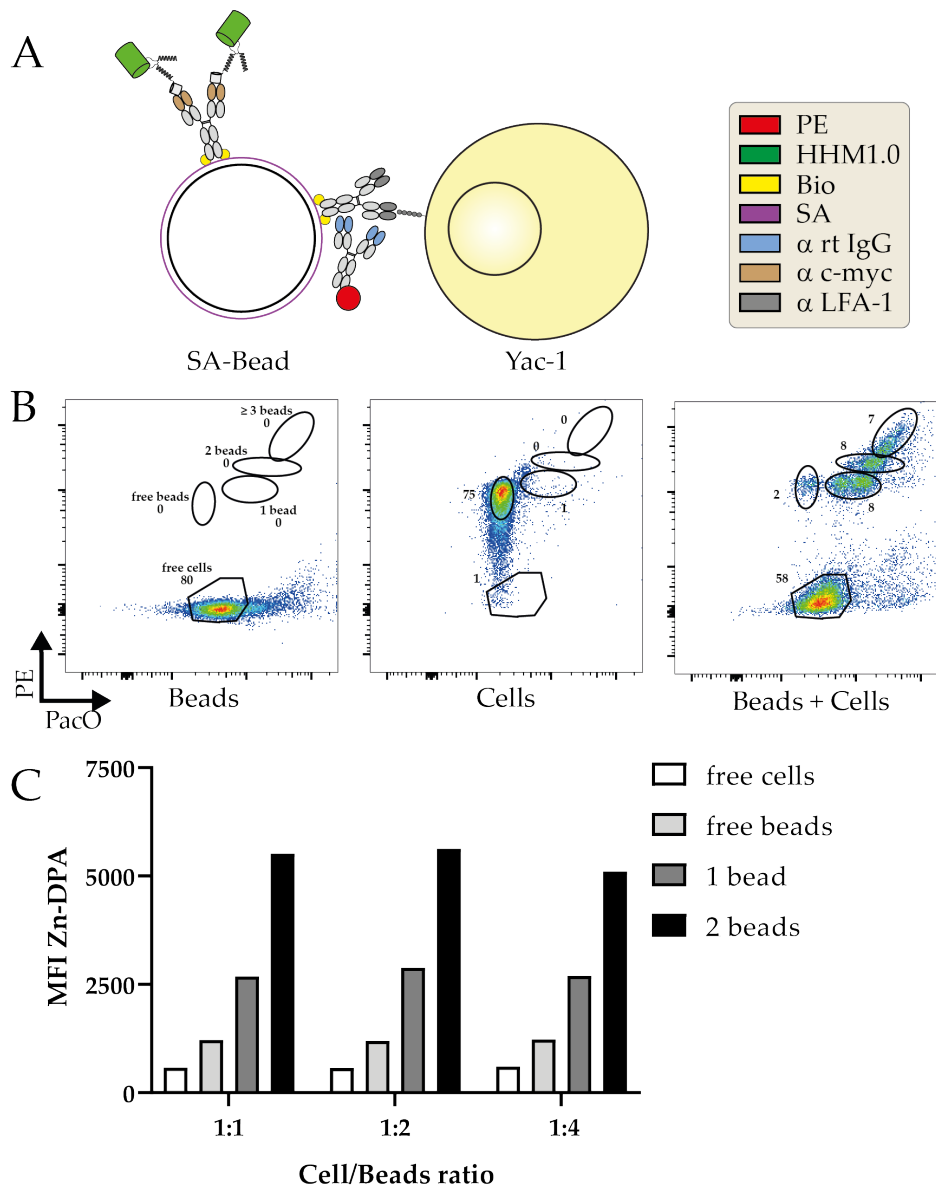


Figure 3.20: Measurement of ATP release with single wavelength ATP sensors

**A** shows a schematic image of the strategy used to bring the single-wavelength ATP sensor HHM1.0 into contact with the surface of Yac-1 cells. Streptavidin- (SA) coated beads were co-coated with biotinylated antibodies against c-myc and the integrin LFA-1. Additionally, a PE-conjugated anti-rat IgG antibody, which binds to the anti-LFA-1 antibody, was used to label the beads. **B** shows the detection of cell/bead complexes by plotting the channels for PE (labels beads) against Pacific Orange (PacO, labels cells) for samples containing beads alone, Yac-1 cells alone, and beads and cells in combination. **C** shows the MFI of the sensor for free cells and beads, and complexes of Yac-1 cells and beads (1 or 2 Beads). Furthermore, different cell/bead ratios were analyzed (1:1, 1:2 and 1:4).

# 4 | DISCUSSION

In this study the relationship between P2X7 activation and ATP release was investigated, using different approaches such as FRET-based ATP sensors to visualize and measure changes in intracellular and extracellular ATP levels.

ATP was discovered early on as the main energy source in cells (Lipmann, 1941) and later on as an important signaling molecule in purinergic signaling. The intracellular concentration of ATP is approximately 10 mM, but in the extracellular space, it is in the low nanomolar range. It is known to be released from dying cells (e.g. apoptosis, necrosis), but can also be released in a regulated fashion, either by vesicular transport or by pore formation. Extracellular ATP acts as a DAMP and its concentration is highly regulated by ectoenzymes which hydrolyzes ATP to Ado. eATP activates P2 receptors which are widely expressed on immune cells. P2X7 is the most studied P2 receptor as it has an important role in inflammation. In comparison to other P2 receptors, P2X7 needs high ATP concentrations in the upper micro-molar range. P2X7 promotes proliferation and activation of T cells and inflammasome assembly in microglia and macrophages.

## 4.1 HALLMARKS OF P2X7 ACTIVATION

P2X7 is expressed in a variety of cell types but is most studied in the context of the immune system. P2X7 activation is associated with specific functions in macrophages and T cells which include T cell differentiation and the release of pro-inflammatory cytokines. Several phenotypic changes can be observed to demonstrate the successful activation of P2X7. In this work shedding of CD62L and the uptake of PI was measured to indicate P2X7-dependent activation of membrane metalloproteinases and pore formation, in accord with other published data (Figure 3.1).

To prove that these effects were P2X7 specific a nanobody and the small-molecule inhibitor A438079 were used (Danquah et al., 2016). Both compounds block the gating of P2X7 in vitro, regardless of whether this occurs by ATP or nicotinamide adenine dinucleotide (NAD<sup>+</sup>)–dependent ADP-ribosylation. Both inhibitors effectively blocked the shedding of CD62L after ATP or NAD<sup>+</sup> ribosylation, but A438079 seemed less effective with regard to hindering pore formation. Why A438079 was less effective at inhibiting pore formation cannot be concluded with the presented data, but it is possible that the two inhibitors may differ in their capacity to inhibit different downstream signaling pathways of P2X7, such as gating of the cation channel vs. the transmission of signals via the long intracellular C-terminal tail. A438079 is a well-established inhibitor for P2X7 that is under consideration for use in chronic pain therapy (Donnelly-Roberts and Jarvis, 2007). However, other groups have also

shown only partial inhibition of pore formation by A438079 (Haanes, Schwab, and Novak, 2012).

Another function of P2X7 is the influx of  $\text{Ca}^{2+}$  after gating of the receptor. This thesis confirms this function by using an inhibitory nanobody directed against P2X7 as well as P2X7-KO mice (Figure 3.3). Even though the difference between  $\text{Ca}^{2+}$  uptake in Yac-1 cells and primary mouse T cells are significant, the difference between WT and P2X7-KO show a higher standard deviation. This could be explained due to the fact that cell lines are highly homogeneous and more robust compared to primary cells (Campisi and Fagagna, 2007).

#### 4.1.1 P2X7 mediated ATP release

Gating of P2X7 also induces cells to the release ATP (Johnsen et al., 2019). However, the mechanism by which this occurs is not clear. Various mechanisms that might be involved in this process will be discussed in more detail in the following section.

To investigate the P2X7-dependent release of ATP from cells P2X7 was gated by  $\text{NAD}^{+}$ -dependent ADP-ribosylation, in order to avoid the addition of exogenous ATP. The release of ATP in response to  $\text{NAD}^{+}$  could be blocked equally well by inhibitory nanobodies against ARTC2.2 or P2X7, or by the P2X7 antagonist A438079. The inhibition of  $\text{NAD}^{+}$ -dependent P2X7 activation might suggest that 13A7 and A438079 sterically prevented the opening of the P2X7 receptor. In fact, it is suggested that the inhibition of P2X7 via A438079 is rather allosteric than orthosteric (ligand binding site) (Allsopp, Dayl, et al., 2018), which would explain the effective inhibition of ADP-ribosylation dependent activation of P2X7. 13A7 could be then suggested to act also in an allosteric manner as A438079 does, considering the small sizes of nanobodies compared to conventional antibodies (Wesolowski et al., 2009).

The described ATP release via gating of P2X7 is also accompanied by an increase of dead cells, as indicated by the uptake of PI by of 3% of Yac-1 cells after treatment with  $\text{NAD}^{+}$ . This raises the question of whether the eATP measured by the luciferin-luciferase assay was caused by the dying cells or through a P2X7-mediated mechanism. The type of assay used to measure the release of ATP (bulk measurement) cannot provide an answer to this question, which made it necessary to use another approach to measure changes in ATP concentrations. Therefore, FRET-based ATP sensors, which are discussed in the following section, were used to address this question.

## 4.2 ATP IMAGING USING FRET BASED SENSORS

In this study, FRET-based ATP sensors were used. They are derived from the ATeam sensor by Imamura et al. (2009). The sensors are composed of CFP a donor-fluorophore and an the YFP variant Venus as an acceptor-fluorophore. These are connected by an ATP-binding domain from the  $\epsilon_0$  subunit of the  $\text{F}_0\text{F}_1$ -ATP synthase from different bacterial strains from the genus *Bacillus*. This binding domain undergoes a conformational change upon binding of ATP, which brings both fluorophores into close proximity to each other, so that FRET occurs (Iino et al., 2005). These sensors were expressed in the cytosol and at the cell membrane of

different cell lines in order to measure local changes of ATP concentration upon activation of P2X7. In general, a decrease of the FRET signal of the ATP sensors expressed in the cytosol means a release of ATP from the cytosol (lower intracellular ATP level). Accordingly, an increase of the signal of FRET sensors located at the cell membrane indicates an increase of the extracellular ATP level at the cell membrane.

#### 4.2.1 *Validating the function of FRET-based ATP sensors*

First, the general function of the FRET-based ATP sensors was confirmed. 3T3 cells expressing the cytosolic ATP FRET variant Bs.cyt were measured both by flow cytometry and confocal microscopy. After the addition of ATP the FRET signal decreased in 3T3 cells expressing both P2X7 and Bs.cyt, as shown by kinetic measurement in the FACS as well as by the live-cell imaging. As a control, the uncoupling agent CCCP was used to decrease intracellular ATP levels by a mechanism that was independent of P2X7.

In the original publication, the specificity of the sensor ATeam was confirmed by testing its reactivity to different nucleotides *in vitro* (Imamura et al., 2009). Additionally, similar to this work, a live-cell imaging approach was used, where HeLa cells were treated with 2DG and KCN to inhibit glycolysis and oxidative phosphorylation, respectively. In this thesis, the addition of 2DG, alone or together with the deprivation of glucose (data not shown), did not cause a decrease in FRET, but the treatment with CCCP caused a steep and fast reduction of the FRET signal (Figure 3.5). Others also showed that the usage of CCCP decreased the intracellular ATP concentration (Ledderose, Bao, Lidicky, et al., 2014). Furthermore, other publications have used this sensor or variants of it in their assays, demonstrating the functionality of this sensor in principle (Lobas et al., 2019; Lerchundi et al., 2019; Botman, Heerden, and Teusink, 2020).

#### 4.2.2 *ATP depletion after gating of P2X7*

ATP and NAD<sup>+</sup>-mediated ADP-ribosylation are the main drivers of P2X7 activation. Next to the already described hallmarks of P2X7 activation P2X7 itself is responsible for the release of its own agonist ATP. In this thesis, cytosolic and membrane-bound variants of the FRET-based ATP sensor were used to measure the release after P2X7 activation.

The release of ATP was long thought to be mainly due to cell death (apoptosis and necrosis). But recently it has been shown that cells release ATP constantly in low amounts by various mechanisms, including release through vesicles (Z. Zhang et al., 2007), pannexins, connexins, volume-regulated anion channels (Gaitán-Peñas et al., 2016), and maxi-anion channels (Sabirov, Dutta, and Okada, 2001). P2X7 itself is also discussed to be directly responsible for the release of ATP. Studies in HEK cells co-expressing P2X7 and a luciferase fusion protein expressed on the cell surface show a P2X7-dependent ATP release (Pellegratti, Falzoni, et al., 2005). Additionally, the interaction of P2X7 and pannexin/connexin hemichannels is discussed, where these form pores that result in the release of ATP. In these experiments, the cells must be handled carefully because mechanic “stress” can result in the

release of ATP or NAD<sup>+</sup>, which then can lead to a gating of P2X7 or a permanent gating of cells expressing both ARTC2.2 and P2X7 (Romanello et al., 2001; B. Rissiek, Lukowiak, et al., 2018; Borges da Silva et al., 2019). Especially the release of NAD<sup>+</sup> should be prevented, as it results in permanent gating of P2X7 and thus possible cell death, which then again results in the release of said nucleotides. Additionally, it must be considered that NAD<sup>+</sup>-dependent ADP-ribosylation is also active at 4 °C (Adriouch, Bannas, et al., 2008; Scheuplein et al., 2009). Thus, careful handling of cells expressing both ARTC2.2 and P2X7 (e.g. YAC-1) is very important to prevent a negative impact on the results and a subsequent misinterpretation of the data. This phenomenon could be observed in some live-cell measurements (confocal microscope) using Yac-1 cells. In some cases, these cells started “blebbing” without the addition of a stimulus from the outside (during the recording of the baseline). Also, the heterogeneous FRET signal between cells might reflect different ATP concentrations in each cell, which could be due to pre-activation of the P2X7 receptors during preparation.

This thesis confirmed the release of ATP in 3T3 cells expressing P2X7 and the cytosolic ATP FRET sensor Bs.cyt stimulated with ATP in kinetic FACS measurements (Figure 3.5). Similar to the measurements of ATP released from Yac-1 shown in Figure 3.4 the measurement using a FACS shows a continuous release of ATP.

ATP release by single cells can be observed with a fluorescence microscope, which can give a better insight as to the mechanics of ATP release. Yac-1 cells show a distinct release of ATP after treatment with the same as well as treated with NAD<sup>+</sup> indicated by the decrease of FRET signal (Figure 3.9).

Additionally, a membrane-bound version of the FRET sensor (PS3.GPI) was used to measure the change of eATP after gating of P2X7 (Figure 3.10). First, the function of the sensor bound to the membrane was tested with the addition of ATP in a range from 2–500 μM. To verify the P2X7-dependent ATP release, the receptor was stimulated with 20 μM NAD<sup>+</sup> in 3T3 cells transfected with P2X7kp, ARTC2.2 and PS3.GPI. Indeed, a release of ATP after ADP-ribosylation of P2X7 could be visualized and measured. These results support the data generated from the experiments with the Bs.cyt variants as well as the NAD<sup>+</sup>-dependent release of ATP in the bulk measurements shown in Figure 3.4 and (Johnsen et al., 2019). Karasawa, Michalski, et al. (2017) obtained similar results, where gating of P2X7 via ATP in liposomes resulted in pore formation and dye uptake, indicating the possibility of a connexin/pannexin-independent ATP release. They showed a P2X7-dependent dye-uptake to be highly dependent on the lipid composition of the cell membrane. These findings are in line with observations by Alberto et al. (2013) who showed that P2X7 pore formation in macrophages is independent of pannexin-1 using different inhibitors and the measurement of dye-uptake. In line with this, other authors have shown a P2X7-dependent pore-formation in bone marrow-derived macrophages of pannexin-1 knock-out mice (Qu et al., 2011). However, other studies show a distinct involvement of connexins/pannexins in the release of ATP. In T cells, for example, the release of ATP through connexin-43 and pannexin-1 could be shown (Woehrle et al., 2010). In agreement with this, the use of pannexin-1 inhibitors prevented the formation of pores and thus dye-uptake in macrophages (Pelegriin and Surprenant, 2006), and co-expression of P2X7 and pannexin-1 in oocytes enabled the formation of pores (Locovei et al., 2007). Furthermore, P2X7-mediated IL1β

release by macrophages is dependent on gasdermin, which forms a pore causing the release of IL-1 $\beta$  and can lead to pyroptosis (He et al., 2015). The release of DAMPs including ATP through gasdermin pores was also shown in the mouse colon carcinoma CL26 (Tsuchiya et al., 2019).

Whether P2X7 itself, alone or in combination with pannexin/connexin, initiates the formation of a pore, or if P2X7 just initiates the formation of a pore by pannexin/connexin cannot be answered in thesis. It is possible that all of these theories are true in individual settings, meaning that the P2X7-dependent pore formation is different in the various cell types and differentiation states. For example, membrane lipid composition varies from cell type to cell type (Harayama and Riezman, 2018) and has an impact on the innate (Köberlin et al., 2015) and adaptive immune response (W. Wu, Shi, and C. Xu, 2018). Robinson et al. (2014) could show the association of P2X7 with cholesterol lipid rafts, and the inhibitory effect of cholesterol on human and mouse P2X7 activation and especially on the formation of a pore. Similarly, Karasawa, Michalski, et al. (2017) showed that, high amounts of cholesterol in the membrane hinder P2X7-mediated pore formation and dye-uptake by interacting directly with the transmembrane domain of P2X7. Taking these findings together, it could be possible that on the one hand in cells with a high amount of cholesterol in the cell membrane P2X7-mediated pore formation is dependent on other cell surface molecules such as connexins/pannexins, which might be recruited via an unknown mechanism. On the other hand, in cells with lower amounts of cholesterol, P2X7 mediated pore formation could be solely dependent on P2X7. Furthermore, cells could use cholesterol homeostasis as a regulator for the P2X7 receptor, where cholesterol-rich lipid rafts could dampen the P2X7 activity.

However, this work supports the notion that P2X7 is directly involved and seems to be important for the release of ATP.

### 4.3 SMALL-MOLECULE ATP SENSORS

Apart from the genetically encoded FRET-based ATP sensors used in this thesis, small-molecule sensors were used and tested if they would be suitable for measuring ATP release from cells. Different approaches for measuring the release of ATP with small-molecule sensors are described in the literature. Among them are fluorescent ATP analogs (Ho et al., 2015), quinacrine, which labels vesicular ATP (Akopova et al., 2012), and a xanthene-based Zn(II) complex (Ojida, Takashima, et al., 2008). The sensors used in this thesis are derived from Moro, Cywinski, et al. (2010) and consist of a naphthalimide chromophore and a Zn(II)-complexed dipicolylamine (DPA) group, where the binding of nucleotides to the DPA group evokes a dose-dependent change in fluorescence. Moro, Cywinski, et al. (2010) could show an increase in fluorescence with increasing ATP concentrations, high selectivity for ATP and ADP compared to other nucleotides (but with a higher fluorescence for ATP), as well as pH stability of the fluorescence ranging from pH 5.6 to pH 8.4. The results in this thesis concur with the mentioned study to the effect that in solution an increase of the

fluorescence signal in the presence of rising ATP concentration as well as a higher selectivity for ATP compared to ADP could be observed (Figure 3.12).

The Zn-DPA harbors a moiety allowing the attachment of different functional groups which in turn can be used to attach the sensor to different surfaces. Here, an azide-coupled variant of Zn-DPA was attached to streptavidin (SA) microtiter plates and SA beads via SPAAC. While a change in fluorescence upon addition of ATP could be observed on microtiter plates the sensor seemed to be not functional anymore (Figure 3.15). It could be argued that the method of how the beads were measured was not ideal. Since the labeled beads were also measured in microtiter plates, the signal inside the well might be not as well distributed as in the case of the coated wells. Thus, the addition of ATP to these labeled beads and the measured of “no difference” in the signal compared to untreated cells might be able with this particular plate reader. An increase of labeled beads per well might influence this observation since the total fluorescence per well would be then increased and a change of fluorescence upon addition of ATP could result. Surprisingly, measured with a confocal microscope, there is also no change of the fluorescent signal after the addition of ATP observed. Moro, Schmidt, et al. (2011) however could label silica beads with their Zn-DPA sensor and could measure a change in fluorescence in the presence of different nucleotides such as ATP in solution, which shows that these sensors should work when attached to surfaces.

Interestingly, addition of the azide group affected the selectivity of the sensor for different nucleotides, so that the azide-coupled sensor emitted the highest fluorescence signal in the presence of AMP instead of ATP (Figure 3.13). The azide-coupled sensor also preferred the monophosphates of other purine nucleosides over the respective tri- and diphosphates, e.g. guanosine monophosphate (GMP) over GDP/GTP (data not shown). A possible explanation for this behavior could be an interaction of the free azide group with the naphthalimide chromophore. Ojida, Mito-Oka, et al. (2002) first described a Zn(II)-DPA chemosensor which has a high affinity towards ATP. They also observed that ATP had a higher association constant towards the Zn(II)-DPA complex compared to ADP or AMP (ATP>ADP>AMP), and concluded that the chemosensor favors the  $\beta$ - and  $\gamma$ -phosphate over the  $\alpha$ -phosphate. Moro, Cywinski, et al. (2010) then added a naphthalimide chromophore to the Zn(II)-DPA complex to make use of the photoinduced electron transfer (PET) effect to further increase the fluorescence (quantum yield). Considering these findings, the azide moiety at the naphthalimide chromophore might influence the PET with the Zn(II)-DPA, resulting in a higher fluorescence of purine monophosphates compared to tri- and diphosphates.

Since the intended use of the sensor was to monitor ATP concentrations at cell surfaces, several strategies were explored to target the sensor to cell membranes. In a first approach, co-labeling of SA beads with the sensor and biotinylated antibodies against CD62L or ARTC2 enabled targeting of the beads to the surface of Yac-1 cells as demonstrated by flow cytometry (Figure 3.15). Another approach was to label an anti-mouse kappa light chain nanobody to label specific molecules on the cell membrane. In this case, a free cysteine at the C-terminus of the nanobody was used to attach an alkyne group that would bind the azide group attached to the sensor. This approach was developed especially for the purpose of binding the sensor to the surface of any human cell of choice. Since the majority

of antibodies against human antigens were developed in the mouse, and the majority of the mouse antibodies use a kappa light chain, attaching the sensor to an anti-mouse-kappa nanobody offers the possibility to target the sensor to any human cell that has previously been labeled by an antibody. This principle was tested using the human myeloma cell line LP1 as an example. Myeloma cells express high levels of the MHC II molecule HLA-DR, and thus an anti-HLA-DR antibody was used as the primary antibody. The results shown in [Figure 3.16](#) show that the labeling worked, but the performance of the sensor at the cell surface could not be investigated further within the time frame of this project. Taken together, the results show that this strategy is a promising tool to label specific cell subsets and to measure the release of ATP during the activation of e.g. T cells or macrophages.

In a third approach, long hydrophobic carbon chains were attached to the Zn-DPA sensor, with the goal of labeling the outer leaflet of cell membranes. The goal was the incorporation of these Zn-DPA-C(n) into cell membranes via lipid interactions. Zn-DPA variants with carbon chain lengths of C13 to C18 were synthesized. In preliminary experiments<sup>1</sup> the sensors with different carbon chain lengths were tested in solution. Compared to the other variants, Zn-DPA-C16 showed the best signal-to-noise ratio in the presence of ATP and thus was used for the experiments in this thesis.

Similar to the “tails” of phospholipids of cell membranes these carbon chains (alkyl) are hydrophobic and should incorporate into the cell membrane. Unfortunately, the sensors only stained the plasma membrane weakly, but entered the cell and incorporated into the cell membranes of intracellular organelles, in particular mitochondria. This could be demonstrated by co-staining with the mitochondria-specific dye MitoTrackerRed ([Figure 3.17](#)). There are many known lipophilic fluorescent dyes which are able to stain cell membranes (Klymchenko and Kreder, 2014). A recent publication specifically addresses this problem. Guo et al. (2020) describe fluorescent dyes with alkyl side chains with varying lengths and their impact on their self-delivery across the cell membrane. They propose that these sensors pass the membrane through diffusion and established a physical model allowing the calculation of the diffusion time. They show that dependent of the length on the carbon chains they either diffuse through the cell membrane and label mitochondria (C1 - 14), cytosol (C15), the cell membrane (C18, C20), or neither stain cellular compartments nor the cell membrane (C22). These findings concur with the results presented in this thesis, with the difference that here both Zn-DPA-C16 and C18 still penetrated the membrane, which can be explained by the different fluorophore groups used in the two sets of experiments.

To circumvent the observed penetration/diffusion of the Zn-DPA-C(n) sensors, PEG spacer and other lipophilic moieties were introduced into the Zn-DPA sensors. PEG is a multimeric hydrophilic molecule, which, besides preventing the diffusion of Zn-DPA sensors, should provide the correct orientation of the sensor (e.g. the alkyl group between the leaflets of the membrane and rest of the sensor extracellular). Interestingly, Zn-DPA-C16 with PEG chains composed of 1 - 5 PEG moieties still diffused through the cell membrane of Yac-1 cells and stained intracellular compartments (mitochondria) and showed only a weak signal located at the cell membrane (data not shown), similar to the sensors lacking

---

<sup>1</sup> This measurement was performed by Alexander Laubach, Department of Chemistry, University of Hamburg

PEG. Improved staining of plasma membrane could be achieved by substituting the alkyl group by cholesterol or tocopherol. Especially Zn-DPA with five PEG groups and cholesterol as a hydrophobic group provided a homogeneously stained membrane with sufficient fluorescence intensity. Other groups also followed his strategy. Jia et al. (2019) for example used a similar sensor with a different fluorophore (Cy5) to successfully stain the cell membrane of embryonic zebrafish, without any diffusion inside the cells.

The same sensor with one PEG group gave in total a weaker signal which was distributed heterogeneously (punctual) on the cell membrane. This might indicate an association of this sensor with lipid rafts caused by the single PEG in combination with the cholesterol group. Lipid rafts are known to be enriched in cholesterol and sphingolipids (K. Jacobson, Mouritsen, and Anderson, 2007), which might favor the association with this Zn-DPA variant. Depending on their composition, cell membranes can exist in two different phases with regard to their fluidity: the liquid-disordered state (Ld), which represents a heterogeneous composition of the membrane and allows lateral movement, and the liquid-ordered (Lo) phase, where the membrane bi-layer contains a high percentage of cholesterol (20-40%) (Quinn and Wolf, 2009) and saturated phospholipids (sphingolipids), the so-called lipid rafts (Heberle and Feigenson, 2011). These phases co-exist and are more common in the outer leaflet. Indeed, Honigmann et al. (2013) developed a fluorescent dye, containing one PEG group which stained specifically those parts of the membrane in the Lo phase. The same dye without PEG did not discriminate between Lo and Ld phase.

#### 4.4 CONCLUSION AND OUTLOOK

In this work, methods for the measurement of changes in local ATP concentrations were established, and protocols for using FRET-based as well as small-molecule ATP sensors to visualize intra- and extracellular ATP concentrations were developed. These tools were successfully used to show the involvement of P2X7 in the release of its own agonist ATP. In the future, these tools can be used to answer important questions in the field of purinergic signaling. In order to overcome the limitations associated with the transfection of cell lines, an important challenge will be to target these sensors to appropriate locations in primary cells. This could be achieved for instance by creating transgenic mice expressing this sensor, either ubiquitously or under the control of a cell-specific promoter. Another possible approach is to introduce the sequence of these FRET sensors into viral vectors in order to induce the expression of these sensors in a variety of cells, including cell lines and primary cells (mouse and human).

A further perspective is the development of pairs of non-interfering FRET-based ATP sensors with different donor/acceptor pairs that could be targeted to different cellular compartments (e.g. cytoplasm and cell membrane) in order to simultaneously visualize e.g. the increase of eATP at the cell surface and the decrease of iATP in the cytosol after gating of P2X7. Furthermore, FRET-based ATP sensors could be combined with a calcium dye to investigate the role of P2X7 gating in T cell activation using appropriate P2X7 knock-out mice or cell lines.

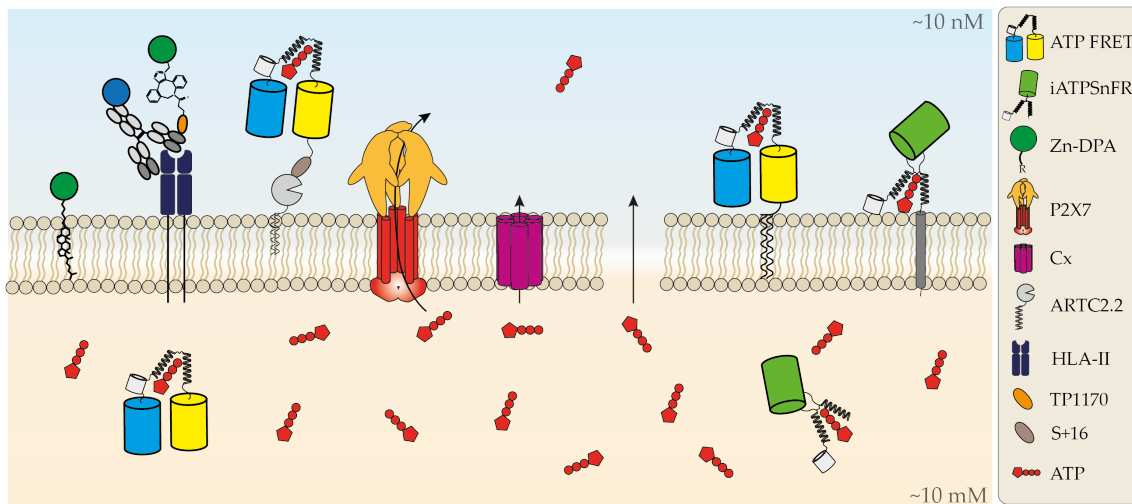


Figure 4.1: Schematic overview of mechanisms of ATP release and of ATP sensors used in this work. Possible pathways of ATP release after gating of P2X7 include the release through pores, such as connexins/pannexins or through P2X7 itself. Additionally, the detection of ATP with different sensors is shown. These include genetically encoded FRET-based ATP sensors and iATPSnFr single-wavelength sensors, which share the same ATP binding domain ( $\epsilon$  subunit of the  $F_0F_1$ -ATP synthase). Both can be expressed in the cytosol or on the cell membrane. Also depicted are small-molecule sensors based on a Zn-DPA complex. A lipophilic variant with a cholesterol group, and one variant connected to a anti-mouse kappa light chain nanobody (TP1170) via DBCO linker, to label antigens on human cells (e.g., HLA-II), are shown. In addition, the approximate resting ATP concentration in the cytosol (10 mM) and extracellular (10 nM) are displayed.

A monochromatic ATP sensor based on the same ATP binding domain as the ATeam sensor, but containing only one modified version of the GFP molecule, was briefly introduced and tested in this thesis. The general functionality in solution could be verified, and protocols to attach this sensor to SA-coated surfaces such as wells from microtiter plates and beads were developed. An advantage of these sensors is that they can be produced easily in bacteria in a short time and in large quantities. Since they can be produced as soluble molecules that carry chemical groups that can be modified to target them to solid phases such as beads or cell surfaces they represent an attractive alternative to the FRET sensors. Since these sensors only have one fluorescent molecule, the combination with other dyes (e.g. calcium dyes) will be easier regarding spectral overlap. Especially the interaction of P2X7 and TCR stimulation in primary T cells would be an interesting application.

Apart from the genetically encoded ATP sensors based on fluorescent proteins, small-molecule sensors were used and seem to be another promising tool. They are based on Zn-DPA and have a moiety to attach different residues for click-chemistry or to be attached directly to the cell membrane with lipophilic residues. Although these molecules are attractive candidates for ATP sensors, the work in this thesis shows that modification of these functional groups with the aim of attaching them to solid phases can carry pitfalls, such as changes in nucleotide selectivity. Even though these sensors did not function in the expected way when attached to a surface, the work in this thesis confirmed that they function well in solution. Given this good functionality in solution, especially Zn-DPA-azide with its increased selectivity for AMP could be used as a simple high-throughput tool for enzyme

assays, e.g. to screen libraries of nanobodies for inhibitory effects against ecto-enzymes such as CD39 and CD73. Additionally, providing the Zn-DPA sensor with a cholesterol group in combination with a PEG group offers a promising approach to label the plasma membrane of target cells, since labeling of cell membranes could be achieved with a signal strength sufficient for measurements in a confocal microscope, but this needs to be tested further.

All in all, the sensors investigated in this thesis offer a large and versatile spectrum of great tools to answer important questions in immunology in general, and purinergic signaling specifically. They hold great promise to gain better insights into the role of extracellular nucleotides in immune regulation, such as solving the mechanistic connection between P2X7-mediated ATP release and T cell activation.

# 5

## ABSTRACT

Adenosine triphosphate (ATP) is the primary energy source in all living organisms. In addition, ATP is an important extracellular signaling molecule as a ligand for P2X and P2Y receptors. P2X7 has been thoroughly studied in the context of immunology since it is expressed on the majority of cells of the immune system. Activation of P2X7 leads to various downstream effects, such as enhancement of T cell receptor (TCR) signals, inflammasome assembly, pore formation, and cell death. Most cells can release ATP in a regulated fashion, but the mechanisms and kinetics of these processes are not well understood yet.

ATP assays are mostly based on the luciferase-luciferin interaction and report only global changes of ATP. By contrast, fluorescent sensors based on ATP-binding proteins, expressed in different cell compartments or small molecules attached to the cell surface enable the visualization of local ATP concentrations by live-cell imaging to help to better understand the mechanisms underlying ATP release.

This study aimed to find and develop appropriate ATP sensors and methods to visualize ATP concentrations at a sub-cellular level. To achieve this, the model of P2X7-dependent ATP release was used. First, genetically encoded, Förster resonance energy transfer (FRET)-based sensors were expressed in the cytosol or the plasma membrane of 3T3 or Yac-1 cells. These sensors did detect changes in cytosolic and cell-surface ATP concentrations after gating of P2X7 via ATP or NAD<sup>+</sup>-dependent ADP-ribosylation. Local ATP concentrations in the cytosol and at the cell surface were visualized and measured by live-cell imaging and flow cytometry. Gating of P2X7 resulted in an increase of ATP at the cell surface accompanied by a slow continuous decrease in cytosolic ATP. By contrast, the loss of cytosolic ATP induced by complement-dependent cytotoxicity (CDC) showed an initial delay of 2 min, followed by a steep decline.

Furthermore, small-molecule sensors based on a Zn(II)-dipicolylamine (DPA) backbone were evaluated. These were synthesized with reactive groups to attach them to cells or solid-phase surfaces by click chemistry. By attaching lipophilic cell anchors, these sensors were also integrated directly into cell membranes. However, in some sensors, modification with reactive groups influenced their sensitivity and selectivity towards nucleotides. Finally, genetically encoded single-wavelength sensors were produced and validated *in vitro*. Compared to their FRET-based counterparts, they could be produced in high quantity in a bacterial expression system. These sensors were targeted to cells of interest by binding them to streptavidin-coated beads, which were additionally loaded with an antibody directed against a cell surface antigen.

The results of this study will contribute to the further development of ATP sensors and lead to a better understanding of ATP release mechanisms and their significant role in immunological processes such as T cell activation.

# 6

## ZUSAMMENFASSUNG

Adenosintriophosphate (ATP) ist die Hauptenergiequelle in lebenden Organismen. Darüber hinaus ist ATP ein wichtiges Signalmolekül für P2X und P2Y Rezeptoren. P2X7 ist der meist untersuchte Purinrezeptor im Kontext der Immunologie, da dieser in einer Vielzahl von Immunzellen exprimiert wird. Die Aktivierung von P2X7 resultiert in einer Vielzahl von Downstream-Effekten, wie die Beeinflussung der T-Zellrezeptor (TZR) vermittelten Signale, Inflammasome Aktivierung, Porenbildung und der Zelltod. Viele Zellen können ATP reguliert freisetzen, der genaue Mechanismus und die Kinetik dieser Prozesse sind jedoch noch nicht vollständig verstanden.

ATP-Assays basieren größtenteils auf einer Luziferase-Luziferin-Reaktion und erlauben lediglich Rückschlüsse auf globale Änderung von ATP. Sensoren mit ATP-Bindedomänen, die in unterschiedlichen Zellkompartimenten exprimiert werden, oder niedermolekulare Sensoren an Zellmembranen, ermöglichen die Visualisierung von lokalen ATP-Konzentrationen mittels Live-Cell-Imaging und tragen so zum besseren Verständnis der Mechanismen zur ATP-Freisetzung bei.

Ziel dieser Arbeit war es, geeignete ATP-Sensoren und Methoden zur Visualisierung von ATP-Konzentrationen auf subzellulärer Ebene zu entwickeln. Dafür wurde das Modell der P2X7-vermittelte ATP-Freisetzung verwendet. Zunächst wurde mittels Transfektion eine zytosolische und membranöse Expression von auf FRET-basierenden ATP-Sensoren in 3T3 und Yac-1 Zellen induziert. Anhand dieser Sensoren wurden mittels Durchflusszytometrie und Live-Cell Imaging Unterschiede in der ATP-Konzentration auf der Zelloberfläche und im Zytosol nach der Aktivierung von P2X7 über ATP oder NAD-abhängige ADP-Ribosylierung gemessen. Die Aktivierung von P2X7 führte zu einer Zunahme extrazellulärem ATPs mit einer gleichzeitigen Abnahme zytosolischem ATPs. Die Induktion der komplementabhängigen Zytolyse (CDC) bewirkte eine verzögerte Abnahme das zytosolischen ATPs.

Außerdem wurden niedermolekulare Sensoren basierend auf einem Zn(II)-Dipicolylamin (DPA)-Rückgrat verwendet. Diese können mittels lipophiler Anker direkt auf Zelloberflächen oder mittels Click-Chemie an Zellen oder andere solide Oberflächen angebracht werden. Diese Modifikationen führten jedoch zu einer Veränderten Sensitivität gegenüber Nukleotiden. Auch wurden genetisch codierte Einzelwellenlängensensoren zur Markierung von Zellen verwendet, die im Gegensatz zum FRET-basierten Gegenstück in einem bakteriellen Expressionssystem produziert wurden. Dafür wurden diese Sensoren an Streptavidin-beschichtete Beads gebunden, die zusätzlich mit einem gegen ein Zelloberflächenantigen gerichteten Antikörper beladen waren.

Die Ergebnisse dieser Arbeit tragen zur weiteren Entwicklung von ATP Sensoren, zu einem besseren Verständnis der ATP Freisetzungsmechanismen und dessen Rolle in immunologischer Prozesse wie der T-Zell-Aktivierung bei.

# 7

## ACRONYMS

AAV	Adeno-associated virus
Ab	Antibodies
Ado	Adenosine
ADP	Adenosine diphosphate
AM	Acetoxymethyl
AMP	Adenosine monophosphate
APC	Antigen-presenting cells
ART	ADP-ribosyltransferase
ARTC	Cholera toxin-like-ADP-ribosyltransferases
ATP	Adenosine triphosphate
BCA	Bicinchoninic acid
BCR	B cell receptor
BSA	Bovine serum albumin
C1q	Complement component 1q
Ca <sup>2+</sup>	Calcium ions
CALHM1	Calcium homeostasis modulator 1
cAMP	Cyclic adenosine monophosphate
CCCP	Carbonyl cyanide m-chlorophenyl hydrazone
CCL3	Chemokine (C-C motif) ligand 3
CDC	Complement-dependent cytotoxicity
CFP	Cyan fluorescent protein
CO <sub>2</sub>	Carbon dioxide
CXCL9	C-X-C motif chemokine 9
DAMP	Danger- or damage-associated molecular pattern
DAPI	4,6-diamidino-2-phenylindole
DBCO	Dibenzocyclooctyne
DC	Dendritic cells
DMEM	Dulbecco's modified eagle medium
ddH <sub>2</sub> O	Double-distilled water

diH <sub>2</sub> O	Deionized water
DNA	Deoxyribonucleic acid
DPA	Dipicolylamine
eATP	Extracellular ATP
EBFP	Enhanced blue fluorescent protein
ECFP	Enhanced cyan fluorescent protein
ECS <sup>-/-</sup>	Extracellular solution
ECS <sup>+/-</sup>	ECS <sup>-/-</sup> with Ca <sup>2+</sup>
ECS <sup>+/+</sup>	ECS <sup>-/-</sup> with Ca <sup>2+</sup> and Mg <sup>2+</sup>
E-NPP	Ecto-nucleoside pyrophosphatase/phosphodiesterase
ENTPDase	Ecto-nucleoside triphosphate diphosphohydrolase
ER	Endoplasmic reticulum
Fab	Fragment antigen-binding
FACS	Fluorescence activated cell sorting
Fc	Fragment crystallizable
FCS	Fetal calf serum
Fiji	Fiji is just ImageJ
FRET	Förster resonance energy transfer
FSC	Forward scatter
GDP	Guanosine diphosphate
GFP	Green fluorescent protein
GMP	Guanosine monophosphate
GPCR	G-protein-coupled receptors
GPI	Glycosylphosphatidylinositol
GTP	Guanosine triphosphate
hcAb	Heavy chain antibody
HCS	Hematopoietic stem cells
HEPES	4-(2-hydroxyethyl)-1-piperazineethanesulfonic acid
HLA	Human leukocyte antigen
HRP	Horseradish peroxidase
iATP	Intracellular ATP
IgSF	Immunoglobulin superfamily
IL	Interleukin
ILC	Innate lymphoid cells

INF	Interferon
IP	Inositol phosphate
IPTG	Isopropyl- $\beta$ -D-thiogalactoside
K <sup>+</sup>	Potassium ions
KCl	Potassium chloride
KO	Knock-out
LUT	Look up table
MAC	Membrane attack complex
MFI	Median fluorescence intensity
Mg <sup>2+</sup>	Magnesium ions
Ca <sub>2</sub>	Magnesium Chloride
MHC	Major histocompatibility complex
MLB	Maleimide labeling buffer
mseCFP	Monomeric super-enhanced CFP
Na <sup>+</sup>	Sodium ions
NaCl	Sodium chloride
NAD <sup>+</sup>	Nicotinamide adenine dinucleotide
NALP3	NACHT, LRR and PYD domains-containing protein 3
Ni-NTA	Nickel-nitrilotriacetic acid
NK	Natural killer cells
O <sub>2</sub>	Oxygen
PBS <sup>-/-</sup>	Phosphate buffered saline
PBS <sup>+/+</sup>	PBS with calcium and magnesium
PCR	Polymerase chain reaction
PEG	Polyethylene glycol
PEI	Polyethyleneimine
PET	Photoinduced electron transfer
PFA	Paraformaldehyde
PI	Propidium iodide
PKA	Protein kinase A
PLC	Phospholipase C
PLL	Poly-l-lysine
PMMA	Poly methyl methacrylate
PPi	Pyrophosphate

PS	Phosphatidylserine
ROI	Region of interest
RPMI	Roswell Park Memorial Institute
RT	Room temperature
SA	Streptavidin
SDS	Sodium dodecyl sulfate
SERCA	Sarco/endoplasmic reticulum Ca <sup>2+</sup> ATPase
SNP	Single nucleotide polymorphism
SPAAC	Strain-promoted azide-alkyne cycloaddition
SSC	Side scatter
SOC	Super optimal broth with catabolite repression
TCR	T cell receptor
THG	Thapsigargin
TNF- $\alpha$	Tumor necrosis factor alpha
UDP	Uridine diphosphate
UTP	Uridine triphosphate
VRAC	Volume-regulated anion channel
WT	Wild type
YFP	Yellow fluorescent protein

## 8

## BIBLIOGRAPHY

- Adriouch, S., P. Bannas, N. Schwarz, R. Fliegert, A. H. Guse, M. Seman, F. Haag, and F. Koch-Nolte (Mar. 2008). "ADP-ribosylation at R125 gates the P2X7 ion channel by presenting a covalent ligand to its nucleotide binding site." In: *FASEB journal : official publication of the Federation of American Societies for Experimental Biology* 22 (3), pp. 861–869. DOI: [10.1096/fj.07-9294com](https://doi.org/10.1096/fj.07-9294com) (cit. on pp. 7, 77).
- Adriouch, S., C. Dox, V. Welge, M. Seman, F. Koch-Nolte, and F. Haag (Oct. 2002). "Cutting edge: a natural P451L mutation in the cytoplasmic domain impairs the function of the mouse P2X7 receptor." In: *Journal of immunology (Baltimore, Md. : 1950)* 169 (8), pp. 4108–4112. DOI: [10.4049/jimmunol.169.8.4108](https://doi.org/10.4049/jimmunol.169.8.4108) (cit. on p. 6).
- Adriouch, S., F. Haag, O. Boyer, M. Seman, and F. Koch-Nolte (Nov. 2012). "Extracellular NAD(+): a danger signal hindering regulatory T cells." In: *Microbes and infection* 14 (14), pp. 1284–1292. DOI: [10.1016/j.micinf.2012.05.011](https://doi.org/10.1016/j.micinf.2012.05.011) (cit. on p. 6).
- Adriouch, S., S. Hubert, S. Pechberty, F. Koch-Nolte, F. Haag, and M. Seman (July 2007). "NAD<sup>+</sup> released during inflammation participates in T cell homeostasis by inducing ART2-mediated death of naive T cells in vivo." In: *Journal of immunology (Baltimore, Md. : 1950)* 179 (1), pp. 186–194. DOI: [10.4049/jimmunol.179.1.186](https://doi.org/10.4049/jimmunol.179.1.186) (cit. on p. 8).
- Akopova, I., S. Tatur, M. Grygorczyk, R. Luchowski, I. Gryczynski, Z. Gryczynski, J. Borejdo, and R. Grygorczyk (Mar. 2012). "Imaging exocytosis of ATP-containing vesicles with TIRF microscopy in lung epithelial A549 cells." In: *Purinergic signalling* 8 (1), pp. 59–70. DOI: [10.1007/s11302-011-9259-2](https://doi.org/10.1007/s11302-011-9259-2). ppublish (cit. on p. 78).
- Alberto, A. V. P., R. X. Faria, C. G. C. Couto, L. G. B. Ferreira, C. A. M. Souza, P. C. N. Teixeira, M. M. Fróes, and L. A. Alves (Sept. 2013). "Is pannexin the pore associated with the P2X7 receptor?" In: *Naunyn-Schmiedeberg's archives of pharmacology* 386 (9), pp. 775–787. DOI: [10.1007/s00210-013-0868-x](https://doi.org/10.1007/s00210-013-0868-x). ppublish (cit. on p. 77).
- Allsopp, R. C., S. Dayl, A. Bin Dayel, R. Schmid, and R. J. Evans (May 2018). "Mapping the Allosteric Action of Antagonists A740003 and A438079 Reveals a Role for the Left Flipper in Ligand Sensitivity at P2X7 Receptors." In: *Molecular pharmacology* 93 (5), pp. 553–562. DOI: [10.1124/mol.117.111021](https://doi.org/10.1124/mol.117.111021). ppublish (cit. on p. 75).
- Allsopp, R. C. and R. J. Evans (June 2015). "Contribution of the Juxtatransmembrane Intracellular Regions to the Time Course and Permeation of ATP-gated P2X7 Receptor Ion Channels." In: *The Journal of biological chemistry* 290 (23), pp. 14556–14566. DOI: [10.1074/jbc.M115.642033](https://doi.org/10.1074/jbc.M115.642033) (cit. on p. 5).
- Antonioli, L., S. V. Novitskiy, K. F. Sachsenmeier, M. Fornai, C. Blandizzi, and G. Haskó (Nov. 2017). "Switching off CD73: a way to boost the activity of conventional and targeted

- antineoplastic therapies." In: *Drug discovery today* 22 (11), pp. 1686–1696. doi: [10.1016/j.drudis.2017.06.005](https://doi.org/10.1016/j.drudis.2017.06.005) (cit. on p. 10).
- Antonoli, L., P. Pacher, E. S. Vizi, and G. Haskó (June 2013). "CD39 and CD73 in immunity and inflammation." In: *Trends in molecular medicine* 19 (6), pp. 355–367. doi: [10.1016/j.molmed.2013.03.005](https://doi.org/10.1016/j.molmed.2013.03.005) (cit. on p. 10).
- Bajar, B. T., E. S. Wang, S. Zhang, M. Z. Lin, and J. Chu (Sept. 2016). "A Guide to Fluorescent Protein FRET Pairs." In: *Sensors (Basel, Switzerland)* 16 (9). doi: [10.3390/s16091488](https://doi.org/10.3390/s16091488) (cit. on p. 11).
- Bass, D. A., J. W. Parce, L. R. Dechatelet, P. Szejda, M. C. Seeds, and M. Thomas (Apr. 1983). "Flow cytometric studies of oxidative product formation by neutrophils: a graded response to membrane stimulation." In: *Journal of immunology (Baltimore, Md. : 1950)* 130 (4), pp. 1910–1917. ppublish (cit. on p. 34).
- Beis, I. and E. A. Newsholme (Oct. 1975). "The contents of adenine nucleotides, phosphagens and some glycolytic intermediates in resting muscles from vertebrates and invertebrates." In: *The Biochemical journal* 152 (1), pp. 23–32. doi: [10.1042/bj1520023](https://doi.org/10.1042/bj1520023) (cit. on p. 9).
- Boehm, T. and J. B. Swann (Feb. 2014). "Origin and evolution of adaptive immunity." In: *Annual review of animal biosciences* 2, pp. 259–283. doi: [10.1146/annurev-animal-022513-114201](https://doi.org/10.1146/annurev-animal-022513-114201) (cit. on p. 1).
- Boeynaems, J.-M., D. Communi, N. S. Gonzalez, and B. Robaye (Apr. 2005). "Overview of the P2 receptors." In: *Seminars in thrombosis and hemostasis* 31 (2), pp. 139–149. doi: [10.1055/s-2005-869519](https://doi.org/10.1055/s-2005-869519) (cit. on p. 4).
- Borea, P. A., S. Gessi, S. Merighi, F. Vincenzi, and K. Varani (July 2017). "Pathological overproduction: the bad side of adenosine." In: *British journal of pharmacology* 174 (13), pp. 1945–1960. doi: [10.1111/bph.13763](https://doi.org/10.1111/bph.13763) (cit. on p. 4).
- Borges da Silva, H., H. Wang, L. J. Qian, K. A. Hogquist, and S. C. Jameson (Apr. 2019). "ARTC2.2/P2RX7 Signaling during Cell Isolation Distorts Function and Quantification of Tissue-Resident CD8, javax.xml.bind.JAXBElement@6749715c, T Cell and Invariant NKT Subsets." In: *Journal of immunology (Baltimore, Md. : 1950)* 202 (7), pp. 2153–2163. doi: [10.4049/jimmunol.1801613](https://doi.org/10.4049/jimmunol.1801613). ppublish (cit. on p. 77).
- Botman, D., J. H. van Heerden, and B. Teusink (Mar. 2020). "An Improved ATP FRET Sensor For Yeast Shows Heterogeneity During Nutrient Transitions." In: *ACS sensors* 5 (3), pp. 814–822. doi: [10.1021/acssensors.9b02475](https://doi.org/10.1021/acssensors.9b02475). ppublish (cit. on p. 76).
- Boussif, O., F. Lezoualc'h, M. A. Zanta, M. D. Mergny, D. Scherman, B. Demeneix, and J. P. Behr (Aug. 1995). "A versatile vector for gene and oligonucleotide transfer into cells in culture and in vivo: polyethylenimine." In: *Proceedings of the National Academy of Sciences of the United States of America* 92 (16), pp. 7297–7301. doi: [10.1073/pnas.92.16.7297](https://doi.org/10.1073/pnas.92.16.7297). ppublish (cit. on p. 31).
- Burnstock, G. (Sept. 1972). "Purinergic nerves." In: *Pharmacological reviews* 24 (3), pp. 509–581 (cit. on p. 3).

- Burnstock, G., T. Cocks, L. Kasakov, and H. K. Wong (May 1978). "Direct evidence for ATP release from non-adrenergic, non-cholinergic ("purinergic") nerves in the guinea-pig taenia coli and bladder." In: *European journal of pharmacology* 49 (2), pp. 145–149. DOI: [10.1016/0014-2999\(78\)90070-5](https://doi.org/10.1016/0014-2999(78)90070-5) (cit. on p. 3).
- Campisi, J. and F. d'Adda di Fagagna (Sept. 2007). "Cellular senescence: when bad things happen to good cells." In: *Nature reviews. Molecular cell biology* 8 (9), pp. 729–740. DOI: [10.1038/nrm2233](https://doi.org/10.1038/nrm2233). ppublish (cit. on p. 75).
- Campwala, H. and S. J. Fountain (May 2013). "Constitutive and agonist stimulated ATP secretion in leukocytes." In: *Communicative & integrative biology* 6 (3), e23631. DOI: [10.4161/cib.23631](https://doi.org/10.4161/cib.23631) (cit. on p. 9).
- Cekic, C. and J. Linden (Mar. 2016). "Purinergic regulation of the immune system." In: *Nature reviews. Immunology* 16 (3), pp. 177–192. DOI: [10.1038/nri.2016.4](https://doi.org/10.1038/nri.2016.4) (cit. on p. 4).
- Crotty, S., P. Felgner, H. Davies, J. Glidewell, L. Villarreal, and R. Ahmed (Nov. 2003). "Cutting edge: long-term B cell memory in humans after smallpox vaccination." In: *Journal of immunology (Baltimore, Md. : 1950)* 171 (10), pp. 4969–4973. DOI: [10.4049/jimmunol.171.10.4969](https://doi.org/10.4049/jimmunol.171.10.4969) (cit. on p. 2).
- Dal Ben, D., M. Buccioni, C. Lambertucci, G. Marucci, A. Thomas, and R. Volpini (Jan. 2015). "Purinergic P2X receptors: structural models and analysis of ligand-target interaction." In: *European journal of medicinal chemistry* 89, pp. 561–580. DOI: [10.1016/j.ejmech.2014.10.071](https://doi.org/10.1016/j.ejmech.2014.10.071) (cit. on p. 4).
- Danquah, W. et al. (Nov. 2016). "Nanobodies that block gating of the P2X7 ion channel ameliorate inflammation." In: *Science translational medicine* 8 (366), 366ra162. DOI: [10.1126/scitranslmed.aaf8463](https://doi.org/10.1126/scitranslmed.aaf8463) (cit. on pp. 2, 9, 74).
- DeLuca, M. and W. D. McElroy (Feb. 1974). "Kinetics of the firefly luciferase catalyzed reactions." In: *Biochemistry* 13 (5), pp. 921–925. DOI: [10.1021/bi00702a015](https://doi.org/10.1021/bi00702a015) (cit. on p. 10).
- Denburg, J. L. and W. D. McElroy (Dec. 1970). "Anion inhibition of firefly luciferase." In: *Archives of biochemistry and biophysics* 141 (2), pp. 668–675. DOI: [10.1016/0003-9861\(70\)90187-6](https://doi.org/10.1016/0003-9861(70)90187-6) (cit. on p. 10).
- Denlinger, L. C., J. A. Sommer, K. Parker, L. Gudipaty, P. L. Fiset, J. W. Watters, R. A. Proctor, G. R. Dubyak, and P. J. Bertics (Aug. 2003). "Mutation of a dibasic amino acid motif within the C terminus of the P2X7 nucleotide receptor results in trafficking defects and impaired function." In: *Journal of immunology (Baltimore, Md. : 1950)* 171 (3), pp. 1304–1311. DOI: [10.4049/jimmunol.171.3.1304](https://doi.org/10.4049/jimmunol.171.3.1304) (cit. on p. 8).
- Di Virgilio, F., V. Bronte, D. Collavo, and P. Zanovello (Sept. 1989). "Responses of mouse lymphocytes to extracellular adenosine 5'-triphosphate (ATP). Lymphocytes with cytotoxic activity are resistant to the permeabilizing effects of ATP." In: *Journal of immunology (Baltimore, Md. : 1950)* 143 (6), pp. 1955–1960. ppublish (cit. on p. 8).
- Di Virgilio, F., D. Dal Ben, A. C. Sarti, A. L. Giuliani, and S. Falzoni (July 2017). "The P2X7 Receptor in Infection and Inflammation." In: *Immunity* 47 (1), pp. 15–31. DOI: [10.1016/j.immuni.2017.06.020](https://doi.org/10.1016/j.immuni.2017.06.020) (cit. on p. 6).

- Donnelly-Roberts, D. L. and M. F. Jarvis (July 2007). "Discovery of P2X7 receptor-selective antagonists offers new insights into P2X7 receptor function and indicates a role in chronic pain states." In: *British journal of pharmacology* 151 (5), pp. 571–579. DOI: [10.1038/sj.bjp.0707265](https://doi.org/10.1038/sj.bjp.0707265). ppublish (cit. on p. 74).
- Duckwitz, W., R. Hausmann, A. Aschrafi, and G. Schmalzing (Dec. 2006). "P2X5 subunit assembly requires scaffolding by the second transmembrane domain and a conserved aspartate." In: *The Journal of biological chemistry* 281 (51), pp. 39561–39572. DOI: [10.1074/jbc.M606113200](https://doi.org/10.1074/jbc.M606113200) (cit. on p. 4).
- Dutta, A. K., R. Z. Sabirov, H. Uramoto, and Y. Okada (Sept. 2004). "Role of ATP-conductive anion channel in ATP release from neonatal rat cardiomyocytes in ischaemic or hypoxic conditions." In: *The Journal of physiology* 559 (Pt 3), pp. 799–812. DOI: [10.1113/jphysiol.2004.069245](https://doi.org/10.1113/jphysiol.2004.069245) (cit. on p. 9).
- Dwyer, K. M., S. Deaglio, W. Gao, D. Friedman, T. B. Strom, and S. C. Robson (Mar. 2007). "CD39 and control of cellular immune responses." In: *Purinergic signalling* 3 (1-2), pp. 171–180. DOI: [10.1007/s11302-006-9050-y](https://doi.org/10.1007/s11302-006-9050-y) (cit. on p. 10).
- Farber, D. L., M. G. Netea, A. Radbruch, K. Rajewsky, and R. M. Zinkernagel (Feb. 2016). "Immunological memory: lessons from the past and a look to the future." In: *Nature reviews. Immunology* 16 (2), pp. 124–128. DOI: [10.1038/nri.2016.13](https://doi.org/10.1038/nri.2016.13) (cit. on p. 1).
- Forrester, T. (Aug. 1972). "An estimate of adenosine triphosphate release into the venous effluent from exercising human forearm muscle." In: *The Journal of physiology* 224 (3), pp. 611–628. DOI: [10.1113/jphysiol.1972.sp009915](https://doi.org/10.1113/jphysiol.1972.sp009915) (cit. on p. 9).
- Förster, T. (1948). "Zwischenmolekulare energiewanderung und fluoreszenz." In: *Annalen der physik* 437.1-2, pp. 55–75 (cit. on p. 11).
- Gaitán-Peñas, H., A. Gradogna, L. Laparra-Cuervo, C. Solsona, V. Fernández-Dueñas, A. Barrallo-Gimeno, F. Ciruela, M. Lakadamyali, M. Pusch, and R. Estévez (Oct. 2016). "Investigation of LRRC8-Mediated Volume-Regulated Anion Currents in *Xenopus* Oocytes." In: *Biophysical journal* 111 (7), pp. 1429–1443. DOI: [10.1016/j.bpj.2016.08.030](https://doi.org/10.1016/j.bpj.2016.08.030) (cit. on pp. 9, 76).
- Gallagher, S. R. and P. R. Desjardins (Nov. 2006). "Quantitation of DNA and RNA with absorption and fluorescence spectroscopy." In: *Current protocols in molecular biology* Appendix 3, Appendix 3D. DOI: [10.1002/0471142727.mba03ds76](https://doi.org/10.1002/0471142727.mba03ds76). ppublish (cit. on p. 41).
- Garbers, C., N. Jänner, A. Chalaris, M. L. Moss, D. M. Floss, D. Meyer, F. Koch-Nolte, S. Rose-John, and J. Scheller (Apr. 2011). "Species specificity of ADAM10 and ADAM17 proteins in interleukin-6 (IL-6) trans-signaling and novel role of ADAM10 in inducible IL-6 receptor shedding." In: *The Journal of biological chemistry* 286 (17), pp. 14804–14811. DOI: [10.1074/jbc.M111.229393](https://doi.org/10.1074/jbc.M111.229393) (cit. on p. 8).
- Glowacki, G., R. Braren, K. Firner, M. Nissen, M. Kühl, P. Reche, F. Bazan, M. Cetkovic-Cvrlje, E. Leiter, F. Haag, and F. Koch-Nolte (July 2002). "The family of toxin-related ecto-ADP-ribosyltransferases in humans and the mouse." In: *Protein science : a publication of the Protein Society* 11 (7), pp. 1657–1670. DOI: [10.1110/ps.0200602](https://doi.org/10.1110/ps.0200602) (cit. on p. 7).

- Gonnord, P., C. Delarasse, R. Auger, K. Benihoud, M. Prigent, M. H. Cuif, C. Lamaze, and J. M. Kanellopoulos (Mar. 2009). "Palmitoylation of the P2X7 receptor, an ATP-gated channel, controls its expression and association with lipid rafts." In: *FASEB journal : official publication of the Federation of American Societies for Experimental Biology* 23 (3), pp. 795–805. DOI: [10.1096/fj.08-114637](https://doi.org/10.1096/fj.08-114637) (cit. on p. 5).
- Gu, B., L. J. Bendall, and J. S. Wiley (Aug. 1998). "Adenosine triphosphate-induced shedding of CD23 and L-selectin (CD62L) from lymphocytes is mediated by the same receptor but different metalloproteases." In: *Blood* 92 (3), pp. 946–951 (cit. on p. 8).
- Guo, L., C. Li, H. Shang, R. Zhang, X. Li, Q. Lu, X. Cheng, Z. Liu, J. Z. Sun, and X. Yu (2020). "A side-chain engineering strategy for constructing fluorescent dyes with direct and ultrafast self-delivery to living cells." In: *Chemical Science* 11.3, pp. 661–670 (cit. on p. 80).
- Haag, F., F. Koch-Nolte, M. Köhl, S. Lorenzen, and H. G. Thiele (Oct. 1994). "Premature stop codons inactivate the RT6 genes of the human and chimpanzee species." In: *Journal of molecular biology* 243 (3), pp. 537–546. DOI: [10.1006/jmbi.1994.1680](https://doi.org/10.1006/jmbi.1994.1680) (cit. on p. 7).
- Haag, F., D. Freese, F. Scheublein, W. Ohlrogge, S. Adriouch, M. Seman, and F. Koch-Nolte (Dec. 2002). "T cells of different developmental stages differ in sensitivity to apoptosis induced by extracellular NAD." In: *Developmental immunology* 9 (4), pp. 197–202. DOI: [10.1080/10446670310001593514](https://doi.org/10.1080/10446670310001593514) (cit. on p. 8).
- Haan, J. M. M. den, R. Arens, and M. C. van Zelm (Dec. 2014). "The activation of the adaptive immune system: cross-talk between antigen-presenting cells, T cells and B cells." In: *Immunology letters* 162 (2 Pt B), pp. 103–112. DOI: [10.1016/j.imlet.2014.10.011](https://doi.org/10.1016/j.imlet.2014.10.011) (cit. on p. 1).
- Haanes, K. A., A. Schwab, and I. Novak (2012). "The P2X7 receptor supports both life and death in fibrogenic pancreatic stellate cells." In: *PloS one* 7 (12), e51164. DOI: [10.1371/journal.pone.0051164](https://doi.org/10.1371/journal.pone.0051164). ppublish (cit. on p. 75).
- Harayama, T. and H. Riezman (May 2018). "Understanding the diversity of membrane lipid composition." In: *Nature reviews. Molecular cell biology* 19 (5), pp. 281–296. DOI: [10.1038/nrm.2017.138](https://doi.org/10.1038/nrm.2017.138). ppublish (cit. on p. 78).
- Hattori, M. and E. Gouaux (May 2012). "Molecular mechanism of ATP binding and ion channel activation in P2X receptors." In: *Nature* 485 (7397), pp. 207–212. DOI: [10.1038/nature11010](https://doi.org/10.1038/nature11010). ppublish (cit. on p. 5).
- Hazlett, L. and M. Wu (Jan. 2011). "Defensins in innate immunity." In: *Cell and tissue research* 343 (1), pp. 175–188. DOI: [10.1007/s00441-010-1022-4](https://doi.org/10.1007/s00441-010-1022-4) (cit. on p. 1).
- He, W.-t., H. Wan, L. Hu, P. Chen, X. Wang, Z. Huang, Z.-H. Yang, C.-Q. Zhong, and J. Han (Dec. 2015). "Gasdermin D is an executor of pyroptosis and required for interleukin-1 $\beta$  secretion." In: *Cell research* 25 (12), pp. 1285–1298. DOI: [10.1038/cr.2015.139](https://doi.org/10.1038/cr.2015.139). ppublish (cit. on p. 78).

- Heberle, F. A. and G. W. Feigenson (Apr. 2011). "Phase separation in lipid membranes." In: *Cold Spring Harbor perspectives in biology* 3 (4). DOI: [10.1101/cshperspect.a004630](https://doi.org/10.1101/cshperspect.a004630). epublish (cit. on p. 81).
- Ho, T., A. I. Jobling, U. Greferath, T. Chuang, A. Ramesh, E. L. Fletcher, and K. A. Vessey (2015). "Vesicular expression and release of ATP from dopaminergic neurons of the mouse retina and midbrain." In: *Frontiers in cellular neuroscience* 9, p. 389. DOI: [10.3389/fncel.2015.00389](https://doi.org/10.3389/fncel.2015.00389). epublish (cit. on p. 78).
- Hofman, P., J. Cherfils-Vicini, M. Bazin, M. Ilie, T. Juhel, X. Hébuterne, E. Gilson, A. Schmid-Alliana, O. Boyer, S. Adriouch, and V. Vouret-Craviari (Mar. 2015). "Genetic and pharmacological inactivation of the purinergic P2RX7 receptor dampens inflammation but increases tumor incidence in a mouse model of colitis-associated cancer." In: *Cancer research* 75 (5), pp. 835–845. DOI: [10.1158/0008-5472.CAN-14-1778](https://doi.org/10.1158/0008-5472.CAN-14-1778). ppublish (cit. on p. 9).
- Hong, S., N. Schwarz, A. Brass, M. Seman, F. Haag, F. Koch-Nolte, W. P. Schilling, and G. R. Dubyak (July 2009). "Differential regulation of P2X7 receptor activation by extracellular nicotinamide adenine dinucleotide and ecto-ADP-ribosyltransferases in murine macrophages and T cells." In: *Journal of immunology (Baltimore, Md. : 1950)* 183 (1), pp. 578–592. DOI: [10.4049/jimmunol.0900120](https://doi.org/10.4049/jimmunol.0900120) (cit. on p. 7).
- Honigsmann, A., V. Mueller, S. W. Hell, and C. Eggeling (2013). "STED microscopy detects and quantifies liquid phase separation in lipid membranes using a new far-red emitting fluorescent phosphoglycerolipid analogue." In: *Faraday discussions* 161, 77–89, discussion 113–50. DOI: [10.1039/c2fd20107k](https://doi.org/10.1039/c2fd20107k). ppublish (cit. on p. 81).
- Hottiger, M. O., P. O. Hassa, B. Lüscher, H. Schüler, and F. Koch-Nolte (Apr. 2010). "Toward a unified nomenclature for mammalian ADP-ribosyltransferases." In: *Trends in biochemical sciences* 35 (4), pp. 208–219. DOI: [10.1016/j.tibs.2009.12.003](https://doi.org/10.1016/j.tibs.2009.12.003). ppublish (cit. on p. 6).
- Hou, B.-H., H. Takanaga, G. Grossmann, L.-Q. Chen, X.-Q. Qu, A. M. Jones, S. Lalonde, O. Schweissgut, W. Wiechert, and W. B. Frommer (Oct. 2011). "Optical sensors for monitoring dynamic changes of intracellular metabolite levels in mammalian cells." In: *Nature protocols* 6 (11), pp. 1818–1833. DOI: [10.1038/nprot.2011.392](https://doi.org/10.1038/nprot.2011.392). epublish (cit. on p. 39).
- Ignowski, J. M. and D. V. Schaffer (June 2004). "Kinetic analysis and modeling of firefly luciferase as a quantitative reporter gene in live mammalian cells." In: *Biotechnology and bioengineering* 86 (7), pp. 827–834. DOI: [10.1002/bit.20059](https://doi.org/10.1002/bit.20059) (cit. on p. 10).
- Iino, R., T. Murakami, S. Iizuka, Y. Kato-Yamada, T. Suzuki, and M. Yoshida (Dec. 2005). "Real-time monitoring of conformational dynamics of the epsilon subunit in F1-ATPase." In: *The Journal of biological chemistry* 280 (48), pp. 40130–40134. DOI: [10.1074/jbc.M506160200](https://doi.org/10.1074/jbc.M506160200) (cit. on pp. 13, 75).
- Imamura, H., K. P. H. Nhat, H. Togawa, K. Saito, R. Iino, Y. Kato-Yamada, T. Nagai, and H. Noji (Sept. 2009). "Visualization of ATP levels inside single living cells with fluorescence resonance energy transfer-based genetically encoded indicators." In: *Proceedings of the National Academy of Sciences of the United States of America* 106 (37), pp. 15651–15656. DOI: [10.1073/pnas.0904764106](https://doi.org/10.1073/pnas.0904764106) (cit. on pp. 11–13, 51, 71, 75, 76).

- Jablonski, A. (1933). "Efficiency of anti-Stokes fluorescence in dyes." In: *Nature* 131.3319, pp. 839–840 (cit. on p. 11).
- Jacobson, K., O. G. Mouritsen, and R. G. Anderson (2007). "Lipid rafts: at a crossroad between cell biology and physics." In: *Nature cell biology* 9.1, pp. 7–14 (cit. on p. 81).
- Jacobson, K. A., S. Paoletta, V. Katritch, B. Wu, Z.-G. Gao, Q. Zhao, R. C. Stevens, and E. Kiselev (Aug. 2015). "Nucleotides Acting at P2Y Receptors: Connecting Structure and Function." In: *Molecular pharmacology* 88 (2), pp. 220–230. DOI: [10.1124/mol.114.095711](https://doi.org/10.1124/mol.114.095711) (cit. on p. 4).
- Jia, H.-R., Y.-X. Zhu, K.-F. Xu, G.-Y. Pan, X. Liu, Y. Qiao, and F.-G. Wu (Apr. 2019). "Efficient cell surface labelling of live zebrafish embryos: wash-free fluorescence imaging for cellular dynamics tracking and nanotoxicity evaluation." In: *Chemical science* 10 (14), pp. 4062–4068. DOI: [10.1039/c8sc04884c](https://doi.org/10.1039/c8sc04884c). epublish (cit. on p. 81).
- Johnsen, B., K. E. Kaschubowski, S. Nader, E. Schneider, J.-A. Nicola, R. Fliegert, I. M. A. Wolf, A. H. Guse, V. O. Nikolaev, F. Koch-Nolte, and F. Haag (June 2019). "P2X7-mediated ATP secretion is accompanied by depletion of cytosolic ATP." In: *Purinergic signalling* 15 (2), pp. 155–166. DOI: [10.1007/s11302-019-09654-5](https://doi.org/10.1007/s11302-019-09654-5) (cit. on pp. 75, 77).
- Karasawa, A. and T. Kawate (Dec. 2016). "Structural basis for subtype-specific inhibition of the P2X7 receptor." In: *eLife* 5. DOI: [10.7554/eLife.22153](https://doi.org/10.7554/eLife.22153) (cit. on p. 5).
- Karasawa, A., K. Michalski, P. Mikhelzon, and T. Kawate (Sept. 2017). "The P2X7 receptor forms a dye-permeable pore independent of its intracellular domain but dependent on membrane lipid composition." In: *eLife* 6. DOI: [10.7554/eLife.31186](https://doi.org/10.7554/eLife.31186) (cit. on pp. 8, 77, 78).
- Kasuya, G., T. Yamaura, X.-B. Ma, R. Nakamura, M. Takemoto, H. Nagumo, E. Tanaka, N. Dohmae, T. Nakane, Y. Yu, R. Ishitani, O. Matsuzaki, M. Hattori, and O. Nureki (Oct. 2017). "Structural insights into the competitive inhibition of the ATP-gated P2X receptor channel." In: *Nature communications* 8 (1), p. 876. DOI: [10.1038/s41467-017-00887-9](https://doi.org/10.1038/s41467-017-00887-9). epublish (cit. on p. 5).
- Kataoka, A., H. Tozaki-Saitoh, Y. Koga, M. Tsuda, and K. Inoue (Jan. 2009). "Activation of P2X7 receptors induces CCL3 production in microglial cells through transcription factor NFAT." In: *Journal of neurochemistry* 108 (1), pp. 115–125. DOI: [10.1111/j.1471-4159.2008.05744.x](https://doi.org/10.1111/j.1471-4159.2008.05744.x). ppublish (cit. on p. 9).
- Kato-Yamada, Y. and M. Yoshida (Sept. 2003). "Isolated epsilon subunit of thermophilic F1-ATPase binds ATP." In: *The Journal of biological chemistry* 278 (38), pp. 36013–36016. DOI: [10.1074/jbc.M306140200](https://doi.org/10.1074/jbc.M306140200) (cit. on p. 13).
- Kawate, T., J. C. Michel, W. T. Birdsong, and E. Gouaux (July 2009). "Crystal structure of the ATP-gated P2X(4) ion channel in the closed state." In: *Nature* 460 (7255), pp. 592–598. DOI: [10.1038/nature08198](https://doi.org/10.1038/nature08198) (cit. on pp. 4, 5).
- Klymchenko, A. S. and R. Kreder (Jan. 2014). "Fluorescent probes for lipid rafts: from model membranes to living cells." In: *Chemistry & biology* 21 (1), pp. 97–113. DOI: [10.1016/j.chembiol.2013.11.009](https://doi.org/10.1016/j.chembiol.2013.11.009). ppublish (cit. on p. 80).

- Knowles, J. R. (1980). "Enzyme-catalyzed phosphoryl transfer reactions." In: *Annual review of biochemistry* 49, pp. 877–919. DOI: [10.1146/annurev.bi.49.070180.004305](https://doi.org/10.1146/annurev.bi.49.070180.004305) (cit. on p. 3).
- Köberlin, M. S., B. Snijder, L. X. Heinz, C. L. Baumann, A. Fauster, G. I. Vladimer, A.-C. Gavin, and G. Superti-Furga (July 2015). "A Conserved Circular Network of Coregulated Lipids Modulates Innate Immune Responses." In: *Cell* 162 (1), pp. 170–183. DOI: [10.1016/j.cell.2015.05.051](https://doi.org/10.1016/j.cell.2015.05.051). ppublish (cit. on p. 78).
- Komatsubara, A. T., M. Matsuda, and K. Aoki (Aug. 2015). "Quantitative analysis of recombination between YFP and CFP genes of FRET biosensors introduced by lentiviral or retroviral gene transfer." In: *Scientific reports* 5, p. 13283. DOI: [10.1038/srep13283](https://doi.org/10.1038/srep13283). epublish (cit. on p. 61).
- Kraft, A. E. and V. O. Nikolaev (2017). "FRET Microscopy for Real-Time Visualization of Second Messengers in Living Cells." In: *Methods in molecular biology (Clifton, N.J.)* 1563, pp. 85–90. DOI: [10.1007/978-1-4939-6810-7\\_6](https://doi.org/10.1007/978-1-4939-6810-7_6). ppublish (cit. on p. 38).
- Kügelgen, I. von (July 2006). "Excitatory P2-receptors at sympathetic axon terminals: role in temperature control of cutaneous blood flow." In: *British journal of pharmacology* 148 (5), pp. 561–562. DOI: [10.1038/sj.bjp.0706767](https://doi.org/10.1038/sj.bjp.0706767) (cit. on p. 4).
- Laemmli, U. K. (Aug. 1970). "Cleavage of structural proteins during the assembly of the head of bacteriophage T4." In: *Nature* 227 (5259), pp. 680–685. DOI: [10.1038/227680a0](https://doi.org/10.1038/227680a0). ppublish (cit. on p. 42).
- Lam, A. J., F. St-Pierre, Y. Gong, J. D. Marshall, P. J. Cranfill, M. A. Baird, M. R. McKeown, J. Wiedenmann, M. W. Davidson, M. J. Schnitzer, R. Y. Tsien, and M. Z. Lin (Oct. 2012). "Improving FRET dynamic range with bright green and red fluorescent proteins." In: *Nature methods* 9 (10), pp. 1005–1012. DOI: [10.1038/nmeth.2171](https://doi.org/10.1038/nmeth.2171) (cit. on p. 12).
- Le Duc, D., A. Schulz, V. Lede, A. Schulze, D. Thor, A. Brüser, and T. Schöneberg (2017). "P2Y Receptors in Immune Response and Inflammation." In: *Advances in immunology* 136, pp. 85–121. DOI: [10.1016/bs.ai.2017.05.006](https://doi.org/10.1016/bs.ai.2017.05.006) (cit. on p. 4).
- Le Stunff, H., R. Auger, J. Kanellopoulos, and M.-N. Raymond (Apr. 2004). "The Pro-451 to Leu polymorphism within the C-terminal tail of P2X7 receptor impairs cell death but not phospholipase D activation in murine thymocytes." In: *The Journal of biological chemistry* 279 (17), pp. 16918–16926. DOI: [10.1074/jbc.M313064200](https://doi.org/10.1074/jbc.M313064200) (cit. on p. 8).
- Ledderose, C., Y. Bao, J. Zhang, and W. G. Junger (Feb. 2015). "Novel method for real-time monitoring of ATP release reveals multiple phases of autocrine purinergic signalling during immune cell activation." In: *Acta physiologica (Oxford, England)* 213 (2), pp. 334–345. DOI: [10.1111/apha.12435](https://doi.org/10.1111/apha.12435). ppublish (cit. on p. 14).
- Ledderose, C., Y. Bao, M. Lidicky, J. Zipperle, L. Li, K. Strasser, N. I. Shapiro, and W. G. Junger (Sept. 2014). "Mitochondria are gate-keepers of T cell function by producing the ATP that drives purinergic signaling." In: *The Journal of biological chemistry* 289 (37), pp. 25936–25945. DOI: [10.1074/jbc.M114.575308](https://doi.org/10.1074/jbc.M114.575308) (cit. on pp. 14, 76).

- Lerchundi, R., K. W. Kafitz, U. Winkler, M. Färfers, J. Hirrlinger, and C. R. Rose (Aug. 2019). "FRET-based imaging of intracellular ATP in organotypic brain slices." In: *Journal of neuroscience research* 97 (8), pp. 933–945. DOI: [10.1002/jnr.24361](https://doi.org/10.1002/jnr.24361). ppublish (cit. on p. 76).
- Lipmann, F. (Nov. 1941). "Metabolic Generation and Utilization of Phosphate Bond Energy." In: *Adv. Enzymol* 1, pp. 99–162. DOI: [10.1002/9780470122464.ch4](https://doi.org/10.1002/9780470122464.ch4) (cit. on p. 74).
- Lobas, M. A., R. Tao, J. Nagai, M. T. Kronschläger, P. M. Borden, J. S. Marvin, L. L. Looger, and B. S. Khakh (Feb. 2019). "A genetically encoded single-wavelength sensor for imaging cytosolic and cell surface ATP." In: *Nature communications* 10 (1), p. 711. DOI: [10.1038/s41467-019-08441-5](https://doi.org/10.1038/s41467-019-08441-5). epublish (cit. on pp. 70, 71, 76).
- Locovei, S., E. Scemes, F. Qiu, D. C. Spray, and G. Dahl (Feb. 2007). "Pannexin1 is part of the pore forming unit of the P2X(7) receptor death complex." In: *FEBS letters* 581 (3), pp. 483–488. DOI: [10.1016/j.febslet.2006.12.056](https://doi.org/10.1016/j.febslet.2006.12.056). ppublish (cit. on p. 77).
- Mackenzie, A. B., M. T. Young, E. Adinolfi, and A. Surprenant (Oct. 2005). "Pseudoapoptosis induced by brief activation of ATP-gated P2X7 receptors." In: *The Journal of biological chemistry* 280 (40), pp. 33968–33976. DOI: [10.1074/jbc.M502705200](https://doi.org/10.1074/jbc.M502705200) (cit. on p. 8).
- Mansoor, S. E., W. Lü, W. Oosterheert, M. Shekhar, E. Tajkhorshid, and E. Gouaux (Oct. 2016). "X-ray structures define human P2X(3) receptor gating cycle and antagonist action." In: *Nature* 538 (7623), pp. 66–71. DOI: [10.1038/nature19367](https://doi.org/10.1038/nature19367) (cit. on p. 5).
- Mantovani, A., C. A. Dinarello, M. Molgora, and C. Garlanda (Apr. 2019). "Interleukin-1 and Related Cytokines in the Regulation of Inflammation and Immunity." In: *Immunity* 50 (4), pp. 778–795. DOI: [10.1016/j.immuni.2019.03.012](https://doi.org/10.1016/j.immuni.2019.03.012). ppublish (cit. on p. 9).
- Margineanu, A., J. J. Chan, D. J. Kelly, S. C. Warren, D. Flatters, S. Kumar, M. Katan, C. W. Dunsby, and P. M. W. French (June 2016). "Screening for protein-protein interactions using Förster resonance energy transfer (FRET) and fluorescence lifetime imaging microscopy (FLIM)." In: *Scientific reports* 6, p. 28186. DOI: [10.1038/srep28186](https://doi.org/10.1038/srep28186) (cit. on p. 12).
- Matsuda, T., A. Miyawaki, and T. Nagai (Apr. 2008). "Direct measurement of protein dynamics inside cells using a rationally designed photoconvertible protein." In: *Nature methods* 5 (4), pp. 339–345. DOI: [10.1038/nmeth.1193](https://doi.org/10.1038/nmeth.1193) (cit. on p. 13).
- McCarthy, A. E., C. Yoshioka, and S. E. Mansoor (Oct. 2019). "Full-Length P2X7 Structures Reveal How Palmitoylation Prevents Channel Desensitization." In: *Cell* 179 (3), 659–670.e13. DOI: [10.1016/j.cell.2019.09.017](https://doi.org/10.1016/j.cell.2019.09.017) (cit. on pp. 5, 6).
- McKinnon, K. M. (Feb. 2018). "Flow Cytometry: An Overview." In: *Current protocols in immunology* 120, pp. 5.1.1–5.1.11. DOI: [10.1002/cpim.40](https://doi.org/10.1002/cpim.40). epublish (cit. on p. 35).
- Menzel, S., B. Rissiek, P. Bannas, T. Jakoby, M. Miksiewicz, N. Schwarz, M. Nissen, F. Haag, A. Tholey, and F. Koch-Nolte (Sept. 2015). "Nucleotide-Induced Membrane-Proximal Proteolysis Controls the Substrate Specificity of T Cell Ecto-ADP-Ribosyltransferase ARTC2.2." In: *Journal of immunology (Baltimore, Md. : 1950)* 195 (5), pp. 2057–2066. DOI: [10.4049/jimmunol.1401677](https://doi.org/10.4049/jimmunol.1401677) (cit. on p. 8).

- Milo, R., P. Jorgensen, U. Moran, G. Weber, and M. Springer (2009). "BioNumbers—the database of key numbers in molecular and cell biology." In: *Nucleic acids research* 38.suppl\_1, pp. D750–D753 (cit. on p. 9).
- Mishra, M., S. Tiwari, and A. V. Gomes (Nov. 2017). "Protein purification and analysis: next generation Western blotting techniques." In: *Expert review of proteomics* 14 (11), pp. 1037–1053. DOI: [10.1080/14789450.2017.1388167](https://doi.org/10.1080/14789450.2017.1388167). ppublish (cit. on p. 43).
- Moon, H., H.-Y. Na, K. H. Chong, and T. J. Kim (Jan. 2006). "P2X7 receptor-dependent ATP-induced shedding of CD27 in mouse lymphocytes." In: *Immunology letters* 102 (1), pp. 98–105. DOI: [10.1016/j.imlet.2005.08.004](https://doi.org/10.1016/j.imlet.2005.08.004) (cit. on p. 8).
- Moro, A. J., P. J. Cywinski, S. Körsten, and G. J. Mohr (Feb. 2010). "An ATP fluorescent chemosensor based on a Zn(II)-complexed dipicolylamine receptor coupled with a naphthalimide chromophore." In: *Chemical communications (Cambridge, England)* 46 (7), pp. 1085–1087. DOI: [10.1039/b919661g](https://doi.org/10.1039/b919661g) (cit. on pp. 14, 62, 78, 79).
- Moro, A. J., J. Schmidt, T. Doussineau, A. Lapresta-Fernandéz, J. Wegener, and G. J. Mohr (June 2011). "Surface-functionalized fluorescent silica nanoparticles for the detection of ATP." In: *Chemical communications (Cambridge, England)* 47 (21), pp. 6066–6068. DOI: [10.1039/c1cc10419e](https://doi.org/10.1039/c1cc10419e) (cit. on pp. 15, 79).
- Nagai, T., K. Ibata, E. S. Park, M. Kubota, K. Mikoshiba, and A. Miyawaki (Jan. 2002). "A variant of yellow fluorescent protein with fast and efficient maturation for cell-biological applications." In: *Nature biotechnology* 20 (1), pp. 87–90. DOI: [10.1038/nbt0102-87](https://doi.org/10.1038/nbt0102-87) (cit. on p. 13).
- Nagai, T., S. Yamada, T. Tominaga, M. Ichikawa, and A. Miyawaki (July 2004). "Expanded dynamic range of fluorescent indicators for Ca(2+) by circularly permuted yellow fluorescent proteins." In: *Proceedings of the National Academy of Sciences of the United States of America* 101 (29), pp. 10554–10559. DOI: [10.1073/pnas.0400417101](https://doi.org/10.1073/pnas.0400417101) (cit. on p. 13).
- Neefjes, J., M. L. M. Jongsmá, P. Paul, and O. Bakke (Nov. 2011). "Towards a systems understanding of MHC class I and MHC class II antigen presentation." In: *Nature reviews. Immunology* 11 (12), pp. 823–836. DOI: [10.1038/nri3084](https://doi.org/10.1038/nri3084) (cit. on p. 2).
- Netea, M. G., A. Schlitzer, K. Placek, L. A. B. Joosten, and J. L. Schultze (Jan. 2019). "Innate and Adaptive Immune Memory: an Evolutionary Continuum in the Host's Response to Pathogens." In: *Cell host & microbe* 25 (1), pp. 13–26. DOI: [10.1016/j.chom.2018.12.006](https://doi.org/10.1016/j.chom.2018.12.006) (cit. on p. 1).
- Neumann, E., M. Schaefer-Ridder, Y. Wang, and P. H. Hofschneider (1982). "Gene transfer into mouse lymphoma cells by electroporation in high electric fields." In: *The EMBO journal* 1 (7), pp. 841–845. ppublish (cit. on p. 33).
- Nicke, A., Y.-H. Kuan, M. Masin, J. Rettinger, B. Marquez-Klaka, O. Bender, D. C. Górecki, R. D. Murrell-Lagnado, and F. Soto (Sept. 2009). "A functional P2X7 splice variant with an alternative transmembrane domain 1 escapes gene inactivation in P2X7 knock-out mice." In: *The Journal of biological chemistry* 284 (38), pp. 25813–25822. DOI: [10.1074/jbc.M109.033134](https://doi.org/10.1074/jbc.M109.033134) (cit. on p. 6).

- Nikolaev, V. O., S. Gambaryan, and M. J. Lohse (Jan. 2006). "Fluorescent sensors for rapid monitoring of intracellular cGMP." In: *Nature methods* 3 (1), pp. 23–25. DOI: [10.1038/nmeth816](https://doi.org/10.1038/nmeth816). ppublish (cit. on p. 38).
- Nutt, S. L., P. D. Hodgkin, D. M. Tarlinton, and L. M. Corcoran (Mar. 2015). "The generation of antibody-secreting plasma cells." In: *Nature reviews. Immunology* 15 (3), pp. 160–171. DOI: [10.1038/nri3795](https://doi.org/10.1038/nri3795) (cit. on p. 2).
- Ojida, A., Y. Mito-Oka, M.-A. Inoue, and I. Hamachi (June 2002). "First artificial receptors and chemosensors toward phosphorylated peptide in aqueous solution." In: *Journal of the American Chemical Society* 124 (22), pp. 6256–6258. DOI: [10.1021/ja025761b](https://doi.org/10.1021/ja025761b). ppublish (cit. on p. 79).
- Ojida, A., I. Takashima, T. Kohira, H. Nonaka, and I. Hamachi (Sept. 2008). "Turn-on fluorescence sensing of nucleoside polyphosphates using a xanthene-based Zn(II) complex chemosensor." In: *Journal of the American Chemical Society* 130 (36), pp. 12095–12101. DOI: [10.1021/ja803262w](https://doi.org/10.1021/ja803262w) (cit. on pp. 14, 78).
- Park, H. I., H. W. Yoon, and S. T. Jung (Nov. 2016). "The Highly Evolvable Antibody Fc Domain." In: *Trends in biotechnology* 34 (11), pp. 895–908. DOI: [10.1016/j.tibtech.2016.04.005](https://doi.org/10.1016/j.tibtech.2016.04.005) (cit. on pp. 2, 36).
- Patterson, G. H., D. W. Piston, and B. G. Barisas (Sept. 2000). "Förster distances between green fluorescent protein pairs." In: *Analytical biochemistry* 284 (2), pp. 438–440. DOI: [10.1006/abio.2000.4708](https://doi.org/10.1006/abio.2000.4708) (cit. on p. 12).
- Pelegrin, P., C. Barroso-Gutierrez, and A. Surprenant (June 2008). "P2X7 receptor differentially couples to distinct release pathways for IL-1beta in mouse macrophage." In: *Journal of immunology (Baltimore, Md. : 1950)* 180 (11), pp. 7147–7157. DOI: [10.4049/jimmunol.180.11.7147](https://doi.org/10.4049/jimmunol.180.11.7147) (cit. on p. 9).
- Pelegrin, P. and A. Surprenant (Nov. 2006). "Pannexin-1 mediates large pore formation and interleukin-1beta release by the ATP-gated P2X7 receptor." In: *The EMBO journal* 25 (21), pp. 5071–5082. DOI: [10.1038/sj.emboj.7601378](https://doi.org/10.1038/sj.emboj.7601378). ppublish (cit. on p. 77).
- Pellegatti, P., S. Falzoni, P. Pinton, R. Rizzuto, and F. Di Virgilio (Aug. 2005). "A novel recombinant plasma membrane-targeted luciferase reveals a new pathway for ATP secretion." In: *Molecular biology of the cell* 16 (8), pp. 3659–3665. DOI: [10.1091/mbc.e05-03-0222](https://doi.org/10.1091/mbc.e05-03-0222). ppublish (cit. on p. 76).
- Pellegatti, P., L. Raffaghello, G. Bianchi, F. Piccardi, V. Pistoia, and F. Di Virgilio (July 2008). "Increased level of extracellular ATP at tumor sites: in vivo imaging with plasma membrane luciferase." In: *PLoS one* 3 (7), e2599. DOI: [10.1371/journal.pone.0002599](https://doi.org/10.1371/journal.pone.0002599) (cit. on p. 9).
- Pleiner, T., M. Bates, and D. Görlich (Mar. 2018). "A toolbox of anti-mouse and anti-rabbit IgG secondary nanobodies." In: *The Journal of cell biology* 217 (3), pp. 1143–1154. DOI: [10.1083/jcb.201709115](https://doi.org/10.1083/jcb.201709115). ppublish (cit. on p. 66).

- Poot, M., L. L. Gibson, and V. L. Singer (Apr. 1997). "Detection of apoptosis in live cells by MitoTracker red CMXRos and SYTO dye flow cytometry." In: *Cytometry* 27 (4), pp. 358–364. ppublish (cit. on p. 34).
- Pope, B. and H. M. Kent (Feb. 1996). "High efficiency 5 min transformation of *Escherichia coli*." In: *Nucleic acids research* 24 (3), pp. 536–537. doi: [10.1093/nar/24.3.536](https://doi.org/10.1093/nar/24.3.536). ppublish (cit. on p. 41).
- Praetorius, H. A. and J. Leipziger (Dec. 2009). "ATP release from non-excitabile cells." In: *Purinergic signalling* 5 (4), pp. 433–446. doi: [10.1007/s11302-009-9146-2](https://doi.org/10.1007/s11302-009-9146-2) (cit. on p. 11).
- Proietti, M., V. Cornacchione, T. Rezzonico Jost, A. Romagnani, C. E. Faliti, L. Perruzza, R. Rigoni, E. Radaelli, F. Caprioli, S. Preziuso, B. Brannetti, M. Thelen, K. D. McCoy, E. Slack, E. Traggiai, and F. Grassi (Nov. 2014). "ATP-gated ionotropic P2X7 receptor controls follicular T helper cell numbers in Peyer's patches to promote host-microbiota mutualism." In: *Immunity* 41 (5), pp. 789–801. doi: [10.1016/j.immuni.2014.10.010](https://doi.org/10.1016/j.immuni.2014.10.010). ppublish (cit. on p. 9).
- Qu, Y., S. Misaghi, K. Newton, L. L. Gilmour, S. Louie, J. E. Cupp, G. R. Dubyak, D. Hackos, and V. M. Dixit (June 2011). "Pannexin-1 is required for ATP release during apoptosis but not for inflammasome activation." In: *Journal of immunology (Baltimore, Md. : 1950)* 186 (11), pp. 6553–6561. doi: [10.4049/jimmunol.1100478](https://doi.org/10.4049/jimmunol.1100478). ppublish (cit. on p. 77).
- Quinn, P. J. and C. Wolf (Jan. 2009). "The liquid-ordered phase in membranes." In: *Biochimica et biophysica acta* 1788 (1), pp. 33–46. doi: [10.1016/j.bbamem.2008.08.005](https://doi.org/10.1016/j.bbamem.2008.08.005). ppublish (cit. on p. 81).
- Rissiek, A., I. Baumann, A. Cuapio, A. Mautner, M. Kolster, P. C. Arck, A. Dodge-Khatami, H.-W. Mittrücker, F. Koch-Nolte, F. Haag, and E. Tolosa (Apr. 2015). "The expression of CD39 on regulatory T cells is genetically driven and further upregulated at sites of inflammation." In: *Journal of autoimmunity* 58, pp. 12–20. doi: [10.1016/j.jaut.2014.12.007](https://doi.org/10.1016/j.jaut.2014.12.007) (cit. on p. 10).
- Rissiek, B., F. Haag, O. Boyer, F. Koch-Nolte, and S. Adriouch (2015a). "ADP-ribosylation of P2X7: a matter of life and death for regulatory T cells and natural killer T cells." In: *Current topics in microbiology and immunology* 384, pp. 107–126. doi: [10.1007/82\\_2014\\_420](https://doi.org/10.1007/82_2014_420) (cit. on p. 7).
- (2015b). "P2X7 on Mouse T Cells: One Channel, Many Functions." In: *Frontiers in immunology* 6, p. 204. doi: [10.3389/fimmu.2015.00204](https://doi.org/10.3389/fimmu.2015.00204) (cit. on p. 10).
- Rissiek, B., M. Lukowiak, F. Raczkowski, T. Magnus, H.-W. Mittrücker, and F. Koch-Nolte (2018). "javax.xml.bind.JAXBElement@6008d197, Blockade of Murine ARTC2.2 During Cell Preparation Preserves the Vitality and Function of Liver Tissue-Resident Memory T Cells." In: *Frontiers in immunology* 9, p. 1580. doi: [10.3389/fimmu.2018.01580](https://doi.org/10.3389/fimmu.2018.01580). epublish (cit. on pp. 8, 77).
- Rizzo, M. A., G. Springer, K. Segawa, W. R. Zipfel, and D. W. Piston (June 2006). "Optimization of pairings and detection conditions for measurement of FRET between cyan and yellow fluorescent proteins." In: *Microscopy and microanalysis : the official journal of*

- Microscopy Society of America, Microbeam Analysis Society, Microscopical Society of Canada* 12 (3), pp. 238–254. DOI: [10.1017/S1431927606060235](https://doi.org/10.1017/S1431927606060235) (cit. on p. 12).
- Robinson, L. E., M. Shridar, P. Smith, and R. D. Murrell-Lagnado (Nov. 2014). “Plasma membrane cholesterol as a regulator of human and rodent P2X7 receptor activation and sensitization.” In: *The Journal of biological chemistry* 289 (46), pp. 31983–31994. DOI: [10.1074/jbc.M114.574699](https://doi.org/10.1074/jbc.M114.574699). ppublish (cit. on p. 78).
- Robson, S. C., J. Sévigny, and H. Zimmermann (June 2006). “The E-NTPDase family of ectonucleotidases: Structure function relationships and pathophysiological significance.” In: *Purinergic signalling* 2 (2), pp. 409–430. DOI: [10.1007/s11302-006-9003-5](https://doi.org/10.1007/s11302-006-9003-5) (cit. on p. 10).
- Roger, S., B. Jelassi, I. Couillin, P. Pelegrin, P. Besson, and L.-H. Jiang (Oct. 2015). “Understanding the roles of the P2X7 receptor in solid tumour progression and therapeutic perspectives.” In: *Biochimica et biophysica acta* 1848 (10 Pt B), pp. 2584–2602. DOI: [10.1016/j.bbame.2014.10.029](https://doi.org/10.1016/j.bbame.2014.10.029). ppublish (cit. on p. 9).
- Roger, S., P. Pelegrin, and A. Surprenant (June 2008). “Facilitation of P2X7 receptor currents and membrane blebbing via constitutive and dynamic calmodulin binding.” In: *The Journal of neuroscience : the official journal of the Society for Neuroscience* 28 (25), pp. 6393–6401. DOI: [10.1523/JNEUROSCI.0696-08.2008](https://doi.org/10.1523/JNEUROSCI.0696-08.2008) (cit. on p. 8).
- Romanello, M., B. Pani, M. Bicego, and P. D’Andrea (Dec. 2001). “Mechanically induced ATP release from human osteoblastic cells.” In: *Biochemical and biophysical research communications* 289 (5), pp. 1275–1281. DOI: [10.1006/bbrc.2001.6124](https://doi.org/10.1006/bbrc.2001.6124). ppublish (cit. on p. 77).
- Sabirov, R. Z., A. K. Dutta, and Y. Okada (Sept. 2001). “Volume-dependent ATP-conductive large-conductance anion channel as a pathway for swelling-induced ATP release.” In: *The Journal of general physiology* 118 (3), pp. 251–266. DOI: [10.1085/jgp.118.3.251](https://doi.org/10.1085/jgp.118.3.251). ppublish (cit. on p. 76).
- Sakaki, H., T. Fujiwaki, M. Tsukimoto, A. Kawano, H. Harada, and S. Kojima (Mar. 2013). “P2X4 receptor regulates P2X7 receptor-dependent IL-1 $\beta$  and IL-18 release in mouse bone marrow-derived dendritic cells.” In: *Biochemical and biophysical research communications* 432 (3), pp. 406–411. DOI: [10.1016/j.bbrc.2013.01.135](https://doi.org/10.1016/j.bbrc.2013.01.135) (cit. on p. 9).
- Scheuplein, F., N. Schwarz, S. Adriouch, C. Krebs, P. Bannas, B. Rissiek, M. Seman, F. Haag, and F. Koch-Nolte (Mar. 2009). “NAD<sup>+</sup> and ATP released from injured cells induce P2X7-dependent shedding of CD62L and externalization of phosphatidylserine by murine T cells.” In: *Journal of immunology (Baltimore, Md. : 1950)* 182 (5), pp. 2898–2908. DOI: [10.4049/jimmunol.0801711](https://doi.org/10.4049/jimmunol.0801711) (cit. on p. 77).
- Schneckenburger, H., P. Weber, M. Wagner, S. Enderle, B. Kalthof, L. Schneider, C. Herzog, J. Weghuber, and P. Lanzerstorfer (Feb. 2019). “Combining TIR and FRET in Molecular Test Systems.” In: *International journal of molecular sciences* 20 (3). DOI: [10.3390/ijms20030648](https://doi.org/10.3390/ijms20030648) (cit. on p. 12).
- Schwarz, N., L. Drouot, A. Nicke, R. Fliegert, O. Boyer, A. H. Guse, F. Haag, S. Adriouch, and F. Koch-Nolte (2012). “Alternative splicing of the N-terminal cytosolic and transmembrane

- domains of P2X7 controls gating of the ion channel by ADP-ribosylation." In: *PLoS one* 7 (7), e41269. DOI: [10.1371/journal.pone.0041269](https://doi.org/10.1371/journal.pone.0041269) (cit. on pp. 5, 6).
- Schwarz, N., R. Fliegert, S. Adriouch, M. Seman, A. H. Guse, F. Haag, and F. Koch-Nolte (June 2009). "Activation of the P2X7 ion channel by soluble and covalently bound ligands." In: *Purinergic signalling* 5 (2), pp. 139–149. DOI: [10.1007/s11302-009-9135-5](https://doi.org/10.1007/s11302-009-9135-5) (cit. on pp. 6, 7).
- Segawa, K. and S. Nagata (Nov. 2015). "An Apoptotic 'Eat Me' Signal: Phosphatidylserine Exposure." In: *Trends in cell biology* 25 (11), pp. 639–650. DOI: [10.1016/j.tcb.2015.08.003](https://doi.org/10.1016/j.tcb.2015.08.003). ppublish (cit. on p. 7).
- Seman, M., S. Adriouch, F. Scheuplein, C. Krebs, D. Freese, G. Glowacki, P. Deterre, F. Haag, and F. Koch-Nolte (Oct. 2003). "NAD-induced T cell death: ADP-ribosylation of cell surface proteins by ART2 activates the cytolytic P2X7 purinoceptor." In: *Immunity* 19 (4), pp. 571–582. DOI: [10.1016/s1074-7613\(03\)00266-8](https://doi.org/10.1016/s1074-7613(03)00266-8) (cit. on p. 8).
- Shrestha, D., A. Jenei, P. Nagy, G. Vereb, and J. Szöllösi (Mar. 2015). "Understanding FRET as a research tool for cellular studies." In: *International journal of molecular sciences* 16 (4), pp. 6718–6756. DOI: [10.3390/ijms16046718](https://doi.org/10.3390/ijms16046718) (cit. on p. 11).
- Sivaramakrishnan, V., S. Bidula, H. Campwala, D. Katikaneni, and S. J. Fountain (Oct. 2012). "Constitutive lysosome exocytosis releases ATP and engages P2Y receptors in human monocytes." In: *Journal of cell science* 125 (Pt 19), pp. 4567–4575. DOI: [10.1242/jcs.107318](https://doi.org/10.1242/jcs.107318) (cit. on p. 9).
- Smith, P. K., R. I. Krohn, G. T. Hermanson, A. K. Mallia, F. H. Gartner, M. D. Provenzano, E. K. Fujimoto, N. M. Goeke, B. J. Olson, and D. C. Klenk (Oct. 1985). "Measurement of protein using bicinchoninic acid." In: *Analytical biochemistry* 150 (1), pp. 76–85. DOI: [10.1016/0003-2697\(85\)90442-7](https://doi.org/10.1016/0003-2697(85)90442-7). ppublish (cit. on p. 44).
- Sonawane, N. D., F. C. Szoka, and A. S. Verkman (Nov. 2003). "Chloride accumulation and swelling in endosomes enhances DNA transfer by polyamine-DNA polyplexes." In: *The Journal of biological chemistry* 278 (45), pp. 44826–44831. DOI: [10.1074/jbc.M308643200](https://doi.org/10.1074/jbc.M308643200). ppublish (cit. on p. 31).
- Sprenger, J. U., R. K. Perera, K. R. Götz, and V. O. Nikolaev (Aug. 2012). "FRET microscopy for real-time monitoring of signaling events in live cells using unimolecular biosensors." In: *Journal of visualized experiments : JoVE* (66), e4081. DOI: [10.3791/4081](https://doi.org/10.3791/4081). epubli (cit. on p. 38).
- Stefan, C., S. Jansen, and M. Bollen (Oct. 2005). "NPP-type ectophosphodiesterases: unity in diversity." In: *Trends in biochemical sciences* 30 (10), pp. 542–550. DOI: [10.1016/j.tibs.2005.08.005](https://doi.org/10.1016/j.tibs.2005.08.005) (cit. on p. 10).
- Stefanati, A., N. Bolognesi, F. Sandri, G. Dini, E. Massa, A. Montecucco, S. Lupi, and G. Gabutti (Sept. 2019). "Long-term persistency of hepatitis B immunity: an observational cross-sectional study on medical students and resident doctors." In: *Journal of preventive medicine and hygiene* 60 (3), E184–E190. DOI: [10.15167/2421-4248/jpmh2019.60.3.1315](https://doi.org/10.15167/2421-4248/jpmh2019.60.3.1315) (cit. on p. 2).

- Sträter, N. (June 2006). "Ecto-5'-nucleotidase: Structure function relationships." In: *Purinergic signalling* 2 (2), pp. 343–350. DOI: [10.1007/s11302-006-9000-8](https://doi.org/10.1007/s11302-006-9000-8) (cit. on p. 10).
- Strober, W. (Nov. 2015). "Trypan Blue Exclusion Test of Cell Viability." In: *Current protocols in immunology* 111, A3.B.1–A3.B.3. DOI: [10.1002/0471142735.ima03bs111](https://doi.org/10.1002/0471142735.ima03bs111). epublish (cit. on p. 31).
- Surprenant, A., F. Rassendren, E. Kawashima, R. A. North, and G. Buell (May 1996). "The cytolytic P2Z receptor for extracellular ATP identified as a P2X receptor (P2X7)." In: *Science (New York, N.Y.)* 272 (5262), pp. 735–738. DOI: [10.1126/science.272.5262.735](https://doi.org/10.1126/science.272.5262.735) (cit. on p. 8).
- Svobodova, I., A. Bhattaracharya, M. Ivetic, Z. Bendova, and H. Zemkova (2018). "Circadian ATP Release in Organotypic Cultures of the Rat Suprachiasmatic Nucleus Is Dependent on P2X7 and P2Y Receptors." In: *Frontiers in pharmacology* 9, p. 192. DOI: [10.3389/fphar.2018.00192](https://doi.org/10.3389/fphar.2018.00192) (cit. on p. 9).
- Taruno, A., V. Vingtdeux, M. Ohmoto, Z. Ma, G. Dvoryanchikov, A. Li, L. Adrien, H. Zhao, S. Leung, M. Abernethy, J. Koppel, P. Davies, M. M. Civan, N. Chaudhari, I. Matsumoto, G. Hellekant, M. G. Tordoff, P. Marambaud, and J. K. Foskett (Mar. 2013). "CALHM1 ion channel mediates purinergic neurotransmission of sweet, bitter and umami tastes." In: *Nature* 495 (7440), pp. 223–226. DOI: [10.1038/nature11906](https://doi.org/10.1038/nature11906) (cit. on p. 9).
- Thastrup, O. (Jan. 1990). "Role of Ca<sup>2+</sup>(+)-ATPases in regulation of cellular Ca<sup>2+</sup> signalling, as studied with the selective microsomal Ca<sup>2+</sup>(+)-ATPase inhibitor, thapsigargin." In: *Agents and actions* 29 (1-2), pp. 8–15. DOI: [10.1007/BF01964706](https://doi.org/10.1007/BF01964706). ppublish (cit. on p. 48).
- Thomas, D. and M. R. Hanley (1994). "Pharmacological tools for perturbing intracellular calcium storage." In: *Methods in cell biology* 40, pp. 65–89. DOI: [10.1016/s0091-679x\(08\)61110-3](https://doi.org/10.1016/s0091-679x(08)61110-3). ppublish (cit. on p. 48).
- Torre-Minguela, C. de, M. Barberà-Cremades, A. I. Gómez, F. Martín-Sánchez, and P. Pelegrín (Mar. 2016). "Macrophage activation and polarization modify P2X7 receptor secretome influencing the inflammatory process." In: *Scientific reports* 6, p. 22586. DOI: [10.1038/srep22586](https://doi.org/10.1038/srep22586). epublish (cit. on p. 9).
- Trautmann, A. (Feb. 2009). "Extracellular ATP in the immune system: more than just a "danger signal"." In: *Science signaling* 2 (56), pe6. DOI: [10.1126/scisignal.256pe6](https://doi.org/10.1126/scisignal.256pe6) (cit. on p. 9).
- Tsuchiya, K., S. Nakajima, S. Hosojima, D. Thi Nguyen, T. Hattori, T. Manh Le, O. Hori, M. R. Mahib, Y. Yamaguchi, M. Miura, T. Kinoshita, H. Kushiya, M. Sakurai, T. Shiroishi, and T. Suda (May 2019). "Caspase-1 initiates apoptosis in the absence of gasdermin D." In: *Nature communications* 10 (1), p. 2091. DOI: [10.1038/s41467-019-09753-2](https://doi.org/10.1038/s41467-019-09753-2). epublish (cit. on p. 78).
- Vignali, D. A. A., L. W. Collison, and C. J. Workman (July 2008). "How regulatory T cells work." In: *Nature reviews. Immunology* 8 (7), pp. 523–532. DOI: [10.1038/nri2343](https://doi.org/10.1038/nri2343) (cit. on p. 10).

- Wang, Z., P. G. Haydon, and E. S. Yeung (May 2000). "Direct observation of calcium-independent intercellular ATP signaling in astrocytes." In: *Analytical chemistry* 72 (9), pp. 2001–2007. DOI: [10.1021/ac9912146](https://doi.org/10.1021/ac9912146) (cit. on p. 10).
- Weisman, G. A., L. T. Woods, L. Erb, and C. I. Seye (Sept. 2012). "P2Y receptors in the mammalian nervous system: pharmacology, ligands and therapeutic potential." In: *CNS & neurological disorders drug targets* 11 (6), pp. 722–738. DOI: [10.2174/187152712803581047](https://doi.org/10.2174/187152712803581047). ppublish (cit. on p. 4).
- Wesolowski, J., V. Alzogaray, J. Reyelt, M. Unger, K. Juarez, M. Urrutia, A. Cauerrhff, W. Danquah, B. Rissiek, F. Scheuplein, N. Schwarz, S. Adriouch, O. Boyer, M. Seman, A. Licea, D. V. Serreze, F. A. Goldbaum, F. Haag, and F. Koch-Nolte (Aug. 2009). "Single domain antibodies: promising experimental and therapeutic tools in infection and immunity." In: *Medical microbiology and immunology* 198 (3), pp. 157–174. DOI: [10.1007/s00430-009-0116-7](https://doi.org/10.1007/s00430-009-0116-7) (cit. on pp. 2, 75).
- Woehrle, T., L. Yip, A. Elkhail, Y. Sumi, Y. Chen, Y. Yao, P. A. Insel, and W. G. Junger (Nov. 2010). "Pannexin-1 hemichannel-mediated ATP release together with P2X1 and P2X4 receptors regulate T-cell activation at the immune synapse." In: *Blood* 116 (18), pp. 3475–3484. DOI: [10.1182/blood-2010-04-277707](https://doi.org/10.1182/blood-2010-04-277707). ppublish (cit. on p. 77).
- Wu, W., X. Shi, and C. Xu (Mar. 2018). "Regulation of T cell signalling by membrane lipids." In: *Nature reviews. Immunology* 18 (3), p. 219. DOI: [10.1038/nri.2018.9](https://doi.org/10.1038/nri.2018.9). ppublish (cit. on p. 78).
- Xing, S., M. W. Grol, P. H. Grutter, S. J. Dixon, and S. V. Komarova (2016). "Modeling Interactions among Individual P2 Receptors to Explain Complex Response Patterns over a Wide Range of ATP Concentrations." In: *Frontiers in physiology* 7, p. 294. DOI: [10.3389/fphys.2016.00294](https://doi.org/10.3389/fphys.2016.00294) (cit. on p. 5).
- Xu, X. J., M. Boumechache, L. E. Robinson, V. Marschall, D. C. Gorecki, M. Masin, and R. D. Murrell-Lagnado (Aug. 2012). "Splice variants of the P2X7 receptor reveal differential agonist dependence and functional coupling with pannexin-1." In: *Journal of cell science* 125 (Pt 16), pp. 3776–3789. DOI: [10.1242/jcs.099374](https://doi.org/10.1242/jcs.099374) (cit. on p. 6).
- Yaginuma, H., S. Kawai, K. V. Tabata, K. Tomiyama, A. Kakizuka, T. Komatsuzaki, H. Noji, and H. Imamura (Oct. 2014). "Diversity in ATP concentrations in a single bacterial cell population revealed by quantitative single-cell imaging." In: *Scientific reports* 4, p. 6522. DOI: [10.1038/srep06522](https://doi.org/10.1038/srep06522). epublish (cit. on p. 11).
- Zhang, Z., G. Chen, W. Zhou, A. Song, T. Xu, Q. Luo, W. Wang, X.-s. Gu, and S. Duan (Aug. 2007). "Regulated ATP release from astrocytes through lysosome exocytosis." In: *Nature cell biology* 9 (8), pp. 945–953. DOI: [10.1038/ncb1620](https://doi.org/10.1038/ncb1620) (cit. on pp. 9, 76).
- Zimmermann, H. (June 1999). "Two novel families of ectonucleotidases: molecular structures, catalytic properties and a search for function." In: *Trends in pharmacological sciences* 20 (6), pp. 231–236. DOI: [10.1016/s0165-6147\(99\)01293-6](https://doi.org/10.1016/s0165-6147(99)01293-6) (cit. on p. 10).

## LIST OF FIGURES

Figure 1.1	Schematic overview of receptors, channels and enzymes taking part in the purinergic signalling cascade . . . . .	3
Figure 1.2	The structure of the P2X7 receptor . . . . .	6
Figure 1.3	Functions of P2X7 in T cells, macrophages and microglia . . . . .	7
Figure 1.4	Fluorescence and the principle of FRET . . . . .	11
Figure 1.5	FRET ATP sensor ATeam . . . . .	13
Figure 1.6	Small molecule ATP Sensor Zn-DPA . . . . .	14
Figure 3.1	Shedding of CD62L and PI uptake after gating of P2X7 . . . . .	47
Figure 3.2	Calcium release after gating of P2X7 in Yac-1 cells . . . . .	48
Figure 3.3	Calcium release after gating of P2X7 in primary CD4 <sup>+</sup> T cells . . . . .	49
Figure 3.4	Bulk measurement of ATP release after ADP-ribosylation of P2X7 . . . . .	50
Figure 3.5	Expression and function of cytosolic FRET sensors . . . . .	54
Figure 3.6	Visualization of cytosolic ATP concentrations by live cell imaging . . . . .	55
Figure 3.7	Monitoring intracellular ATP depletion after CDC in Yac-1 cells with FRET-based ATP sensors . . . . .	56
Figure 3.8	Gating of P2X7 is associated with a depletion of cytosolic ATP . . . . .	58
Figure 3.9	Visualization of P2X7-dependent cytosolic ATP depletion in Yac-1 lymphoma cells . . . . .	59
Figure 3.10	Validation of the membrane bound ATP FRET sensor . . . . .	60
Figure 3.11	Release of ATP after ADP-ribosylation of P2X7 . . . . .	61
Figure 3.12	Functionality testing of Zn-DPA sensors . . . . .	63
Figure 3.13	The Zn-DPA-azide variant of the small-molecule ATP sensor shows an altered specificity for ATP . . . . .	64
Figure 3.14	Labeling of SA surfaces with Zn-DPA-azide . . . . .	65
Figure 3.15	Labeling of SA beads/plates Zn-DPA-C-Azid variants . . . . .	66
Figure 3.16	Targeting TP1170-Zn-DPA to LP1 cells via an anti-HLA-DR antibody . . . . .	67
Figure 3.17	Localization of the Zn-DPA-C(n) sensor in Yac-1 cells . . . . .	69
Figure 3.18	Functionality testing of cholesterol- and tocopherol-modified Zn-DPA sensors . . . . .	70
Figure 3.19	Cholesterol and tocopherol Zn-DPA variants label cell membranes . . . . .	71
Figure 3.20	Measurement of ATP release with single wavelength ATP sensors . . . . .	73

Figure 4.1	Schematic overview of mechanisms of ATP release and of ATP sensors used in this work . . . . .	82
------------	--	----

## LIST OF TABLES

Table 2.1	Antibodies/nanobodies used for FACS and microscopy . . . . .	16
Table 2.2	Bacterial strains . . . . .	17
Table 2.3	Buffers and solutions . . . . .	17
Table 2.4	Cell lines . . . . .	19
Table 2.5	Chemicals and reagents . . . . .	20
Table 2.6	Consumables . . . . .	23
Table 2.7	Used enzymes . . . . .	25
Table 2.8	Kits . . . . .	26
Table 2.9	Laboratory equipment . . . . .	26
Table 2.10	Mouse lines used for T cell preparation . . . . .	28
Table 2.11	Plasmids . . . . .	28
Table 2.12	Primers used for sequencing and genotyping . . . . .	29
Table 2.13	Software . . . . .	29
Table 2.14	Reagents needed for transfections using jetPEI® . . . . .	32
Table 2.15	Reagents needed for transfections using PEI . . . . .	32
Table 2.16	PCR mixture . . . . .	40
Table 2.17	PCR program . . . . .	40

## DANKSAGUNG

Zunächst danke ich Prof. Dr. Friedrich Haag für die Bereitstellung des Themas und der Unterstützung und Betreuung während der gesamten Arbeit, sei es im Labor oder bei der Fertigstellung dieser Arbeit. Zudem danke ich Prof. Dr. Viacheslav Nikolaev für das Übernehmen des Zweitgutachtens und die Möglichkeit einen großen Teil der Live-Cell Imaging Versuche in seinem Labor durchführen zu dürfen. Prof. Dr. Andreas Guse und Dr. Björn Diercks danke ich für die Unterstützung und Möglichkeit der Calcium-Messungen. Bei Herrn Dr. Virgilio Failla bedanke ich mich für die Einweisung in die verschiedensten Mikroskopiesysteme und die Hilfestellung bei der Auswertung der generierten Daten.

Gudrun Dubberke, Fabienne Seyfried und Joana Schmid danke ich für die Unterstützung in allen laborrelevanten Themen und darüber hinaus, sowie für die netten Kaffee- und Mittagsrunden, bei denen interessante Themen besprochen wurden und es immer etwas zum Lachen gab. Darüber hinaus danke ich allen Mitarbeitern der AG Haag, die ich in meiner Zeit dort kennengelernt habe; Felix Scherg, Samantha Wittke, Fathen Habib, Antonia Lehmann und Sonja Klose für die tolle Zusammenarbeit und die experimentelle Hilfe. Außerdem danke ich Sana Javed und Carolina Pinto-Espinoza, die zur gleichen Zeit promoviert haben, für die nette Zeit im gemeinsamen Büro und im Labor. Nicole Schwarz möchte ich für lustige Zeit und das Korrekturlesen meiner Arbeit danken. Weiterhin möchte ich mich bei Alexander Laubach für die gute Zusammenarbeit und die Synthese und Bereitstellung der Zn-DPA Sensoren bedanken, die einen großen Beitrag zu meiner Arbeit geliefert haben.

Auch danke ich all meinen Freunden, die teilweise das gleiche durchgemacht haben oder durchmachen und mir mit motivierenden Worten in schwierigen Zeiten sowie bei der Korrektur meiner Arbeit geholfen haben. Natürlich geht mein Dank auch an meine Familie, die mich während des Studiums und der Promotion unterstützen, auch wenn Ihnen nie ganz klar war, was ich eigentlich mache. Den größten Dank spreche ich vor allem Lea aus, die immer für mich da war und ohne die die Fertigstellung dieser Arbeit nicht möglich gewesen wäre.

## CURRICULUM VITAE

Lebenslauf wurde aus datenschutzrechtlichen Gründen entfernt.

## EIDESSTATTLICHE VERSICHERUNG

Ich versichere ausdrücklich, dass ich die Arbeit selbständig und ohne fremde Hilfe verfasst, andere als die von mir angegebenen Quellen und Hilfsmittel nicht benutzt und die aus den benutzten Werken wörtlich oder inhaltlich entnommenen Stellen einzeln nach Ausgabe (Auflage und Jahr des Erscheinens), Band und Seite des benutzten Werkes kenntlich gemacht habe.

Ferner versichere ich, dass ich die Dissertation bisher nicht einem Fachvertreter an einer anderen Hochschule zur Überprüfung vorgelegt oder mich anderweitig um Zulassung zur Promotion beworben habe.

Ich erkläre mich einverstanden, dass meine Dissertation vom Dekanat der Medizinischen Fakultät mit einer gängigen Software zur Erkennung von Plagiaten überprüft werden kann.

*Hamburg, 2020*

---

Klaus Eric Kaschubowski